Magnetic based micro-indentation catheter for soft tissue characterization in minimally invasive surgery

Design, prototypes and measurements

N.J. Zaanen

Master of Science Thesis

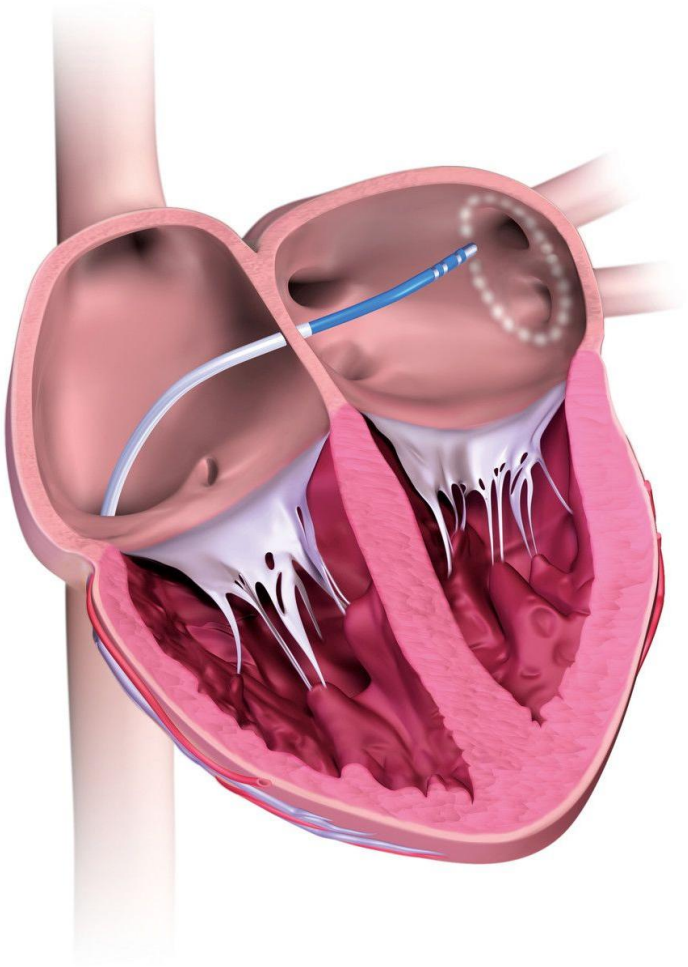

TU Delft Delft University of Technology

Magnetic based micro-indentation catheter for soft tissue characterization in minimally invasive surgery

Design, prototypes and measurements

Master of Science Thesis

For the degree of Master of Science in Precision and Microsystems Engineering at Delft University of Technology

N.J. Zaanen

November 26, 2015

Report number: MNE 2015.036
Faculty of Mechanical, Maritime and Materials Engineering (3mE) · Delft University of Technology

The work in this thesis was conducted in the Multi-Scale Robotics Lab, ETH Zurich. Their cooperation is hereby gratefully acknowledged.

Delft University of Technology
Department of
Mechanical Engineering (pme)

The undersigned hereby certify that they have read and recommend to the Faculty of Mechanical, Maritime and Materials Engineering (3mE) for acceptance a thesis entitled

Magnetic based micro-indentation catheter for soft tissue characterization in minimally invasive surgery

by

N.J. Zaanen

in partial fulfillment of the requirements for the degree of

Master of Science Precision and Microsystems Engineering

Dated: November 26, 2015

Supervisor(s):

prof. dr. U. Staufer

ir. G. Chatzipirpiridis

Reader(s):

ir. J.W. Spronck

dr. L. Sasso

Abstract

In the last ten years, open heart surgery has increasingly been replaced by Minimally Invasive Surgery (MIS), which has three main advantages. There is reduced blood loss, small scars to reduce infections, and a shorter recovery time. However, MIS still lacks full surgical capabilities. Firstly, not all surgical movements can be performed, since manipulation through an incision reduces catheter dexterity. Solutions for this problem are medical robotic surgery (e.g. Zeus or DaVinci system) or external guidance (e.g. with a magnetic field). Secondly, contact force determination is more difficult, since the force measured *ex vivo* is not equal to the contact force, due to forces and moments imposed by organs, arteries and the incision. Force determination is important however, in order to prevent tissue puncture and to assist in thermal ablation. Commercially available solutions for this problem are Thermocool (measurement with strain gauges) and TactiCath (optical measurement). Lastly, tissue characterization is more difficult, since palpation is not possible in MIS. Tissue characterization is used to detect tissue abnormalities and to determine the effectiveness of thermal ablation, by measuring the resulting increase in stiffness of the lesion. Thermal ablation is used to treat Atrial Fibrillation by destroying tissue and therefore blocking an electrical pathway. There are currently no solutions available for this problem, and this research therefore focuses on this problem.

Therefore, the main goal of this research is the development of a catheter capable of force and soft tissue stiffness measurement in the human heart, in order to distinguish ablated from non-ablated tissue. This is reflected in the research objective:
Develop an accurate and robust micro-scale catheter tip prototype for combined stiffness and force sensing of soft biological heart tissue during minimally invasive surgery by making use of a 3D magnetic Hall sensor and micro-indentation technique. During this research, such a catheter tip has been designed. Force and stiffness sensing is performed based on load-displacement determination, as opposed to e.g. resonance-based sensing. Measurement is performed in a displacement-controlled mode, in which force is measured in the catheter tip.

Measurement is performed with a 3D magnetic Hall sensor and a permanent magnet, each attached to one end of the spring (resilient structure). Deflection of the spring creates a changed magnetic field, which is measured by the Hall sensor. Through calibration, the applied force and the spring deformation can be deduced from this magnetic field. Since the actuation displacement is controlled, the tissue indentation can be determined as the difference between the actuation and spring deformation. Tissue stiffness can then be calculated as the

slope of the measured load-displacement curve.

Besides this basic measurement principle, three other key design features are worth mentioning. Firstly, actuation of the catheter can occur *ex vivo*, since a stiff guidance tube concentrically encloses the catheter tube. Therefore, a force can be applied outside of the body, which is then transferred to the catheter tip without influence of the incision or internal organs. Secondly, guidance of the catheter can also occur *ex vivo*, since the magnet used for force and stiffness sensing is fixated in the catheter tip. This enables guidance of the whole catheter based on an external (i.e. *ex vivo*) magnetic field. Thirdly, mechanical stoppers are implemented in the design to enable pre-loading of the spring. This is essential to achieve repeatable and reliable results, since the initial spring length (before actuation) is always the same. Furthermore, these stoppers protect tip components and prevent them from falling out of the tip.

Several prototypes have been made, in which most components are 3D printed out of Vero-Clear. The only two exceptions are the spring and Hall sensor, which are both commercially available at low cost. Consequentially, the catheter tip weighs only 0.32 gram and costs less than €4, making it disposable. Other key design features of the catheter tip are its diameter of 4 mm and its force range of 0 - 0.2 N. Calibration and measurement of the final prototype is performed with several experiments in order to assess the repeatability, accuracy and effectiveness of the catheter tip design. The main conclusions from these experiments were:

- The prototype measurements are repeatable, with a measured force deviation of mostly 0% to 5% in different measurements of the same material.
- The prototype measurements directionality correspond to measurements with a verified load-displacement machine. However, the prototype systematically underestimates the stiffness by approximately 30% to 40%, due to an indentation speed difference between the measurements with the prototype and with the verified machine. Further research is required.
- The prototype is effective towards its goal of distinguishing non-ablated and ablated tissue, and even different ablated tissues. This is mainly the case because of the high measurement repeatability (i.e. precision) and the fact that the lower accuracy was mainly caused by a systematic error (instead of a random one).

Based on these measurement results, it can be concluded that the developed catheter tip meets the main objective of robust and effective force and stiffness sensing of soft biological heart tissue. Although there seems to be a systematic inaccuracy (to be verified with new measurements) in stiffness measurement, the catheter tip is still effective in reaching its goal of distinguishing ablated and non-ablated heart tissue.

To increase the force resolution and signal-to-noise ratio of the catheter tip, a design study has been undertaken as a side-project during the research. Based on this study, the use of a displacement amplifying compliant mechanism (DACM) is proposed based on a spring-mass lever model and stiffness mapping. A mechanism with an amplification of 2.2 has been designed, and a review of fabrication methods is recommended.

Contents

List of Figures

List of Tables

Acknowledgements

This thesis report is written as a part of the master programme in Precision and Microsystems Engineering at the Faculty of Mechanical Engineering of Delft University of Technology. The research has been performed at the Eidgenössische Technische Hochschule Zürich, in the Multi-Scale Robotics Lab which is part of the Institut für Robotik und Intelligente Systeme.

During the last six months, I have truly enjoyed working on my thesis research and can look back at a valuable time for which I would like to thank the following people. First of all, I would like to express my gratitude towards my supervisor, prof. dr. Urs Staufer, for his excellent guidance and valuable advice during the project. Furthermore, I would like to thank dr. ir. Bradley Nelson, for providing me with the opportunity to conduct my research in the Multi-Scale Robotics Lab. In addition, I would like to especially thank my supervisor ir. George Chatzipirpiridis, for his enormous enthusiasm, excellent guidance and valuable contributions during my whole research. I would also like to thank ir. Jo Spronck and dr. Luigi Sasso, for completing my graduation committee.

Furthermore, I would like to thank K-Tube Technologies for providing the required stainless steel tubes for laser cutting my spring design and Polyfluor for sending sample material for the test set-up. Moreover, dr. ir. Hamdi Toren and dr. ir. Olgaç Ergeneman for their effort in making possible the fabrication of the custom spring I have designed.

Many thanks to all people that have helped, educated and stimulated me during my educational period as well as to my roommates, friends and colleagues that have made my time as a student absolutely terrific. Although there are too many to mention here, I would like to extend a special thanks to the people that helped me during this thesis research: the fellow students working in the Multi-Scale Robotics Lab, in specific Simone, Alessandro and Kathrin and my friends Jasmin, Parmiss and Yvonne in the Netherlands for the good times and support over Skype. Besides this, I would like to express my gratitude towards my parents and my beloved sister for their unconditional support, love and care in everything I have pursued as a student and in life. Finally, I would like to thank a very special person in my life, my boyfriend Roelant, for his enormous support, encouragement and devotion since the beginning of my studies.

Nanda Zaanen

Zürich, November 2015

Chapter 1

Introduction

In this chapter, the research is introduced as well as the thesis purpose and objective. Section 3-1-2 discusses the background of the research which includes minimally invasive surgery as well as trends towards medical robotic surgery. The research purpose is given in section 1-2, followed by the research objective in section 1-3 and the scope and limitations in section 1-4. The chapter concludes with an overview of the thesis structure, which is presented in section 1-5.

1-1 Background

Surgery has been performed since medieval times and can be described as physically changing body tissues by means of cutting, abrading, saturing or other methods to treat disease or injury. During traditional open heart surgery, surgeons are opening the chest of the patient and perform various types of operations on the heart muscle, valves or connected parts such as the aorta. Soft tissue mechanical properties and anatomical structures, such as soft tissue stiffness, thickness and abnormalities, are obtained by means of palpation [1]. Palpation is a medical procedure by which surgeons apply a small force on organs and tissue with their fingers to ascertain possible abnormalities [2]. Tumors or tissue abnormalities can efficiently be identified based on mechanical properties, since these are changed by disease. Alterations in tissue stiffness are commonly caused by exudation of fluids from the vascular system into the extra- and intracellular space or due to loss in the lymphatic system [3, 4]. Therefore, local measurement of tissue mechanical properties can be used for the successful identification of disease during open heart surgery.

1-1-1 Minimally invasive surgery (MIS)

In the last decade, open heart surgery, illustrated in figure 1-1a, has been increasingly replaced by Minimally Invasive Surgery (MIS), depicted in figure 1-1b. The surgical tool, a heart catheter, is inserted through a small incision in the neck, groin or axilla and manually pushed

through the vascular system towards the target location. Compared to open heart surgery, MIS offers many advantages and is becoming the preferred procedure due to its minimal invasiveness. This results in a reduction of blood loss, tissue trauma, risk of post operative infection and overall recovery time of the patient [5].

(a) Traditional open heart surgery

(b) Minially invasive surgery

Figure 1-1: Traditional open heart surgery compared to minimally invase surgery

Despite of the aforementioned benefits, surgeons still face many technical challenges as well as ergonomic difficulties. Technical challenges include but are not limited to depravation of direct hand-eye coordination because of the remote and *in vivo* measurement site. Furthermore, loss of intuitiveness in the usage of the minimally invasive tools is a common problem, since the incision reverses the movement from hand to tool-tip, leading to imprecise movements. Moreover, MIS induces increased difficulty in reaching the surgical location without causing internal damage on blood vessels or soft tissue since the maximum force to prevent tissue puncture is easily exceeded without force feedback [6, 7, 8].

Furthermore, the surgeon experiences a restricted vision of the operation site and relies on 2D imaging techniques resulting in a lack of depth. Currently, real-time projection images with X-ray fluoroscopy are used to perform catheter navigation inside the human body [8]. This technique involves an X-ray source, detector and a contrast agent which is injected in the blood vessels to increase imaging quality and resolution. Unfortunately, imaging quality of soft tissue and organs is still poor despite of the added contrast agent which increases risk of kidney failure [9]. Moreover, the interventional procedure time is limited due to the increasing risks associated with exposure to ionization radiation for the patient and medical staff.

Therefore, innovative methods for imaging are desired in order to perform cardiac catheterization [10, 11]. One of these methods is the so called Magnetic Resonance Imaging (MRI), in which a strong magnetic field is able to capture three dimensional high contrast images of soft tissue by making use of the magnetic properties of atomic nuclei. These nuclei, in particular hydrogen nuclei which are present in water, thereby making up most of the human body, have a magnetic spin that can be aligned by a burst of radio-frequency waves. Subsequently, the nuclei oscillate and are distorted out of the spin alignment by means of a second burst. The realignment to equilibrium position differs per tissue which makes them possible to distinguish and image. This method does not require a contrast agent or involves

radioactivity or ionising radiation. Magnetic materials can not be implemented in surgical tools because of the strong magnetic field. They cause image distortion and possible displacement of magnetic components [9, 12]. Furthermore, conductive materials can act as magnetic resonance-antennas which means that the objects are heated. This may possibly result in tissue burning, thereby putting the patient in critical condition [13]. Hence, non-magnetic surgical tools and devices must exclusively be used in combination with MRI to fully guarantee safety of the patient.

Ergonomic challenges are inflicted during MIS, firstly because of the restricted degrees of freedom on the instrument operated by the surgeon. The instruments degrees of freedom are limited to four, since as the instrument enters the trocar point (point where catheter enters the body) it can only slide and rotate, illustrated in figure 1-2. The missing two degrees of freedom need to be compensated for by elbow, wrist and shoulder movements of the surgeon causing fatigue and tremor of the hands on the tool, which leads to surgical inaccuracy. Secondly, surgeons are not able to rest, support or lean their hands on the patients body for fixation and tool orientation in order to perform fine operations as in traditional surgery [14].

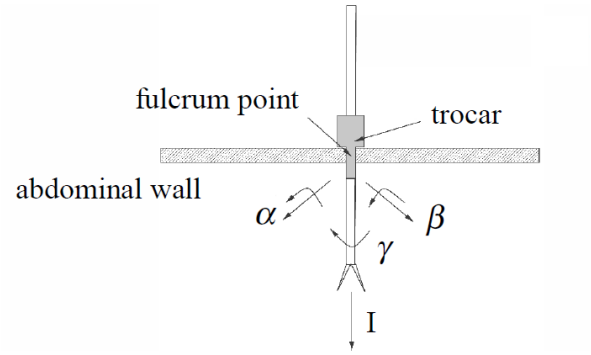

Figure 1-2: Degrees of freedom $(\alpha, \beta, \gamma, I)$ in MIS: Instrument is moved around an invariant fulcrum point [7]

Furthermore, obtaining tactile and kinesthetic force feedback from the interaction between the instrument and tissue, also referred to as haptic feedback, is highly influenced during MIS. Figure 1-3 presents the force components and tractions originating from friction and transversal moments between the catheter shaft and insertion port as well as friction between the blood vessel wall and the catheter shaft [15, 16]. The forces acting on the catheter at the incision are a combination of friction caused by the trocar and moments are generated when tilted by the abdominal wall [17]. The force component of actual interest to the surgeon is the contact force of the catheter tip with the soft tissue on the surgical site. However, distinction between components, desired tip-tissue contact force or unwelcome friction and force components, of the received force feedback during catheterization procedures requires extensive training, especially to achieve the same level of palpation (tissue property identification) as during open heart surgery [18].

1-1-2 Medical robotic surgery

The increased use of minimally invasive surgery has also highly impacted the area of medical robotics. The motivation for using surgical systems and sophisticated catheters is twofold

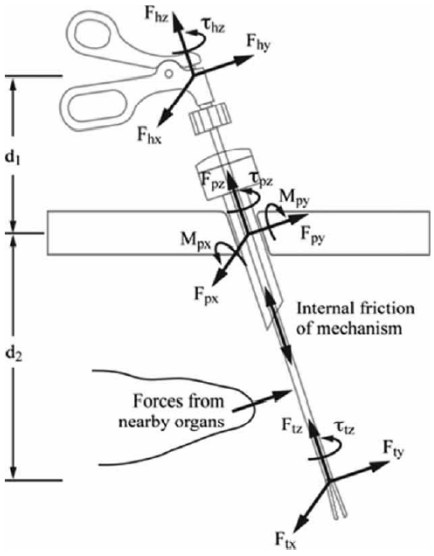

Figure 1-3: Force and moments on surgical instruments during MIS [16]

and explains the rapid growth and development of these devices.

Firstly, as discussed in the previous section, MIS necessitates movement stretching the limits of human performance and levels of dexterity [19]. Substantial improvements in the capabilities of physicians are required and can be achieved by the use of robotic surgical system. The improvements include increased precision, tremor filtering, movement control and enhanced dexterity [20].

Secondly, the increased capabilities during robotic surgery allow to perform complicated and scarless operations in comparison with MIS, by entering the body through smaller incisions or natural orifices.

Figures 1-4 and 1-5 show the information flow for the whole system during conventional MIS and when using a master-slave system, respectively. In these overviews the information flow is mapped starting with the tissue-tool interaction, followed by sensor signals and finally the delivery of force information through a user interface to the clinicians. The main difference is that force feedback is given by means of an interface for robotic surgery while it is direct but distorted for conventional MIS.

For cardiac robotic surgery, two master-slave systems have recently been developed. A master-slave system is defined as a model where one device has unilateral control over one or more devices [21]. In the context of medical surgery, the slave is the robot that performs the surgery while the master is a control device operated by the surgeon. The surgeon uses a remote interface to manipulate and control the surgical tool.

The first system is called the Da Vinci system, consisting of a control unit and a four-arm surgical manipulator [22, 23]. The manipulator offers three degrees of freedom for the catheter shaft (pitch, yaw and insertion), and three additional degrees (pitch, yaw and roll)

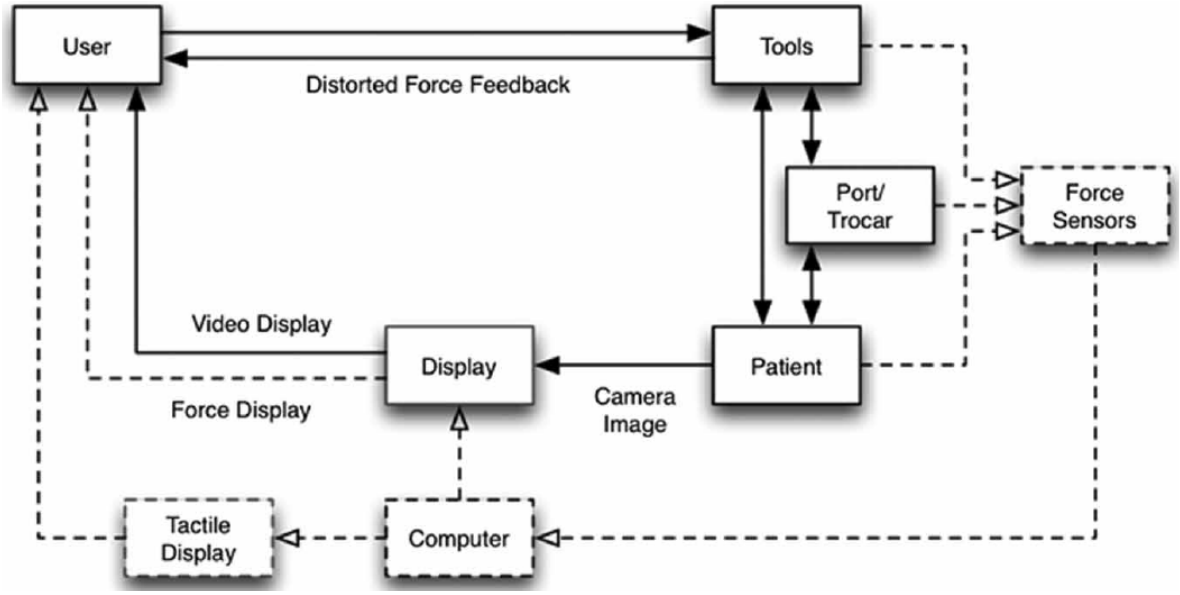

Figure 1-4: Information flow during conventional MIS [16]

can be added by the end-effector which is the tool-tip. A similar system, called Zeus, is a slave system mounted on the operation table consisting of three interactive robotic arms: two endoscopic instrument arms and one endoscopic camera arm [24]. This computer motion system has only four degrees of freedom and therefore less dexterous than the Da Vinci system. Higher dexterity can be obtained by introducing one or two additional degrees of freedom at the instrument tip. Several tips have been developed either with rotating joints at the tip [25] or by means of a flexible tip [26, 27].

Robotic surgery has become a key technology in for example coronary artery bypass operations and miral valve surgery achieving much better outcomes than without these systems. However, force and tactile information is still lacking, limiting the clinical use of commercially available systems because of the urge for this information during certain surgical procedures [28].

1-2 Research purpose

The research purpose, for developing a force sensing and soft tissue stiffness measurement catheter is twofold.

Firstly, common needs for all cardiac MIS procedures are to restore tactile sensation and enhance the capability of surgeons by appropriate sensors in the catheter tip. Improvements would able the surgeon to determine hardness and tension in tissue, measure variation in properties and control force application in a more precise manner to prevent tissue puncture. Secondly, to increase the success rate in treatment of Atrial Fibrillation (AF) by measuring contact force during ablation and soft tissue stiffness before and after surgery in specific. Atrial fibrillation is the most common type of heart arrhythmia in which the heart rhythm

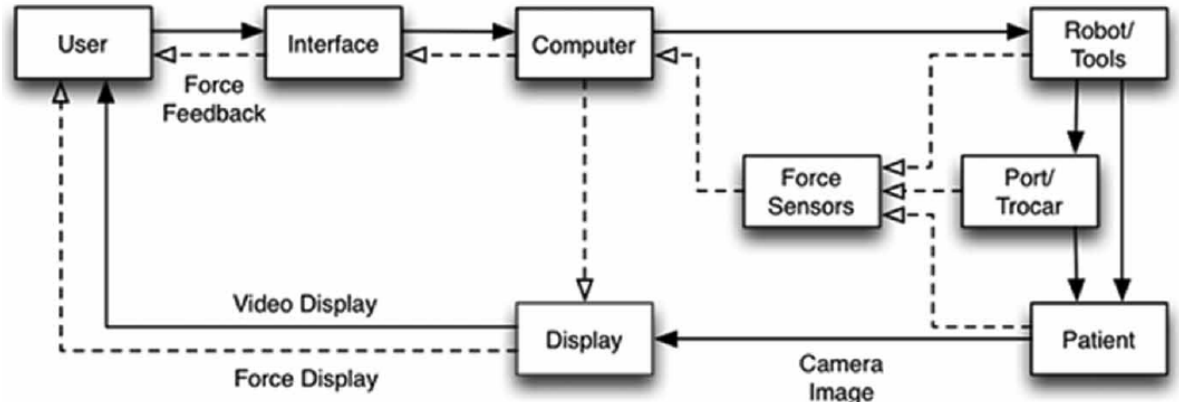

Figure 1-5: Information flow during robotic minimally invasive surgery by means of master-slave system [16]

is disturbed and is either too fast, too slow or irregularly. This disease is caused by incorrect and disorganized electrical signals of the sinoatrial node resulting in a missing correlation of contraction between the two upper heart chambers. In Europe 2% of the population has atrial fibrillation of which 50% suffers from a continuous form, which highly increases the risk for a fatal heart stroke [29].

Atrial fibrillation can be treated with (radio frequency based) catheter ablation. Non-isolated electrodes at the end of the catheter tip emanate radio waves, heat is produced as the radio waves find their ground (foil package attached to patients back) due to resistive forces surrounding the electrode. The heat burns the soft tissue, creating so called lesions, which can encircling the pulmonary veins in order to isolate electrical pulses from the left atrium [30, 31]. Accurate and reliable methods to determine the adequacy of the treatment are essential to prevent under- or overheating of lesion which determines the lesion size. The lesion size, including depth, responsible for blocking the electrical pulse dependents on the catheter tip temperature and contact force [32]. Several studies have shown that catheter contact force is an important determinant of lesion size and decreased the incidence of ablation complications, both enhancing the success of the treatment.

Currently, diagnostic imaging techniques are used to accomplish three different tasks concerning catheter ablation [33]. Firstly, the optimal positioning of the ablation catheter with respect to the targeted ablation location. Secondly, the guidance for energy deposition during the surgical ablation. Thirdly, assessment of the results of the created lesion to decide upon relevant post surgical treatments. Most of the imaging-guidance for thermal ablation procedures are performed by means of sonography because due to associated low-cost, real-time visualization, portability and nearly universal availability. The main limitation of this technique is however that poor visualization of the lesion can occur because of a lack in innate tissue conspicuity or overlying bone- or gas-containing structures. The greatest lesion-to-tissue contrast can be achieved by means of MRI imaging, as discussed in section 1-1-1. Here, the main drawbacks are the high costs and the required MR compatible tools.

Given the likelihood of successful treatment, additional techniques for lesion size and depth de-

termination are aspired. Stiffness measurement of soft tissue before and after lesion formation provides valuable insight in the lesion depth and quality. The relation between tissue heating and increased soft tissue stiffness has been researched in several studies [34, 35, 36, 37] and is found to increase on average 5 times for an increase of 30 °C [38]. Dehydration of soft tissue occurs for increased heating which leads to protein denaturation and resulting in increase of the tissue stiffness. To conclude, measuring soft tissue stiffness qualifies as a valuable tool for lesion size analysis and providing assistance in qualitative lesions, which provide long-term electrical signal isolation while not stiffening the heart muscle.

1-3 Research objective

The main goal of this research is the development of a catheter capable of force and soft tissue stiffness measurement in the human heart. This is highly relevant because it would result in increased effectiveness and success of tissue ablation while reducing tissue trauma and patient recovery time. The research objective, based on the performed literature study of which the investigations leading to this statement will be treated in chapter 2, is formulated as follows:

Develop an accurate and robust micro-scale catheter tip prototype for combined stiffness and force sensing of soft biological heart tissue during minimally invasive surgery by making use of a 3D magnetic Hall sensor and micro-indentation technique.

In this research objective, 'accurate' is defined as the best possible result given the sensor and actuator resolution, tool compliance and non-linear tool-tissue interaction. The accuracy of the whole system may be evaluated by a reference measurement, conducted by a verified stiffness measurement device. The samples for this measurement should not be too stiff such that the indentation approaches the indentation resolution of the machine.

Soft tissue stiffness measurement can be accomplished by two techniques, these involve either resonance based sensing or indentation (displacement) based sensing. Resonance based stiffness sensing has been studied prior to the current research and will not be in the scope of the current thesis for technical reasons elaborated on in section 2-2.

The meaning of 'micro-indentation technique' includes the choice for optimal indenter geometry and relevant indentation technique. Indentation for stiffness sensing can be performed by means of distinguish between passive or active soft tissue indentation.
In the passive technique, the indenter sticks out with respect to a reference, biasing the indenter with an initial displacement. In contrary to this passive technique, active indentation requires an actuator mechanism to actively indent soft tissue from a reference at the tissue surface to ultimately generate a load-displacement curve.
Little is described in literature concerning the best approaches for *in vivo* biological tissue indentation, to perform measurement of mechanical properties therefore additional research is needed.

Subordinate to the main objective are three sub-objectives:

1. To create effective catheter tip concept design(s) for the combined stiffness and 3D force

sensing by making use of a Hall sensor and fixed permanent magnet;

2. To study the design and application of a displacement-amplifying compliant mechanism to amplify the indentation displacement and thereby improve the force and stiffness sensing accuracy;

3. To perform experiments with the assembled prototypes on samples of varying stiffness under prescribed boundary & environmental conditions.

The first sub-objective mentions the creation of 'effective catheter tip concept design(s)'. In this thesis, this means that the fabrication cost, the *in vivo* safety of material and design as well as the essential measurement accuracy of the prototype are taken into account in the design phase. A remark concerning the assessment of *in vivo* safety will be made in section 1-4. Furthermore, the positioning of the permanent magnet, which will be fixed in the device, related to the 3D magnetic Hall sensor will be discussed in section 1-4.

In the second sub-objective, a displacement-amplifying compliant mechanism is studied to assess whether this can improve the force sensing accuracy and therefore also the soft tissue stiffness. The small indentation displacement (input displacement) is amplified to the sensor side resulting in a larger output displacement provided for measurement by the Hall sensor.

The last and third sub-objective focuses on prototyping and testing of the concept design(s) developed in subobjectives 1 and 2. In order to effectively test the prototype, samples of varying stiffness will be measured under specified boundary conditions. These boundary conditions include *inter alia* the specific angle under which the catheter approaches the sample.

1-4 Research scope and limitations

The research scope has been defined at the beginning of the research given the limited amount of time to perform the thesis. The current research focuses on the development of an *in vivo* cardiac catheter, capable of measuring the contact force between catheter and soft tissue and determining soft tissue stiffness. The ranges for soft tissue stiffness as well as force sensing are discussed in the design requirement, section 3-2, aiming to be in close accordance with realistic MIS values. In addition, the catheter prototype needs to be compatible with the *in vivo* environment and safety regulations, as well as suitable to be guided by an external magnetic field. The research concerning magnetic guidance is conducted in parallel by the Multi-Scale Robotics Lab (ETH, Zürich)[39] in cooperation with Aeon Scientific.

Soft tissue measurement and modeling nor a clinical study of prototype(s) is included in the scope of this research. Primarily because of the initial stage of the research and limited time to conduct the research. However, a clinical study and designing an associated user interface for the catheter can be a subject for further research after the current work.

The main limitation of soft tissue surgery and the design of the associated systems and measurement tools is the deformability and mobility of soft tissue. The complex non-linear and viscous behavior can not be solely based on preoperative and documented data. There-

fore, additional data during surgery needs to be determined by means of imaging, indentation, boundary conditioning methods and mathematical modeling. However, a model containing and accounting for all complex intrinsic properties is challenging since the bio mechanical properties of the soft tissue depend on intraoperative conditions [20] and differ for each individual [40]. Hence, assumptions regarding soft tissue stiffness and the influential nature on the measurement need to be made because of lacking qualitative data, which will be described in section 3-1-2.

1-5 Thesis structure

This thesis consists of two parts, reflecting the two main phases of the research which are aligned with the followed research method.

Part I covers the development of the combined force and stiffness measurement catheter tip and consists of four chapters. Chapter 2 provides a summarized overview of the state-of-the-art of force sensing catheters and the mechanics and associated methods of (soft tissue) indentation. The design methodology is the subject of chapter 3, i.e. how the theory of force and stiffness sensing is used to develop different design solutions. Chapter 4 discusses the design of the spring flexure mechanism. Furthermore the chapter provides analytically as well as finite element modeling analysis. This is used as design tool and adding further to the credibility to the design. Finally, chapter 5 discusses the design and analysis of the Displacement Amplifying Compliant Mechanism (DACM).

Part II in this thesis, consisting of four chapters, discusses the catheter prototype(s) and evaluates these based on measurements. In chapter 6, the fabrication of the prototype(s) will be discussed. Chapter 7 discusses the experimental setup and different measurements that will be conducted. The results of these measurements are presented and discussed in chapter 8. Lastly, the conclusions and recommendations for further research are treated in chapters 9 and 10, respectively.

Chapter 2

State-of-the-art

This chapter summarizes the main findings of the conducted literature review prior to the research. The goal of this literature review, and therefore this chapter, is to provide an overview of the state-of-the-art of the transducer and measurement techniques in catheter force sensing and soft tissue stiffness characterization.

Section 2-1 discusses the state-of-the-art in medical catheters. This section treats the force sensing transducer principles used for catheters in MIS in section 2-1-1. The state-of-the-art in soft tissue stiffness measurement is the subject of section 2-2. Section 2-3 concludes the chapter with a short summary.

2-1 State-of-the-art in medical catheters for MIS

In this section, the state-of-the-art and the latest development in catheter force sensing transducer techniques by outlining the most relevant literature in academia, patents and commercial available endeavors. The review focuses on the the research scope or closely related topics to catheters and MIS.

The medical definition of a catheter is [41]:
A catheter is a hollow flexible tube that can be inserted into a vessel or cavity of the body to withdraw or instill fluids, directly monitor various types of information, visualize a vessel or cavity or perform a surgical operation.

There are many types of catheters all invigorated to the specific MIS procedure and *in vivo* location such as bladder, heart, kidney et cetera. Most catheters are very small in size, only a few french (1 Fr is 1/3 mm) and made of soft plastic, rubber, or silicon which are biocompatible and therefore save to use inside the human body.

Cardiovascular (heart) catheters can have multiple functions, they can be used for catheterization purposes such as examination of the heart valves, measuring the oxygen level or search

for tissue abnormalities (these include heart function and diagnose cardiovascular conditions). Furthermore, they are used for surgical procedures such as biopsy (a small sample is taken for testing), open up restricted veins by balloon inflation or when performing tissue ablation [42].

Because of this decreased level of invasiness during minimally invasive surgery, the surgeon experiences a loss in tactile feedback and tissue contact force, as has been discussed in the introduction. This 'sense of feel' needs to be restored by artificial means to find tumors, which are during open heart surgery easy to locate, determine the ablation effectiveness by measuring the stiffness of the lesion and prevent tissue puncture [43, 5]. This can be achieved by implementing force and artificial tactile sensing systems (see Explanatory box 1) in MIS tools.

Explanatory box 1: **Background on tactile feedback**

According to Lee a tactile sensor is defined as *"a device or system that can measure a given property of an object or contact event through physical contact between the sensor and the object"* [44].

Tactile sensing is the process of determining the physical properties through physical contact. The measured characteristics could be properties like temperature, texture, shape, composition and different force components (shear and normal forces). A tactile sensor does not necessarily have to be limited to measure only one property.

Mostly, tactile sensing is a spatially distributed measurement to develop a 3D reconstruction of a surface or the shape and size of an object [45]. However, much of the literature describes devices that are applications based on localized sensing, which are for example mounted on a gripping surface of a robot end-effector or MIS gripper [46].

The field of tactile sensing started to develop in the 1970s, considerable effort in developing new transducer techniques have been undertaken from 1991 onward [47, 48]. The main reason was the great potential in robotics applications used in industrial automation. During the 1980s new transducer techniques were developed and a large number of new sensors and prototypes were built.

However, in order to completely imitate tactile sensing a few challenges such as multiple transducer effects (not only texture but also friction, force, temperature etcetera) needed to be addressed as well as how to measure certain physical quantities.

A decade later, a range of sensors has been developed who could detect the shape, size, presence, position of an object as well as the forces and temperature. The sensors could not yet detect surface texture, hardness or consistency [48]. Interesting to mention is that researchers in that time, such as Harmon [44], argued that the potential application for tactile sensing was in the field of robotics and unqualified for areas such as medicine or agriculture. Their primary reason was because of low return on investment and technical challenges.

The following points need to be taken into account when designing a tactile sensor [48]:

1 What parameters need to be measured and the corresponding range?

2 What is the spatial resolution and dimension of the sensing area, is this restricted by boundary conditions?

3 What is the sensor response to changing sensor stimulus (is it either stable or showing hysteresis)?

Common transducer techniques for tactile sensing are based on capacitive, piezoresistive, thermoresistive, inductive, piezoelectric, magnetic and optical methods [47].

2-1-1 MIS force sensing

In this section, the different catheter force sensing techniques are discussed and the advantages and disadvantages thereof. Eight different transducer techniques for force sensing in MIS can be distinguished, these include (note that the techniques require additional components, for example a resilient element when measuring displacement, the transducer technique names should therefore not be taken literally):

1. Displacement-based
2. Current-based
3. Pressure-based
4. Resistive-based
5. Capacitive-based
6. Piezoelectric-based
7. Optical-based sensing

In this research, a new force sensing technique is used which is introduced at the end of this section. The technique used in this research is based on the Hall effect and therefore magnetic-based. The theory of Hall effect sensors will be discussed in section 2-1-7.

Each of the force sensing techniques will be discussed separately based on the working principle and the most relevant literature, patents and commercially availability catheters. In general, the transducer technique requiring the least steps are the most accurate and reliable. The advantages and disadvantages of these force sensing principles are extensively studied in literature and will not be repeated [5, 16, 47].

2-1-2 Displacement-based sensing

Measuring the displacement of an elastic element, such as a spring, is the simplest method to conduct force sensing. This is known as the force-displacement relationship. The force can easily be calculated for a measured deflection, by multiplication with the spring stiffness, assuming that this is accurately known or verified by calibration.

A patent based on this principle is by Govari [49], the distal end of the tip is coupled to the catheter tube by a resilient member. A spring is used as resilient member, figure 2-1a, the spring deformation is measured based on a position change of the distal end with respect to the catheter tube. The position is determined based on the superposition of two magnetic field generators, one outside the body and the second in the distal tip. Note that with this technique, the position coordinates inside the human body can also be determined. A similar principle is patented by Clark et al. and given in figure 2-1b [50].

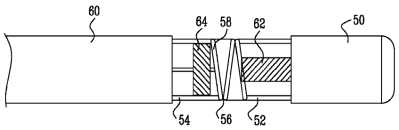

(a) Patent of catheter tip by Govari [49]

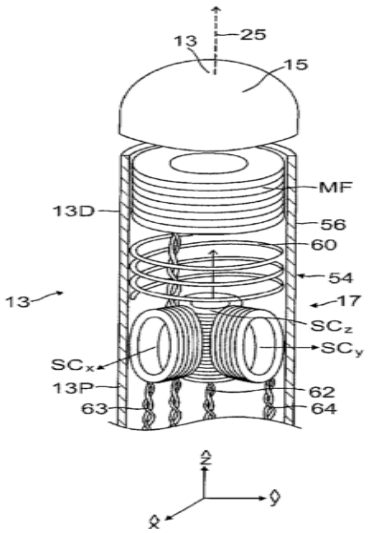

(b) Patent of catheter tip by Clark [50]

Figure 2-1: Two patents of displacement-based catheter tip force sensing

Pressure-based sensing

Pressure-based sensing makes use of a pressure sensor in an enclosed volume. The forces are detected because of an increase in pressure [51]. Tanomoto et al. have developed a force sensing catheter tip as small as 1.6 mm by using an IC pressure sensor by [52].

A second catheter based on this principle is shown in figure 2-2 [53], forces are detected on the distal end of the catheter tube. The semiconductor pressure chip in the tip is bend due to a pressure difference between a reference and measurement volume. The chip is equipped with distortion gauges, these are located on the substrate of the chip (numbers 6a, 6b). As silicon gel, indicated by number 37, functions as pressure transmitting medium from the tip to the chip, generating a change in electrical resistance value of the chip. The reference pressure

can either be atmospheric (relative pressure type) or an absolute pressure type in which the volume under the chip is enclosed.

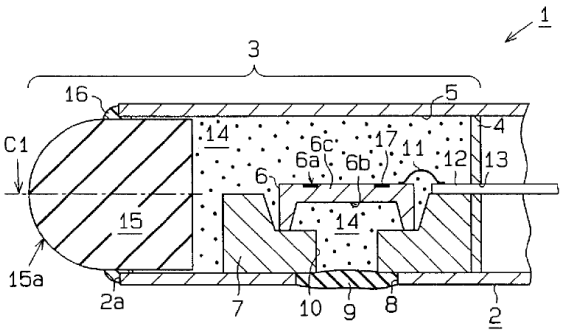

Figure 2-2: Patent of catheter tip by Iwata [53]

2-1-3 Piezoresistive based sensing

A very common force sensing measuring technique is resistive-based sensing by means of strain gauges. The underlying principle of resistive based sensing from a physical point of view is a change in electric resistivity in a metal or semiconductor when mechanical strain is applied. Some property of the voltage (or current) is fixed and a change in resistance is measured by a change in the current (or voltage). Strain gauges are mounted on flexible structures that either bend or are compressed. Therefore there is always a trade off needs to be made between structural stiffness and sensitivity of the measurement [54]. For increased stiffness, the sensitivity decreases however the manipulations as well as hysteresis effects decreases and vice versa. Hysteresis effects can be minimized by using a monolothic flexure; the flexure part is made out of one piece of material [55].

For two patents and one commercial available catheter force sensor, the measurement principal is based on strain gauges. In 2011, Selkee patented a mapping and ablation catheter with contact sensing capabilities based on strain gauge technology [56]. In the same year, another configuration for contact force sensing based on strain gauges has been patented by Govari, see figure 2-3a [57]. A plurality of strain gauges are mounted on the surface of an elastic tube located at the distal end of the catheter. Their configuration on the tube is such an optimal signal in response to deformation of the sensor tube is acquired, i.e. placed at different and respective locations in vertical and orthogonal direction.

A commercial available contact force ablation catheter, Thermocool, is based on the deflection of a precision spring measured by strain gauges has been FDA approved. The ablation is based on radiofrequency (RF) energy, the temperature is measured by a thermocouple or thermistor temperature, and has a total tip diameter of 3.5 mm [58], see figure 2-3b.

2-1-4 Piezoelectric based sensing

No literature or patents have been found for a contact force catheter based on piezoelectric sensing. There are however several MIS force sensors (for in laparoscopic grasper) based

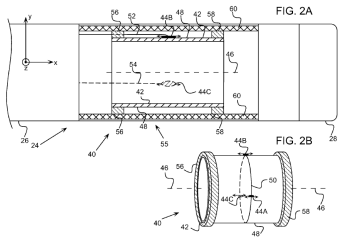

(a) Patent of catheter tip by Govari [57]

(b) Thermocool ablation catheter [59]

Figure 2-3: Strain gauge based sensing in catheter tip

on the piezoelectric effect, which is physically different than the piezoresistive effect. The piezoelectric effect, generates a voltage when a piezoelectric material is deformed due to polarization changes. Especially crystals and some ceramics can generate a voltage once the crystal structure is deformed.

A very common used piezoelectric material is polyvinylidene fluoride also known and referred to as PVDF or PVDF2, mostly used for the construction of thin sheet tactile sensors [60]. They need no external power source for sensing, and generated voltage is directly proportional to the applied force, pressure or strain. Moreover, they have a high sensitivity and are considered reliable resulting in a broad application range. Because of very good high-frequency response piezoelectric-based sensing is ideal for measuring vibrations.

The main drawback is that they are limited to dynamic force measurement and unable to measure static forces. This is caused by the fact that these materials have a large internal resistance. The developed charge decays with a time constant, this depends on the internal impedance and dielectric constant of the piezoelectric material [5].

2-1-5 Capacitive based sensing

Capacitive based sensing principles is recognized as being the most powerful detection for extremely small deflections of structures. Despite this fact, no literature or patents have been found on capacitive based force sensing in catheters. However capacitive tactile sensors are used in endoscopic tools, ground breaking research have been performed by Gray and Fearing. They have developed a consisting of an array of 8 by 8 cells of capacitive elements less than 1 mm^2 [61]. The array is covered with a thin protective silicon rubber, therefore the forces are spatially distributed and low-pass filtered at the same time. The forces, as small as millimeter newton, cause the thin membrane to deflect which change the capacitance in the sensing elements. Other examples of capacitive-based tactile sensors are given in an overview by Eltaib et al. [62]

2-1-6 Optical based sensing

Till now the most frequent implemented technique for force sensing is by making use of optics. Primarily because these sensors are compatible to use in MRI-environment. They are

having a high spatial resolution, and the influence of lower frequency electronics interference is low. However, they could be very rigid which is not beneficial for catheter purposes and the sensitivity could be decreased by dust or other light sources.

Optical sensors employ a light source, a transducer element (modulator) and an optical detector. The working principle is based on light modulation in proportion to the applied force. The light generated by the light source, like a LED or laser, travels through an optical fiber (transduction element, also called modulator), modulated and send back to an optical detector to be converted into an electrical signal [8]. The optical sensor can be intrinsic, extrinsic or more advanced and based on sensing the phase and spectrum of the light. The main difference is that for the extrinsic sensor the delivering optical fiber also receives the modulated light, in most cases the modulation of the light takes place outside the transducer element. For the intrinsic sensor the light modulation is inside the fiber itself, the conductivity changes when a force or pressure is applied.

An overview of fiber-optic force/pressure sensors for catheters are provided by Polygerinos et al. [8]. For most fiber-optic catheters, the force sensing principal is based on light intensity modulation. Because of the applied force, a reflective surface in the tip at a predefined distance is varied in distance and orientation with respect to the optical fibers [9, 15, 63, 64], see figure 2-4a. The same kind of principle can be applied with three optical fibers in a circular flexible structure [14].

A second principle of light modulation is in combination with a chromium half mirror [65]. A change in cavity volume causes a change in distance of the reflective surface with respect to the half mirror. Part of the light is transmitted through the mirror while the other part is directly reflected and is serving as a reference. The measure of deformation is reflected in the phase delay between the two signals.

Since 2014 a second catheter, Tacticath, has been approved by the FDA, this ablation contact force catheter is based on optics [66], see figure 2-4b.

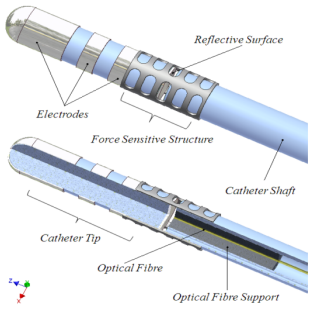

(a) Fiber optic force sensor [9]

(b) Tacticath contact force ablation catheter [67]

Figure 2-4: Two examples of optical based force sensing catheters

2-1-7 Magnetic-based force sensing

In this research, a Hall sensor in combination with permanent magnet and resilient structure will be used for force sensing, as discussed in chapter 1.
This principle has been used for in a tactile sensor by Ledermann et al. [68], however has not yet been implemented for catheter contact force sensing apart from prior studies in the research group.

A magnetic field (or change in magnetic field) can be measured by a voltage difference, so called 'Hall voltage', in the transverse direction of the current direction, see figure 2-5. Because of the Lorentz force experienced by the electron in a magnetic field, the electrons are therefore deflected to the side of the Hall plate building up a voltage. An electric field is created which counteracts the Lorentz force in approximately 10^{-14} s such that the current flows again in the original direction [69].

The Hall voltage increases for increased thickness of the Hall plate [70], and is inversely proportional to the number of charge carriers resulting in a much higher voltage for semiconductor materials.

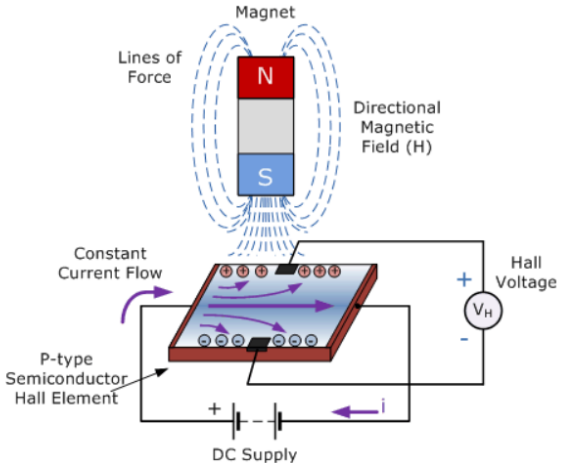

Figure 2-5: The Hall effect [71]

2-2 State-of-the-art in soft tissue characterization

Soft tissue characterization is performed by the surgeon to extract soft tissue mechanical properties as an indicator for tissue condition. Interest in techniques to obtain mechanical properties of materials is not very recent and constant development and research is pursued through history [72]. This section aims at summarizing the field of soft tissue characterization, in particular with respect to techniques and underlying theory to perform soft tissue stiffness determination. Two techniques are identified: resonance based stiffness sensing, see explanatory box 2, and load-displacement based stiffness sensing.

In this research, resonance based stiffness sensing will not be implemented for two reasons.

First of all because this technique does not provide an absolute stiffness value and requires rough approximation models and reference data acquired by testing on samples of known stiffness [73]. Secondly, the resonance frequency changes continuously in a fluid environment, since the blood flow creates a non constant pressure density [74]. Research shows overlap in tissue stiffness results for small differences in stiffness value and therefore it is suggested that this technique is always used in combination with other methods to increase the diagnostic power [75]. Therefore, soft tissue characterization is performed by indentation.

Indentation is a technique to obtain mechanical characteristics of samples by poking the tissue with known geometries while measuring the penetration depth and forces applied on the sample in real-time. Indentation can be defined as the probing depth into the tissue with respect to the tissue surface. Indentation of soft biological tissue (*ex vivo*) is a common method of assessing biomechanical properties [40], the stiffness value is the slope of the load-displacement curve. In section 2-2-1, the development of instrumented indentation is described. Section 2-2-2 discusses the indentation mechanics, which is the interaction between the indenter and sample material. The indentation of soft tissue and instruments are the topic of section 2-2-3.

Explanatory box 2: Resonance based stiffness sensing

Most resonance based sensor technology is based on bringing a small cantilever in resonance, this is also called dynamic stiffness sensing. The principle is based on a shift in resonance frequency [76, 77]. The sensor element consist of a piezoelectric cylindrical transducer made of a ceramic material, generally Lead Zirconate Titanate (PZT). The element is divided in a driving element and a second element is used for detection. An alternating voltage, close to the resonance frequency of PZT is applied, and a chance in resonance frequency can be measured when part of the device is pressed against the soft tissue surface.

There are two techniques for resonance based stiffness sensing, the first operation principle is based on the principle of contact compliance [78] and the phase shift method [79]. The change in resonance frequency between the loaded and the unloaded situation is given in equation (2-1) [80]

$$\Delta f_0 = \frac{1}{2\pi^2}\left(\frac{k_x}{Z_0}\right) \tag{2-1}$$

$$C_x = \frac{1}{2}\left(\frac{\pi}{S}\right)^{1/2}\frac{1-\nu^2}{E} \tag{2-2}$$

In this equation Z_0 is the equivalent impedance of the sensor and k_x is the stiffness. The stiffness is defined as $1/C_x$, which is called the surface compliance, and depends on S the surface contact area (πr^2, r is radius of the indenter) and v and E the Poisson ration and Young modulus respectively.

A second theory, approximates the system behavior by the theory of vibration modes in a finite rod. In this model, the change in resonance frequency is related to the acoustic impedance of the object.

Methods applied in acoustics use the concept of mechanical impedance. The impedance of a body is determined by applying a known alternating force F to a given surface area. The vibrating area, having velocity u, is measured such that the velocity amplitude and its phase lag are known relative to the exciting force [81]. The acoustic impedance of an object, Z, can be separated into an acoustic resistance α, which is the real part, and an imaginary part which is the acoustic reactance β.

$$Z = \frac{F}{u} = \alpha + j\beta \; with \; j = \sqrt{-1} \tag{2-3}$$

The change in fundamental resonance frequency for a rod with length l is defined as [82]:

$$\delta f_{PZT} = -\frac{V_0}{2\pi l}\frac{\beta}{Z_0} \tag{2-4}$$

In this equation Z_0 is the acoustic impedance of the sensor element and V_0 the sound velocity in the sensor element. The acoustic reactance contains information concerning the stiffness, it can be divided into a mass load part, m, and a surface compliance part C_x, equation 2-5, in which ω is the angular frequency.

$$\beta = \omega m_x - \frac{1}{\omega C_x} \tag{2-5}$$

The resistance nearly remains constant with frequency while it increases for an increase in indenter inversely until it passes through the zero line where it becomes a mass reactance. This means that it increases proportionally for increasing frequency [81]. The frequency at which the reactance is zero, also called the resonance point, is nearly inversely proportional to the indenter area. The mass load part, m_x, and the surface compliance, C_x are functions of the contact area S which is given in equation 2-6.

$$m_x = \frac{\rho S}{10(1-\nu)} S^{1/2} \tag{2-6}$$

$$C_x = \frac{1}{2}\left(\frac{\pi}{S}\right)^{1/2} \frac{1-\nu^2}{E} \tag{2-7}$$

In this equation, ρ is the density of the measured material, ν is the Poisson's ratio, E is the Young's modulus, S is the contact area defined as $S = \pi r^2$ in which r is the the diameter of the contact area, and not the diameter of the resonance tip. The relation between the geometry of the probe radius and the material constants of the object, in this case the soft tissue, determines whether the mass load or stiffness mode is dominant. This relationship can easily be studied by substituting S and expressing the stiffness as $k_x = 1/C_x$:

$$m_x = \frac{\rho \pi^{3/2}}{10(1-\nu^2)} r^3 \tag{2-8}$$

$$k_x = \frac{2E}{1-\nu^2} r \tag{2-9}$$

The radius of contact area is in the third power for the mass load and proportional to the stiffness of the tissue. The force of the hemisphere tip with radius r which is pressed against the object and the area of contact are related according to the following equation 2-10.

$$F = \frac{4}{3}(2\pi)^{3/2}) \cdot \frac{E}{1v - \nu^2} \cdot r \cdot S \tag{2-10}$$

For constant F, objects with high stiffness result in large E and small S and vice versa. Therefore, the resonance frequency of the sensor decreases for softer objects and increases for harder objects, this is implemented in β, see equation 2-4, 2-5. Through β the change in resonance frequency is dependent on the contact area between the tip and the tissue.

Among all the available resonance-curve-shift detection techniques (incl. vibration amplitude, gain detection method, open-loop resonance frequency, frequency-shift method based on PLL and resonance curve method) there have been sufficient signal-to-noise developed. However this was only applied for metals since the sensitivity was not adequate for soft bodies. The phase shift method has been developed, having a very high signal-to-noise ratio.

The shift in resonance frequency depends on [82]:

- Acoustic impedance of the object, Z;
- Contact area of tip with the sample;
- Frequency characteristic of the unloaded PZT-element;
- Frequency characteristics of the feedback circuit through the zero-phase condition which totally determines the oscillator frequency, this condition states that: the sum of the phase shifts around the feedback loop (feedback circuit and PZT-element) must be zero.

There is only one main sensor configuration, one vibrating element and one pickup element controlled by means of feedback of which the phase shift method is preferred.

2-2-1 Development of instrumented indentation

Instrumented indentation is the method where tissue (or samples in general) are indented with controlled force or displacement, the force applied on the sample and the indentation into the sample are monitored. Using well-established equations [83], mechanical properties (such as material Young's modulus) of materials can be determined based on load displacement data and elastic contact theory or inverse analysis in Finite Element software [84, 85]. This section presents a high level overview of theoretical development in the field of mechanical property determination by indentation.

The very first recognized theory for material indentation, and of major contribution to the field of indentation and material characterization, is the linear elastic contact theory between two spheres of Heinrich Hertz in 1880. At present, this theory is still widely used for contact analysis during spherical indentation [86]. The contact between indenter and sample determines the stress distribution in the material which is experienced by the indenter. Around 1900, the first standardized indentation based hardness test, better known as Brinell test, was development by which the imprint of indentation with a hard ball (of 1-10 mm) was measured with a microscope [87].

The Vickers hardness test, based on indentation of material with a diamond pyramid allowed for more consistent results. Mainly because of more precise indenter fabrication [72]. An important addition to the field of indentation has been made by Tabor in 1948. He concluded that the indent formed by the indenter has a larger radius of curvature than the actual indenter radius, see figure 2-7. He experimentally proved that a second indentation with similar load does not change the size or shape of the indent made by the previous indentation. Hereby concluding that the unloading process is purely elastic despite that the material undergoes elasto-plastic deformation. The contact problem was much later (1960) extended to viscoelastic bodies, based on Hertz theorem and use of Boltzman operators, which is relevant for soft tissue indentation since it exhibits viscoelastic behavior.

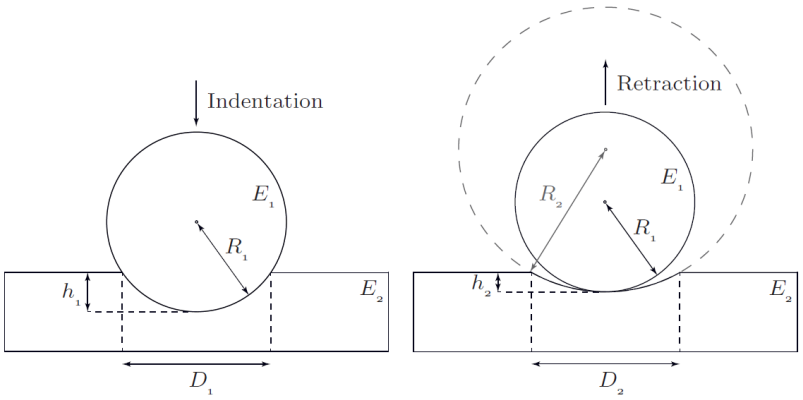

Figure 2-6: The indenter has a larger radius of curvature than the actual indenter radius [72]

A more advanced contact problem related to rigid conical indention in a semi-infinite half plane by Sneddon in 1948. He extended the solution to axisymmetric indentation in a semi-infinite half plane a few years later.

Calculation for the reduced Young's modulus to which is commonly referred to as the contact stiffness equation, proposed by Bulychev in 1975 based on the work of Tabor and Sneddon [88]. The stiffness is a function of the reduced modulus and of the projected area, however the accurate determination of of this area was impossible. The first complete contact stiffness equation has been described by Doerner and Nix in 1986 since they assumed the change in contact area to be small such that the indenter can be treated as a flat punch [89]. Finally, Oliver and Pharr contributed a great deal to the field of indentation, leading to a standardized model for mechanical property extraction of load-displacement data, with the following three findings [83, 90]:

1. The contact stiffness equation of Bulychev is valid for any axisymmetric indenter;
2. Proposed power laws for the first part of the unloading curve instead of the linear fitting curve defined by Doerner and Nix;
3. Renewed area functions to improve the determination of the projected area.

Note that the solutions are under the assumption that the indenter has an ideal geometry, indenting an infinite half-space specimen limited to small deformation such that linear elasticity holds.

2-2-2 Indentation mechanics

Important for the indentation mechanics are the contact problem, this describes the interaction between the indenter and the sample subjected to indentation. Furthermore, the indentation models developed by Doerner and Nix as well as Oliver and Pharr are briefly discussed, by which material Young's modulus based on load-displacement data can be determined.

Contact theory
Contact theory describes the interaction between the touching interface of two bodies with a model based on assumptions. Two contact theories are shortly discussed, first of all the Hertzian contact and subsequently the contact theory for viscoelastic bodies.

Hertzian contact
The elastic contact theory by Hertz describes the shape of the contact area, the corresponding magnitude and distribution of surface forces as well as the stress in both bodies and components of deformation.

For any point on the surface profiles of two bodies in the vicinity of contact, see figure 2-7, the separation the points can be expressed as

$$h_{initial} = z_1 - z_2 \tag{2-11}$$

To express this equation in terms of the geometry of the two bodies, the surfaces are considered smooth (disregard surface irregularities) and the surfaces at the origin can be seen as ellipses functions in the first assumption of Hertz. The terms A_1, A_2, B_1, B_2 can be expressed as the radius of curvature, this results in

$$h_{initial} = z_1 - z_2 = Ax^2 + By^2 \tag{2-12}$$

$$= \frac{1}{2}\left(\frac{1}{R_1} + \frac{1}{R_2}\right)(x^2 + y^2) = \frac{1}{2R}r^2 \tag{2-13}$$

For the deformed situation, the separation between the same two points is smaller because the bodies displace collinear towards each other. The initiated contact pressure between the surfaces, causes local elastic deformation of the contact surface, shifting the actual surface

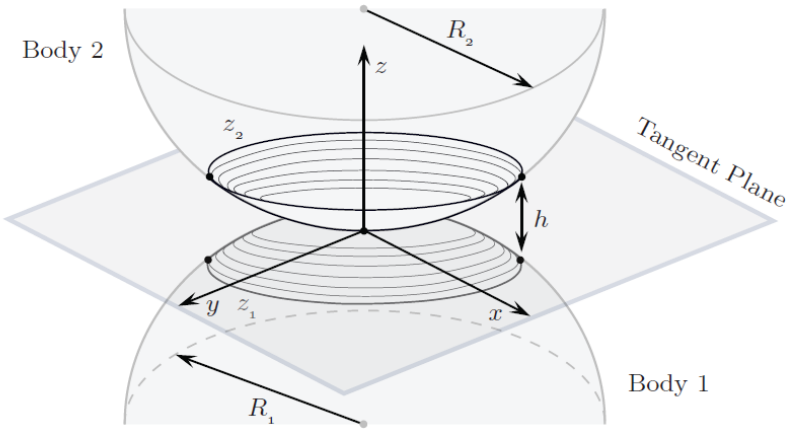

Figure 2-7: Surface profiles in the vicinity of contact [72]

points parallel to the z-axis. Assuming these points do not change in any other spatial direction than the z-axis, the equation for the separation between the two bodies is given by

$$h_{contact} = h_{initial} - \delta + u_z \tag{2-14}$$

$$= \frac{1}{2}\left(\frac{1}{R_1} + \frac{1}{R_2}\right)(x^2 + y^2) - (\delta_1 + \delta_2) + (u_{z1} + u_{z2}) \tag{2-15}$$

In which δ is the vertical displacement and u_z the elastic displacement, which equals $(u_{z1} + u_{z2}) = \delta - h_{initial}$ in the contact zone and $(u_{z1} + u_{z2}) < \delta - h_{initial}$ outside the contact area.

The pressure distribution for the contact region proposed by Hertz, figure 2-8.

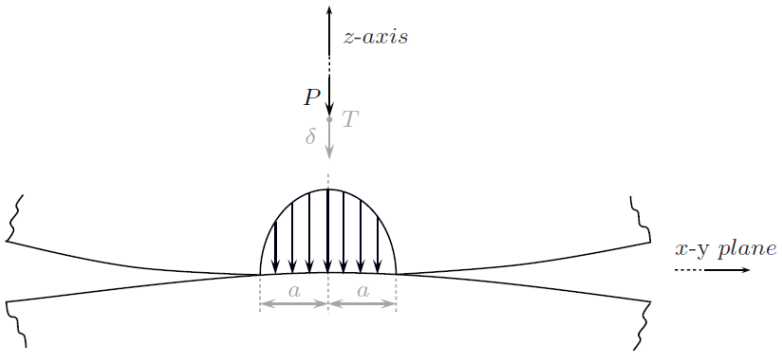

Figure 2-8: Pressure distribution introduced by Hertz and described by Johnson [72]

Hertzian contact extended for viscoelastic materials
In 1960, the Hertzian contact theory has been extended by Lee and Rabok [91] for viscoelastic material properties. The model assumptions of Hertz are maintained, small strain elastic deformations theory is used to extend the model. Note that the model is only valid for small deformation. Moreover, material and geometric nonlinearities are not accounted for in the solution. The small strain elastic deformation for spherical indentation of viscoelastic bodies can be described by

$$\frac{4\sqrt{R}}{3}h^{3/2} = \frac{1-v^2}{E}P \tag{2-16}$$

The relationship between the force and displacement is non-linear, which is expected for viscoelastic behavior to account for the increase in strain during constant applied stress. The elastic constant $(3/2E)$ in equation2-16 can be replaced by a linear viscoelastic integral operator which depends on the material Poisson's ratio [91], the equation is given by

$$\frac{4\sqrt{R}}{3}h^{3/2} = \int_0^t J_{AS}(t-u)\frac{dP}{du}du \tag{2-17}$$

The creep compliance function is described by $J_{AS}(t)$, and u is the variable of integration.

Indentation analysis
The analysis model of force-displacement data, obtained during indentation, to extract elastic property are well-described by Oliver and Pharr [83, 90]. Their work is an improvement on the analysis method proposed by Doerner and Nix, which on their turn based the stiffness equations established by Bulychev. These three models will be described in historical order.

Contact Stiffness Equations (Bulychev)
In 1975, a simple experimental method for extracting elastic properties of material form load-displacement data has been proposed by Bulychev [88]. This method is based on experimental measurement of the upper part of the unloading curve, see figure 2-9, given by equation

$$S = \frac{dP}{dh} = \frac{2}{\sqrt{\pi}}E_r\sqrt{A} \tag{2-18}$$

In this equation the stiffness $S = d\mathrm{P}/dh$ is a function of the projected area of elastic contact A and reduced Young's modulus (E_r) defined in [92]. The projected area is optically measured and assumed to equal the contact area at maximum indentation depth for conical, spherical and cylindrical indenters. Technical limitations in contact area determination, as well as approximation by assuming an equal are for maximum depth and the projection after indentation [90].

Contact Area function (Doerner and Nix)
The contact stiffness equation requires the accurate determination of the contact area of indentation, Doerner and Nix extended this equation by proposing [89]:

1. The early phase of the unloading curve behaves like a flat cylindrical punch and therefore the curve can be assumed linear;
2. The projected contact area, necessary in the contact stiffness equation, can be expressed as a function of contact depth (h_c).

$$A = f(h_c) \tag{2-19}$$

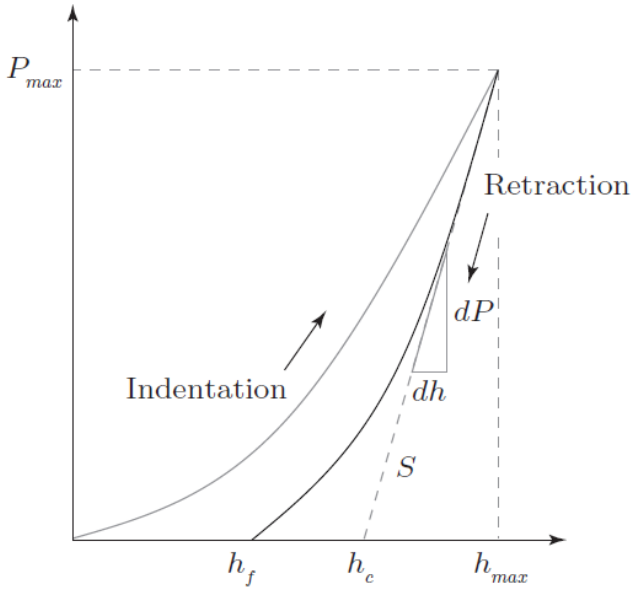

Figure 2-9: Experimental determination of elastic properties from retraction, further extended by Doerner & Nix and Oliver & Pharr [72]

$$h_f = h_i - d_s \tag{2-20}$$

The contact depth is defined as the distance over which contact is made, see figure 2-10.

Oliver and Pharr model
Oliver and Pharr observed that the initial part of the unloading curve, as assumed by Doerner and Nix to be linear, would far better be described by a power law function to account for changes in the contact area during unloading

$$P = \alpha h^m \tag{2-21}$$

In this equation, P is the indentation force, h the elastic displacement and α, m constants related to the indenter tip geometry which are between 1.2-1.6 [83]. The contact stiffness of is defined as the slope at maximum load.

Furthermore, a new area function has been defined to better describe the projected area and has been defines as

$$h_c = h_f - \lambda \frac{P_{max}}{S} \tag{2-22}$$

The depth of the indent as indicated in figure 2-9 is h_f, the factor λ is a constant dependent on indenter geometry. This value equals 1 for a flat punch, 0.75 for spherical shape or 0.72 for a conical geometry [83]. Both of these new relations are used in in the contact stiffness function, note that the contact still needs to be purely elastic and the tip geometry is ideal.

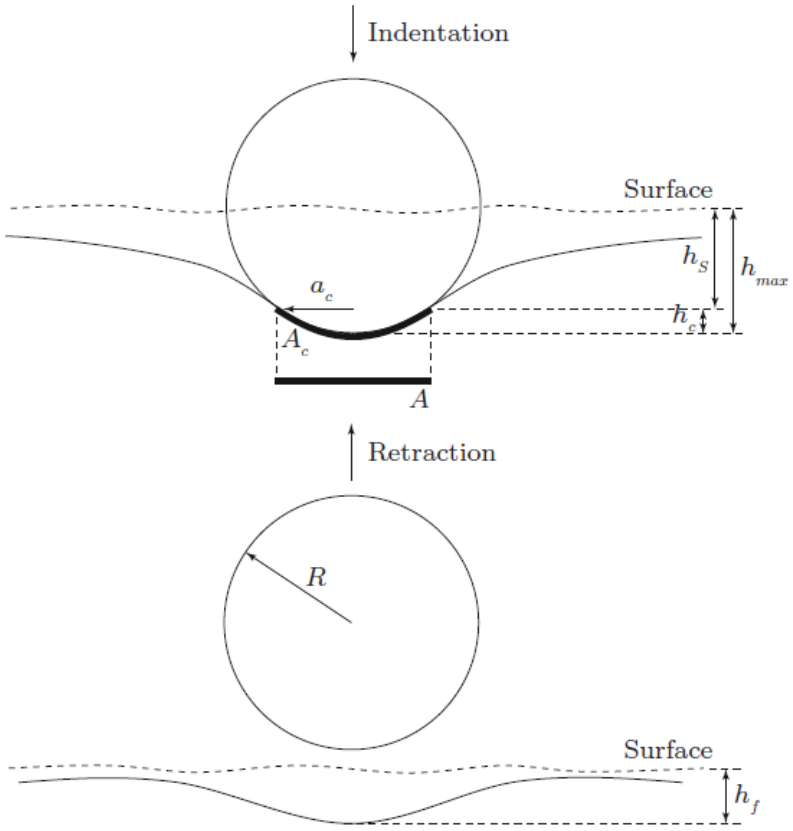

Figure 2-10: Representation of area of contact and related contact depth [72]

The best choice for indenter geometry depends partly on the indented material, and is of relevance to minimize pile up or sink in around the indenter tip [93]. For static indentation, the soft tissue is slowly indented until the indenter allows no more displacement, this could be performed at a certain rate (mm/s) in order to characterize a force-displacement curve [84].

2-2-3 Overview of soft tissue indentation devices

Biological tissue is linearly elastic for small deformations [94], and becomes non-linear for larger deformations. This is caused by a non-linear increase in force during increased indentation, therefore a number of non-linear tissue modeling models have been proposed [94, 95]. The nonlinearity occurs due both the inherent nonlinearity of the tissue stiffness as well as the possible tissue geometry. Relevant literature on biomechanical properties, most obtained by *ex vivo* indentation, are given by Ahn et al. [95], insights for soft material indentation are described by Zhang [96].

Instrumented indentation has been shown over the past 10 years to be a promising potential technique for soft tissue characterization [72]. In 1992, Bicchi et al. addressed the challenges related to MIS and the need for soft tissue stiffness measurement. He proposed a device based on a commercial which has been modified into a prototype by which forces are measured with

strain gauges and the position has been sensed optically [1].

A device for *in vivo* cartilage stiffness sensing, the instrument is inserted through a trocar into the knee. The reference plate of the instrument is adjusted by means of video feedback and pressed longitudinal against the examined surface with a constant force [97]. The deflection of a suspended beam is measured with strain gauges.

Ottensmeyer developed an *in vivo* indentation device based on an LVDT force sensor and a voice coil linear actuator [98]. The force and displacement resolutions are respectively $\pm 70mN$ and $\pm 0.2\mu m$, with a force range up to 0.3 N. A second tool for *ex vivo* load-displacement data generation has been described by Carter et al. [99]. The soft tissue is indented by a manual winding mechanism in the probe and the force is measured with a load-cell.

A hand-held device for *ex vivo* use on skin has been proposed by Arokoski et al. in 2005 [100] and consists of a indenter connected to a load cell measuring up to 98.2 N.
In the same year, an indenter for laparoscopic MIS has been developed by Samur et al. [101] consisting of a force-torque transducer (Nano 17 from ATI industrial Automation) with a force range of $\pm 50N$ in x, y direction and $\pm 70N$ in z-direction. Controlled indentation is performed by making use of a haptic device.

Finally, the hand-held soft tissue indentation device by Iivarinen et al in 2014, consists of two coaxial load cells [102]. The first to measure the force of the reference plate and the second load cell is used to measure the indenter force, which are in summed to obtain the total indenter force. The indenter has a fixed part that sticks out with respect to the reference plate.

All of above mentioned devices are very rigid or only for *ex vivo* usage, no device for stiffness sensing by means of a catheter has been proposed.

2-3 Conclusion

In this chapter, the state-of-the-art in catheter force and the development and techniques for soft tissue stiffness sensing have been discussed. Catheter force sensing can be performed by six different transducer techniques, optical based sensing has been implemented most frequent thus far. In this research a new force sensing technique based on the Hall effect will be implemented in a catheter tip.

The measurement of soft tissue stiffness can be performed based on a change in resonance frequency or by tissue indention. The last technique will be used in this research, whereby the penetration depth and forces applied on the sample are measured in real-time. Major contributions in the field of material indentation have been made by Doerner and Nix, and Oliver and Pharr. In the last 10 years, several instruments for soft tissue stiffness measurement have been proposed *ex vivo* as well as *in vivo*. However, stiffness sensing by using a catheter device in MIS has not been succesfully researched yet.

Chapter 3

Design methodology

This chapter discusses the implemented design methodology to effectively address the research objective and systematically evaluate high-level concept designs for force sensing and soft tissue indentation. The design methodology consists of several subsequent steps, chronologically discussed in this chapter. Section 3-1 elaborates on the research objective, stated in the introduction, thereby pointing out challenges for the design. Subsequently, section 3-2 provides an outline of the design requirements and design considerations. Based on these two sections, the design methodology resulting in the high-level measurement concepts on combined force and stiffness sensing are presented and discussed in section 3-3. Finally, section 3-4 concludes the chapter with a short summary.

3-1 Measurement goal

The first step towards effective concept design, is the accurate and explicit formulation of the combined force and indentation-depth measurement problem and associated challenges. The primary reason for defining a measurement goal and description is to address the requirements and challenges and to gain an understanding of and insight in the required measurement working principal. Moreover, appropriate assumptions have to be made to simplify the measurement problem in order to enhance the design process.

The research objective, specified in chapter 1 and repeated below, addresses on a high-level the requirements as well as the challenges.

Develop an accurate and robust micro-scale catheter tip prototype for combined stiffness and force sensing of soft biological heart tissue during minimally invasive surgery by making use of a 3D magnetic Hall sensor and micro-indentation technique.

In the research objective, two interlinked measurement elements can be identified. These are the technical aspects of the combined force and stiffness measurement and the implications because of the *in vivo* conditions during MIS. For the purpose of clarification, these topics will be treated separately. At the end of the section the interdependencies and associated interactions are discussed.

The second interlinked component is related to the environmental nature in which the measurement is conducted, there are some challenges because of the *in vivo* conditions. These could possibly impact and distort the measurement itself as well as impose additional challenges on the design criteria because of regulation and safety requirements. These influences will be discussed in the next section 3-2.

3-1-1 Technical aspects

The technical aspects involve the requirements for the combined force and indentation-depth measurement with the catheter tip, to obtain the material's load-displacement curve for stiffness determination. The state-of-the-art in force sensing catheters provides several transducer techniques. This research introduces a new force sensing transducer technique based on the Hall effect. General Hall effect sensor theory has been explained in section 2-1-7. The working principle of how this is implemented for catheter tip force sensing will be explained next.

A change in magnetic field intensity is caused by the changing distance between the permanent magnet and the Hall sensor. One of the two components needs to be fixed, while the second component can move freely and is attached to a flexible element (for example a membrane or flexure mechanism), see figure 3-1. The force applied on the tissue by the catheter tip, correlates directly to the force on the catheter force-sensing mechanism. The force can be determined by means of calibration or can be calculated based on the measured displacement and known flexure stiffness. The range and sensitivity of the force-sensing system will be quantified in section 3-2.

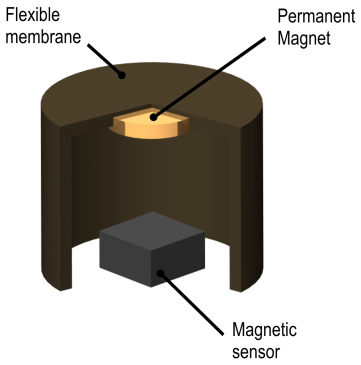

Figure 3-1: Example of possible configuration by which the permanent magnet is fixed on a membrane with respect to the magnetic Hall sensor (at the bottom in figure)

The state-of-the-art in (soft tissue) stiffness measurement, as far as data is available on tissue measurement in specific, shows that the measurement requires force and tissue indentation. In this thesis, indentation is defined as the 'probing' depth in soft tissue with respect to a fixed reference at the soft tissue surface, producing a force-displacement response. This response can be used to estimate the effective shear, hardness or elastic modulus by using linear elastic contact theory and small indentation assumption, further discussed in section 2-2-2 [101]. According to the studied literature discussed in section 2-2, soft tissue stiffness is best characterized by the last part of the unloading curve in the load displacement curve [83].

3-1-2 *In vivo* measurement conditions

Prior to defining the design requirements, it is important to gain an understanding of the aspects and inflicted disturbances on the force and stiffness measurement, associated with the *in vivo* conditions. The most relevant factors are discussed in this section. Medical concepts are described more extensively, to provide a basic explanation of these non-engineering topics.

- **Geometrical complexity of measurement site**: To reach the distant location of operation in MIS, catheters can only be pushed through the vascular system for approximately $100 - 110$ cm [103], resulting in contradictory design requirements. On the one hand, the catheter needs to be stiff to assure optimal force transmission between the externally applied force by physician or robot. On the other hand, the MIS environment requires a flexible catheter to allow for bending to trail the internal histology (see Explanatory Box 1). Several commercially available MIS heart catheters, without incorporated force sensing, are addressing this requirement. In these catheters, the shaft is bent with guide wires [104] or the shaft consists contains an active bending structure [105]. Because these solutions already exist, this requirement will not be considered in depth in this research.
  Furthermore, current measurement set-ups rely on remote signaling techniques, consisting of an ex vivo signal processor connected to the catheter tip. The distance between the site of measurement and processing leads to signal degradation. However, in the context of this work, this error is considered as a constant, which has been accounted for by calibration measurements.

Explanatory Box 1: Introduction to histology and the vascular system
The aim of this explanatory box is to give a high-level overview of the anatomy and histology of the vascular system:

The human heart consists of four chambers, two upper smaller chambers (right and left atrium) and two larger lower chambers (right and left ventricle), see the figure below. The heart wall in between the left and right atria and ventricles is called the interventricular septum, which can transfer loads from one chamber to another. This is useful during filling of the heart chambers since an increase in volume of the right chambers, due to inflow of blood, automatically reduces the volume in the left chambers causing outflow of blood. Between the chambers, valves assure that blood flows one directional and these increase support heart functionality in pumping blood through the body. The interior surface of the heart is characterized by many trabeculae, which are muscular ridges as shown in the figure below.

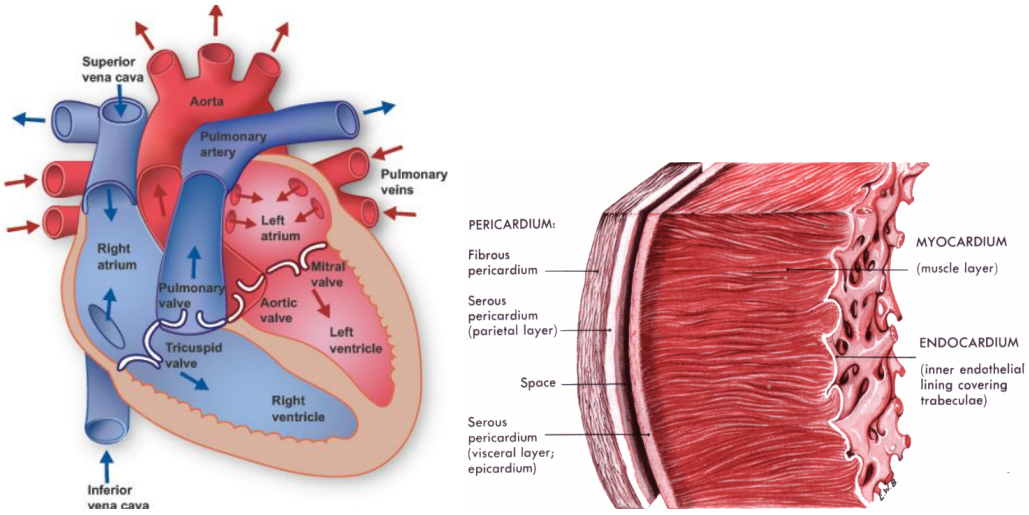

The heart walls are the most important structure for the pumping mechanism of the heart [106]. The ventricles are thick-walled 3D pressure vessels; their curvature and thickness varies locally and temporally. The heart wall consists of three distinct layers: the outer layer called the epicardium, the middle layer called the myocardium and the inner layer called the endocardium. The three layers differ in composition and thickness, which determines the mechanical properties of the tissue.

The endocardium covers up all the chambers on the inside and is a serous membrane consisting primarily of 2D plexus of collagen and elastin. A serous membrane is a membrane consisting of two layers of epithelial cells with a benign, transparent or yellow body fluid in between. Furthermore, one single layer of endothelial cells being in direct contact with the blood serves as interface between the blood and heart wall.

The middle layer is the actual functional layer which allows for the heart contraction to pump blood. The myocardium consists of mainly myocytes (arranged in locally parallel muscle fibres) and fibroblast. These fibres are embedded in an extracellular matrix which is built up of collagen I (75-85%) and III (10-20%), which are the most abundant proteins in the body and are synthesized by fibroblast. The collagen are only a few percent of the myocardian's dry weight in comparison to the myocytes, which account for 90% of the dry weight. The collagen fibre renders anisotropic mechanical properties and has many functions in the myocardium. These range from protecting the myocytes against excessive stressing, to actively transferring the generated force throughout the tissue. Because of these two functions, the passive stiffness of the heart is important for the overall heart functioning.
Lastly, the outer layer, the epicardium is as thin as the endocardium and also serous in nature.

- **Heart rhythm contraction**: The constant contraction of the heart chambers alters the curvature of the heart walls on which measurements are performed. Additionally, the contraction translates and rotates the measurement site. When aiming at describing this motion and deformation of the heart, the evolution of the deformation needs to be

tracked over time using either a Lagrangian or Euler description [107]. The Langrangian description uses a fixed reference coordinate system to describe motion while Euler describes motion through spatial coordinates corresponding to the current configuration. To define a deformation gradient using the Lagrangian description, a relation between the reference (K) at a fixed point and current (k) state, see figure 3-2, are expressed by the function h as follows [107]:

$$\bar{x} = h(\bar{X}, t) \quad ; \bar{x} = (x_1, x_2, x_3)^T \quad \bar{X} = (X_1, X_2, X_3)^T \tag{3-1}$$

In this equation, $\bar{x}$ is the position vector of a particle in the current configuration and $\bar{X}$ is the position vector in the reference configuration. The deformation gradient is subsequently defined as

$$\bar{\bar{A}} = \frac{d\bar{x}}{d\bar{X}} = \begin{bmatrix} \frac{\partial x_1}{\partial X_1} & \frac{\partial x_1}{\partial X_2} & \frac{\partial x_1}{\partial X_3} \\ \frac{\partial x_2}{\partial X_1} & \frac{\partial x_2}{\partial X_2} & \frac{\partial x_2}{\partial X_3} \\ \frac{\partial x_3}{\partial X_1} & \frac{\partial x_3}{\partial X_2} & \frac{\partial x_3}{\partial X_3} \end{bmatrix} \tag{3-2}$$

The deformation tensor for change in heart wall curvature and spatial location is very difficult to measure, and therefore difficult to simulate and to account for as input for the design.

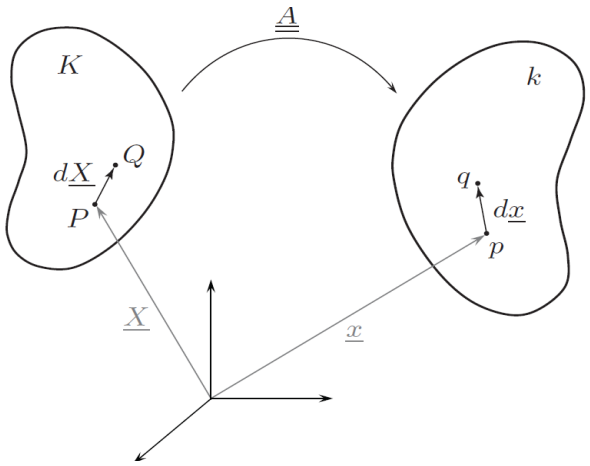

Figure 3-2: Langrangian description of undeformed ($d\bar{X}$) and deformed configuration ($d\bar{x}$) [72, 107]

- **Blood pulsation**: During *in vivo* surgery and examination, tools are constantly surrounded by blood and exposed to pulsation of the blood in the veins. To avoid influence of blood on the measurement system, preventing for example blood clotting on the flexure or the short circuiting of electronics, a hermetical sealing should be implemented to avoid blood entering the catheter. Note that this sealing, for example a thin membrane, will influence the designed measurement system in two ways. The membrane could change the stiffness of the total system when covering the flexure, since it provides a counteracting force on the flexure. Furthermore, the sealing introduces a pressure difference between the *in vivo* environment and the measurement system resulting in incorrect forces on the flexure mechanism and therefore systematic measurement errors. Moreover, depending on the catheter tip and shaft orientation with respect to the flow

direction, the pulsating blood can produce a small impulse on the catheter shaft or tip. This influence can be neutralized by superimposed external forces, for example a magnetic guidance field by which the tip is constantly aligned with the applied field direction. These forces on the tip are dominant over the impulse and thereby canceling the influence. Another option could be to temporarily fixate the catheter *in vivo*, for example by expansion of a balloon in vessels. The downside of this is an increased risk of internal damage.

- **Body temperature**: The difference between room and body temperature is approximately 12 °C on average, under the assumption that temperature values are 25 °C and 37 °C respectively. This change in ambient temperature can impact the measurement because of calibration errors or increased probability of temperature-induced offset and offset drift of the Hall sensor. Both of these aspects will be explained briefly.
  The sensor will initially be calibrated outside the body (at room temperature), creating a temperature offset in relation to a potential *in vivo* measurement location (*in vivo* measurements are not performed in this research). Temperature rise can cause an increase in electron mobility of the signal over the full cable length from tip to external signal processing. This phenomenon evolves in time since heat conduction through the wall requires an incubation time. However, the temperature difference is too small and the catheter tube material has a low thermal conductivity (for PTFE $0.25 W/m \cdot K$ [108]), such that heat conduction through the walls is limited and this influence therefore can be neglected.
  Besides this, temperature offset and offset drift increase for increasing temperature [109]. Depending on the Hall cell configuration (45 °, XL, Basic or with Narrow conactss) temperature offset drift changes. For a basic Hall cell geometry, the average offset drift is $0.409 \mu T/°C$. In practice, the temperature difference is too small for causing errors in the measurement data.

- **Biomechanics and constitutive equations of soft tissue**: Soft tissue response to externally induced deformation and indentation is very hard to model or describe with constitutive equations because of its non-linear, anisotropic and viscous behavior, which moreover varies per location and per individual [110]. However to determine the best measurement method to obtain tissue mechanical properties, a solid understanding of soft tissue response to externally induced deformation and indentation is desired. In the last twenty years, much research has been devoted to the development of soft biological tissue models (see explanatory box 2), in the emerging field of biomechanics. So far, no single model (FEM or constitutive equations) exactly describes or predicts soft tissue behavior. However there is an overall consensus that soft tissue mechanical properties can be modeled by the coupling of springs and dampers [111]. Soft tissue is modeled as in figure 3-3 and for example viscoelasticity can be described with the Kelvin, Maxwell or Voigt models, see explanatory box 2.

Explanatory Box 2: Biomechanics of soft biological tissue

Knowledge of indentation and biomechanics of soft tissue are important for the catheter design, since these provide insight in the mechanical properties of soft tissue which need

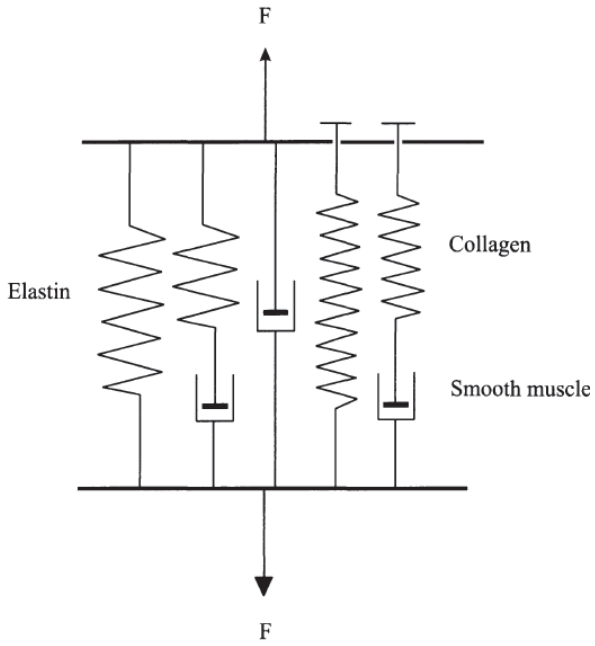

Figure 3-3: Model for soft biological tissue [111]

to be measured. The first paragraph, describes the research field of biomechanics, and its relevance and main challenges. In the second paragraph, the mechanical properties of soft biological tissue will be elaborated on.

Background of biomechanics
The research field of biomechanics, and in specific biomechanics of soft tissue, was not very clear and active until the mid 1960s. It can be argued that the origin of biomechanics could even be mechanics itself [110]. For example, Galileo Galilei (1564 - 1642) was interested in the strength of bones and suggested these are hollow to optimize the strength with minimum weight.
Scientific achievements in history which have led to the development of biomechanics are [110]:

- The development of a theory to describe nonlinear mechanical behavior:
  Soft biological tissue exhibits inherently nonlinear mechanical behaviour over finite strains requiring new frameworks such as finite elasticity, viscoelasticity and mixture models;
- Advances in computer technology:
  Computers are essential for controlling experiments, performing simulations to test hypotheses and solving complex boundary and initial value problems;
- Development of the finite element method (FEM):
  Introduced in 1956, based on mathematical advances which developed significantly throughout the 1960s, where Oden (1972) published a nonlinear finite-element method suitable for tissue mechanics [112];

- Enormous increase in the motivation to perform research in this field:
  During the exploration of the moon in the 1960s, investigation into the possible effects of mechanical loads on the human body received significant interest.

Analyzing the mechanical response of soft tissue contributes to the understanding of human health as well as of disease, rehabilitation, injury and clinical treatment. In particular, biomechanics is of importance for clinical intervention. The understanding on physiology, cell biology, physical models and the solutions to boundary and initial value problems are of great influence. Therefore, biomechanics is not limited to the 'mechanics applied to biology' [113] but rather needs to be defined as a development, extension and application of mechanics. The main purpose is to gain a better understanding of physiology and pathophysiology as well as to diagnose and provide treatment in cases of disease or injury.

The proteins, cells and tissues in the human body reveal incredible diversity in structure and properties, reflected in the variety of possible functions. Learning more about the characteristics of living materials requires a broader view on mathematical models and even in some cases basic postulates and concepts in mechanics [110].

Continuum biomechanics
In 1847, M.G. Wertheim concluded that soft tissue, including veins and arteries, does not obey Hooke's law based on force-elongation data [114]. Hooke's law describes a linear relation between Cauchy stress and linearized measures of strain, and therefore does not support large nonlinear deformation in soft tissue. In 1880, C.S. Roy drew a similar conclusion and observed anisotropic response and viscoelastic behaviour in arteries. Furthermore, he showed that material properties in arterial walls differ with radial location and point in the vascular tree, which can be additionally be changed by age, disease, exercise and time post-mortem [115].

The constitutive equations are used to describe the response of a material to an applied load, based on the internal constitution. To quantify the response, relations based on histology and mechanical properties of the components need to be developed by means of close examination. However, since these structures are incredibly complex, and therefore require approximations of the underlying structure and phenomenological descriptions. Therefore, these relations are focused on specific problems and do not comprehensively describe material behavior [110].

At present, there are three main areas of study within continuum biomechanics: i) identification of fundamental concepts, postulates and principles, ii) formulation of constitutive equations that describe material behavior and iii) solutions of initial-boundary-value problems.

Mechanical properties of soft tissue
The mechanics of a material in response to an applied load depends upon the internal constitution, i.e. the interconnections, orientations and distribution of microstructural components. Despite differences between the many forms of soft biological tissue, the basic constituents are the extracellular matrix and cells. The latter is the fundamental structural and functional unit of tissues and organs. The extracellular matrix mainly

consists of proteins and has many functions, mainly providing strength and resilience to the tissue and maintaining its shape.

Biological tissues can roughly be divided in hard tissues which contain minerals such as bone and teeth, and soft tissues like skin, muscle and blood vessels. The mechanical properties, such as Young's modulus, are different between hard and soft tissue. For soft biological tissue, theories for infinitesimal deformations (e.g. used for metals) do not apply. Instead, finite (large) deformation theories are used to describe the mechanics of soft tissue. Understanding the mechanical properties of soft biological tissue is fundamental for biomechanics and the extraction of useful mechanical properties such as Young's modulus.

The mathematical framework to describe the mechanical behavior of biological soft tissue can be approximated by the one used for rubber elasticity since they both exhibit elastomers which are long-chained, cross-linked polymeric structures [116]. However, there are significant differences in the structure as well as the response to applied stress. In the figure below, a stress-stretch response is shown to compare the response of rubber (left) and soft tissue (right) [117]. The main discrepancies in characteristics are that rubber-like materials exhibit isotropy with respect to the natural unloaded configuration. This is in contradiction with soft tissue, which is anisotropic.

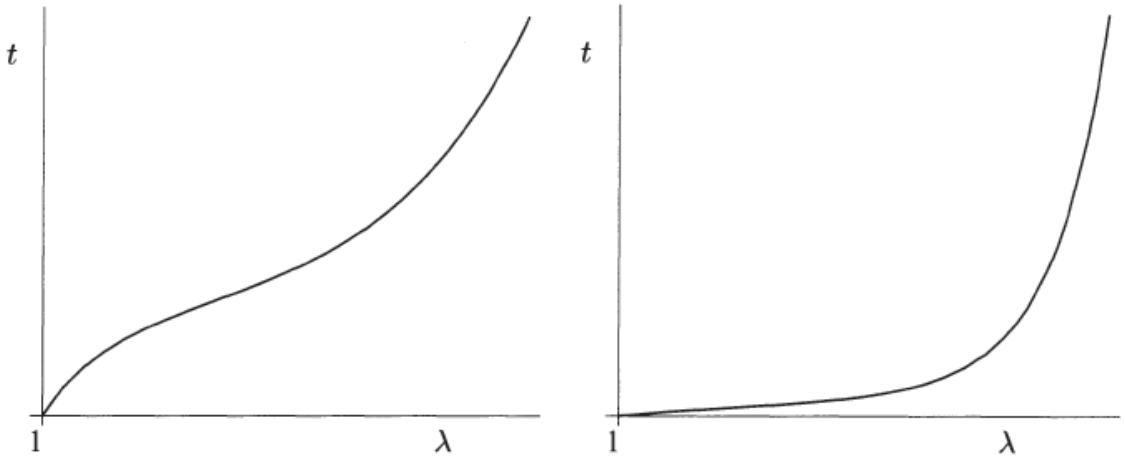

The initial large extension, which can be achieved for relatively low stress levels, followed by the stiffening at higher extension levels, is a very important characteristic. This is caused by the collagen fibres, which first unfold to reach their natural length, after which their stiffness overrides that of the underlying matrix material [117]. The distribution of collagen fibers causes the anisotropy in the material which is one of the key differences with (isotropic) rubber. Several properties unique for soft tissue can be distinguished [111]:

1. *Inhomogeneous structure*: Biological soft tissue consists of cells and intermediate substances which have different physical and chemical properties and the contents differ from point to point.

2. *Nonlinear deformation*: Each of the soft tissue components exhibits nonlinear mechanical properties as well as non-linearities in geometry. The nonlinearity is enhanced by the

assembly of the individual components and behaves at high tension like collagen while for low tension the behavior is similar to collagen, see figure below.

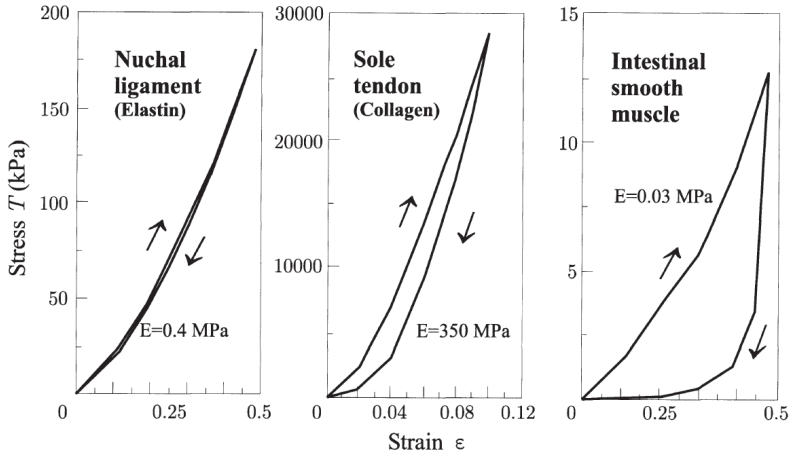

3. *Anisotropy*: Elastin and Collagen are long-chained polymers, these are intrinsically anisotropic. Additionally, the orientation in tissue depends on the functionality, which further adds to the anisotropy. This implies that the mechanical properties differ for soft tissue since elastin and collagen are the building blocks.

4. *Strain rate intensity*: Different strain rates (speed by which the material is tested) result in different mechanical properties of the tissue because of the viscoelastic behavior. Higher strains are characterized by higher stresses. However, these are not very large in soft biological tissue.

5. *Incompressibility*: Most of the soft biological tissue consists of 70% water. This is the main reason that soft tissue hardly changes in volume. Being isochoric, even when load is applied they are almost incompressible [118]. The incompressibility characteristic of soft tissue is very important for the formulation of constitutive equations since the sum of all principal strain is always zero.

6. *Viscoelasticity*: Viscoelastic materials are characterized by hysteresis. They show both 'viscous' (fluid-like) and 'elastic' (solid-like) behaviour. Therefore, according for *in vivo* testing of mechanical properties, the measurement site needs to be pre-conditioned by applying appropriate force and deformation several times before actual measurement [119]. Typical models which are often used to represent viscous behavior are the Maxwell, Voigt and Kelvin model, given respectively in the figure below [111].

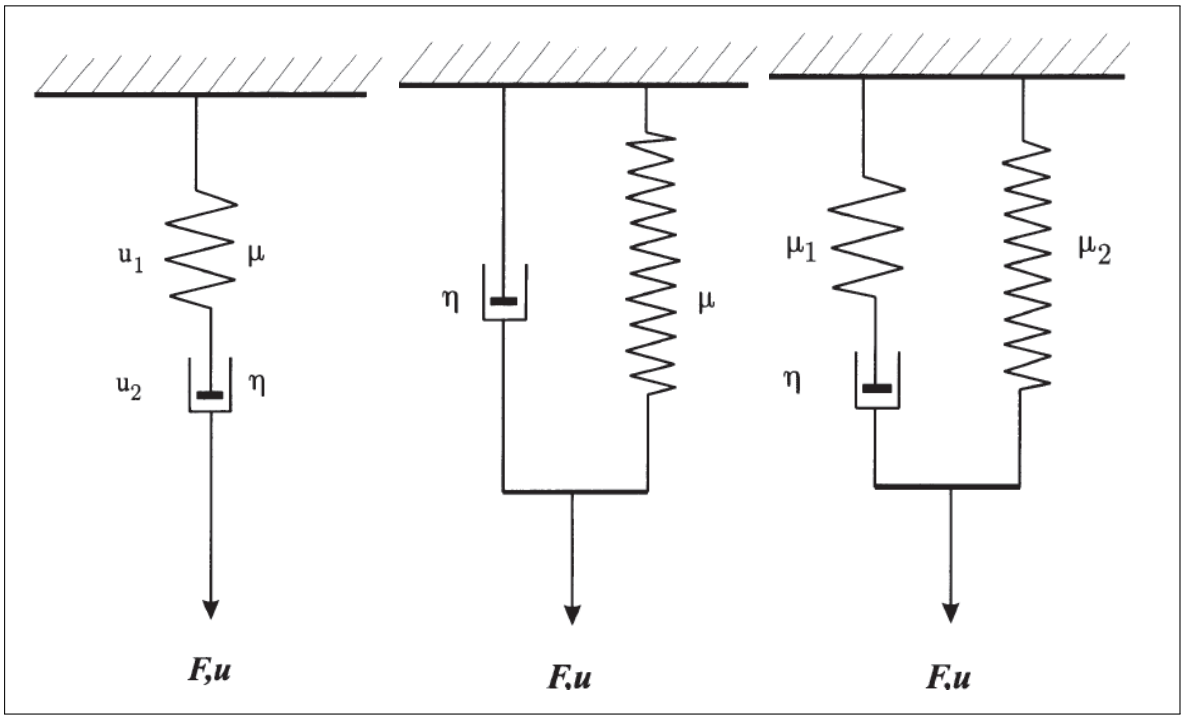

3-2 Design requirements

The design requirements for the catheter tip are defined along two topics, in accordance to the segregation made in section 3-1. Firstly, the technical design requirements, which are the force sensing range and accuracy, distance between the sensor and the Hall magnet, repeatability of the measurement and the indentation reference. Secondly, the design requirements related to *in vivo* conditions, which are tool dimensions, magnetic guidance, hermetical sealing and mandatory safety regulations. At the end of this section, some design considerations are discussed.

Force sensing range and accuracy
The expected force range needs to be quantified, before design of the force sensing mechanism. The required range for force sensing during the treatment of Atrial Fibrillation (AF), i.e. ablation and lesion size determination by means of stiffness sensing, is between 0 and 0.2 Newton per 5.7256 mm ^{2} (d_{tip} = 2.7 mm) [32, 120] resulting in an ablation pressure by the catheter on the tissue of:

$$P_{tissue} = \frac{0.2}{5.7256} = 0.0349MPa \tag{3-3}$$

Larger contact forces during ablation are less effective and could moreover result n tissue puncture [121]. The range of precision necessary for MIS application varies from a few microns to about a few millimeters, depending on the MIS application and required dexterity [122]. The minimum force sensing resolution is set at 0.01 N [14], this is 10 times more sensitive than what could be achieved human fingers during palpation [123].

Distance between magnet and Hall sensor
The second design requirement concerns the maximum allowed distance between the perma-

nent magnet and the 3D Hall sensor. This maximum distance is defined by the decay in magnetic field strength of the permanent magnet and the sensitivity of the Hall sensor. For increased sensitivity of the Hall sensor and/or a stronger magnetic field of the magnet, the distance between sensor and magnet can become larger. The decay in magnetic field strength of the magnet is determined by the geometry (e.g. rectangular, cylinder, ring, disc,..), dimensions, magnetic field remittance of material and pole direction (i.e. axial, diametrical, radial,..). Note that for a small or zero gap distance, the sensor could have the tendency to saturate. The requirement strongly depends on the magnetic Hall sensor and dimensions of the permanent magnet. The requirement could be set by the lower bound of the least sensitive commercial available sensor and expected dimensions of the magnet. However it would serve more as a guideline instead of requirement and therefore the corresponding analysis, based on the choice of Hall sensor, is given in the technical design chapter.

Repeatability
Repeatability of the measurement is another design requirement to assure robustness of the catheter force and indentation measurement. This requirement encompasses firstly the restorative nature of the measurement system. This implies that the measurement system needs to return to the initial position, preferably without hysteresis, such that the full force sensing range remains intact. Furthermore it needs to provide constant accuracy for every measurement. Secondly, the components of the system should have a long life cycle to repeat measurements without any component failure.

Indentation reference
To determine the depth of the soft tissue indentation, a reference indicating the initial catheter-soft tissue contact is required. This reference could be an *in vivo* reference, although internal references have an increased risk to shift because of the heart, lungs or blood movement. It could also be an external reference.

Tool dimensions
The practiced invasiveness level demands the overall dimension to be compatible with the human vascular system. Most cardiac catheter devices are defined in French, where one Fr is 1/3 mm. For regular catheters, the diameter range is between 6 Fr (2 mm) and 12 Fr (4 mm) [103]. For commercially available cardiac force-sensing catheters from Thermocool and Tacticath, the tip diameter is around 11 Fr (3.5 mm) [124]. The increase in catheter diameter can be attributed to the incorporated force sensor mechanisms in the tip. The maximum catheter tip diameter for this design is fixed at 4 mm, i.e. 12 Fr.

***In vivo* safety**
There are many safety regulations regarding catheter devices, therefore the scope of this research is limited by maximum current levels (<0.01 A) to prevent tissue burning [125] and the use of biocompatible material. These are natural or synthetic materials, used to remain *in vivo* when replacing a part of the human body or used in surgery. They are required to avoid infection or allergic reactions. appropriate host response in a specific application.

Magnetic guidance
Normally, catheter guidance is performed by means of MRI or X-Ray navigation and manual catheter manipulation of skilled surgeons. In this thesis, the catheter should be suited to be externally (ex-vivo) guided by a strong magnetic field. This spatial guidance field is created by means of six magnetic coils positioned outside the human body. A magnet needs to be incorporated in the catheter tip such that the superimposed gradient aligns the catheter tip.

Undesired manipulation as well as *in vivo* influence such as pulsation and contraction can thus be minimized or diminished.

Hermetical sealing
The catheter requires a hermetical sealing which is biocompatible to prevent blood from entering the catheter for two reasons. Firstly, blood can clot on the sensing mechanism because of protein agglomeration. For example the blood can clot in cavities, thereby influencing the deflection leading to inaccuracies. Secondly, the hermetical sealing allows for sterilization of the device, although mostly catheters are disposable of nature. The downside is that the sealing affects the deflection mechanism and can only be properly accounted for by means of calibration which is quite time consuming for all possible configurations of force components.

Design considerations
Besides the design requirements, several design considerations have been taken into account during the design process. Note that considerations are not treated as hard criteria. Firstly, the device should be comprehensive, easily accessible in nature for the surgeon and convenient to handle. This includes the need for a clear and useful display of acquired force and stiffness information to provide added value during surgery.
Besides this, the overall fabrication cost of the assembled components creating the catheter need to be taken into consideration. Especially considering that a possible disposable nature is desired to avoid effort and cost of sterilization, which are equal to $0.51 per component [126]. Closely related are the method of fabrication and the associated opportunity for batch fabrication of the catheter prototypes.

3-3 Methodological design approach

This section covers the methodological design approach, including preliminary design choices resulting in a high-level measurement concept. Section 3-3-1, discusses several assumptions concerning the environmental *in vivo* conditions. In section 3-3-2, the measurement problem is analyzed and formulated in a simplified free body diagram. Section 3-3-3, contains a discussion on the measurement concepts and feasibility thereof, leading to a final high-level concept. Further design and analysis of this concept is discussed in chapter 4.

3-3-1 Assumptions

In this section, the assumptions leading to simplification of the *in vivo* are discussed. Three assumptions are made:

i. Soft tissue model
The soft tissue model, presented in section 3-1-2, and viscoelastic models presented in 'Explanatory Box 2' contain spring and damper components to account for the soft tissue characteristics. However, in chapter 2 the load-displacement, or indentation, method has been discussed. In this method, the soft tissue model does not change the requirements of the device because the indentation data analysis accounts for this. Therefore, the soft tissue can be modeled as a single spring for analysis of the force and indentation measurement.

ii. Indentation frame compliance
In this thesis, the frame compliance is assumed to be negligible since the tubes are very

stiff compared to the applied forces (< 0.2 N). Normally, for small force and displacements, additional variations may arise during the indentation process. The load applied on the soft tissue via the indenter, induces displacement in the sample and the load frame of finite stiffness.

iii. Friction forces and protection tube
The forces and moments induced by the trocar point and internal organs, as discussed in the introductory chapter, are assumed not to be of influence on the force measurement. The force measurement is conducted at the tip, therefore the trocar point is no part of the measurement system. Furthermore, the catheter is "protected" against buckling and influence of organs by means of an additional tube surrounding the catheter (also see chapter 4). These tubes are used in MIS to easily change surgical tools in limited time. Moreover, it increases tool performance since it limits material friction and has constant friction conditions.

3-3-2 Freebody diagram of force and indentation measurement

In figure 3-4, the soft tissue stiffness can be modeled by a single spring indicated by k_1, based on the assumption in section 3-3-1. This spring is grounded on the left, while the right end is free to move and represents the tissue surface, indicated by the red vertical line. The deformable element in the catheter tip, used for force sensing in combination with the permanent magnet and Hall sensor, is indicated by k_2. The applied force on the catheter tip is indicated by $P_{actuation}$.

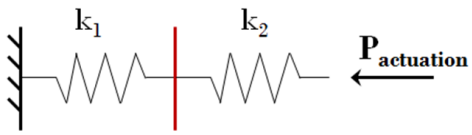

Figure 3-4: Model for soft tissue (k_1) and catheter tip spring (k_2)

Figure 3-5 shows a free body diagram of the problem. If the assumption is made that the system is in equilibrium during measurement, the force on the tissue spring on the left (F_1) is equal to that on the catheter spring on the right (F_2).

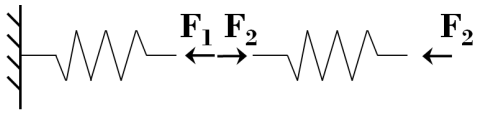

Figure 3-5: Free body diagram of tissue and catheter tip spring

The catheter spring on the right is calibrated over the full range of possible (spring) deflections such that the force F_2 (and therefore F_1) can be determined accurately if the spring displacement is known. Thus, by measuring the displacement x_2 of the catheter spring, the forces F_1 and F_2 can be calculated with equation (3-4).

$$F_1 = F_2 = k_2 \cdot x_2 \tag{3-4}$$

Now that the force on the tissue can be calculated, only determination of the tissue stiffness k_1 remains. To that end, the deflection x_1 of tissue spring needs to be determined, which

reflects the indentation into the tissue. The deflection of the tissue spring (x_1) with respect to its initial position, can be calculated with equation (3-5), assuming that an equilibrium state is studied. In this equation, $x_{actuation}$ is the actuation displacement of the right end of the catheter spring, and x_2 is the catheter spring deflection. As was stated earlier, $x_{actuation}$ is known since it is controlled, and x_2 is measured.

$$x_1 = x_{actuation} - x_2 \tag{3-5}$$

Equation (3-5) is further explained by figure 3-6. This figure shows the catheter spring, and the tissue surface (the red line). It shows that actuation of the catheter spring $x_{actuation}$ leads to spring shortening x_2 and tissue indentation x_1. Since the initial spring length L_0 is known, equation (3-5) can be used to determine x_1 from the controlled $x_{actuation}$ and the measured x_2.

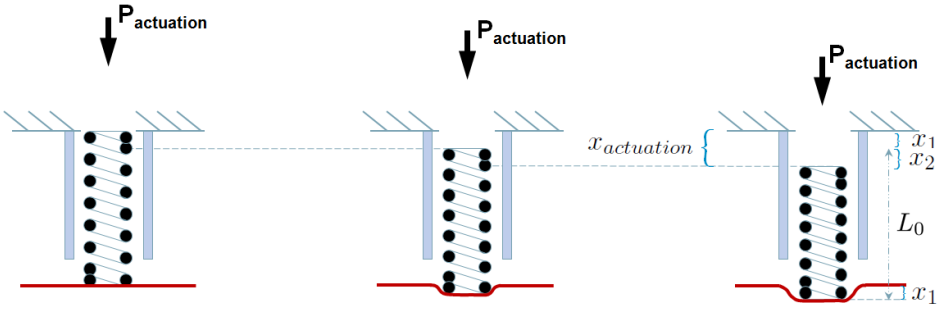

Figure 3-6: Schematic illustration to determine soft tissue indentation

Equation (3-6) then follows from equations (3-4) and (3-5). This equation can be used to determine the tissue stiffness k_1, which was the only remaining unknown.

$$k_1 = \frac{F_1}{x_1} = \frac{k_2 \cdot x_2}{x_{actuation} - x_2} \tag{3-6}$$

3-3-3 Measurement techniques

To determine the load-displacement response of soft biological tissue, the applied force and associated indentation need to be known. Indentation is defined as the probing depth of the indenter into the sample with respect to a reference. Therefore, indentation can only be achieved for a force exceeding the restistant force induced by the soft tissue on the indenter. Two high level indentation principles can be distinguished:

1. Indentation of soft tissue from a physical reference placed at the tissue surface, figure 3-7a;
2. Indentation of soft tissue in which the initial tool-tissue contact point determines the reference for depth-sensing, figure 3-7b.

In the first principle, either the force or the displacement can be controlled to generate load-displacement data:

(a) Reference placed at tissue surface

(b) Initial tool-tissue contact serves as reference

Figure 3-7: Two principles for the reference during indentation

1. Force controlled indentation: the force is prescribed and the associated indentation is measured by the decay in magnetic magnetic field strength of the permanent magnet location in relation to the Hall sensor, which can be mounted in the indenter tip.
2. Displacement controlled indentation: the force is measured for prescribed actuator displacement.

For both configurations in this first principle it is of vital importance for the accuracy of the measurement to have constant reference-tissue contact. However, when the catheter tip is actuated, it might push the reference from the tissue if the force on the reference is not high enough. On the other hand, the force applied on the reference to ensure tool-tissue contact should not be too high, because that would influence the indentation. When the forces on the reference are too high, the reference also indents the tissue and by doing so adds additional displacement, see figure 3-8. This principle is therefore not pursued for further design.

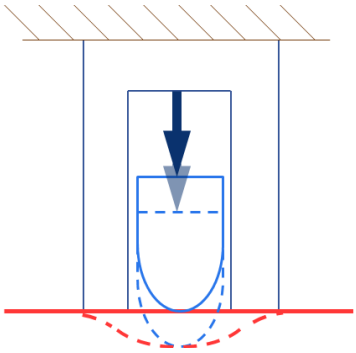

Figure 3-8: Influence on reference on tissue indentation (depth)

The second principle is based on methods where the initial tool-tissue contact serves as the reference for indentation. There are three methods to determine this initial-tool tissue contact:

1. Force signal, which can be measured by a change in the magnetic field, since tissue contact deforms the flexible element and thus changes the distance between the permanent magnet and Hall sensor [68];
2. Change in electrical resistivity since blood and tissue have separate values for electrical conductance [127];

3. Change in resonance frequency (discussed in chapter 2) [73, 76, 80]

The easiest method to determine the initial tool-tissue contact is by means of a change in force signal. Above all, the generated data (magnetic field strength and actuation displacement) is only used for the load-displacement curve as soon as a change in signal magnetic field strength is measured. Besides this, the other two techniques require either additional components (PZT elements) or are less desired in terms of *in vivo* safety (maximum current and voltage levels). Moreover, the resonance based technique can damage components inside the Hall sensor or tip because of dynamic loading.

In this principle, the actuation needs to be performed *ex vivo*. The implementation of a guidance tube is proposed to guide the catheter and transmit the force through the long catheter length inside of the body. This technique will be used for further design. The actuation can be force controlled or displacement controlled:

- Force-controlled indentation: the force is controlled and the sample indentation is measured. However, the indentation/contact force needs to be measured as close as possible to the surface as possible [5], which is not the case for *ex vivo* actuation. Because of the distance between *ex vivo* actuation and *in vivo* force application, additional forces and moments are imposed by organs, arteries and the incision point, which makes force control inaccurate. Therefore this is an infeasible configuration, which will not be pursued further.

- Displacement-controlled indentation: actuation displacement is controlled and the corresponding indentation force is measured at the tip. Technically, indentation by means of imposing a known displacement requires a force in itself. However this force is assumed to differ from the indentation force, because of the length of the catheter tube inside the body (see the previous point).

Because force-controlled indentation is inaccurate, displacement-controlled indentation will be pursued. This requires force measurement, which could be done with a flexure or with a spring. Springs have already been discussed extensively, and some background on flexures is given in Explanatory Box 3.

Explanatory Box 3: Flexures

In mechanism design for relatively small displacements or rotations, elastically deforming parts called "flexures" can be used [55]. Approximate points of rotation or parallel guides with relatively high stiffness in constrained direction can be created based on different geometries achieving high or low compliance, such that upon force application a defined relative motion between linkages is achieved.

The goal of a flexure mechanism is very well defined by Smith [128] and states:
"The goal of a flexure mechanism is to maintain a precise geometric relation between links while simultaneously providing sufficient compliance to accommodate relative motion in specific directions".

This requires flexures to be suitably constrained while on the the other hand having the freedom for relative motion.

The advantages of flexure mechanisms are [128]:
1. They are wear-free, as long as no fatigue cracks develop; 2. They can be designed to be resistive against thermal variation and mechanical disturbances;
2. They can be used for easy implementation of mechanical leverage;
3. They are inexpensive to manufacture can be made of one solid. They are easy to assemble, and provide continuous and smooth displacement;
4. For small distortions a linear relationship between applied force and displacement exists, which is independent of manufacturing tolerances for elastic distortions.

Disadvantages of flexures include:
1. They cannot tolerate large loads, since for large loads more than one state can correspond to equilibrium, which possibly results in instabilities or even buckling. Besides that, accidental overload is often destructive;
2. For accurate prediction of the load-displacement relation, accurate knowledge of the geometry as well as the elastic modulus is necessary;
3. The length of translation for a flexure is restricted by size and stiffness.

Flexures can consist of a leaf spring (see the figure below on the left [129]) or a notch hinge (see the figure below on the right [130]). The principles behind these flexures will be discussed briefly, for the leaf spring. The reader interested in notch hinges is referred to literature on this topic [130].

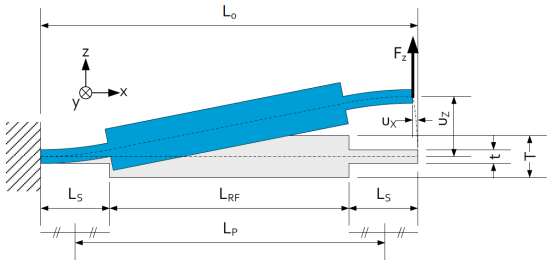

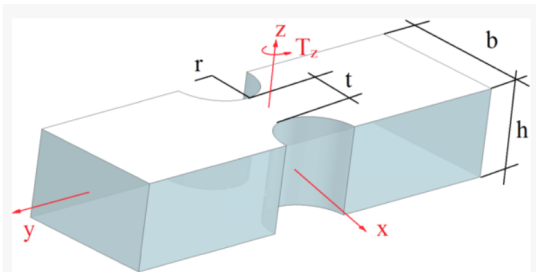

Parallel guided leaf springs are appropriate when the application requires the end angle of the flexible element to remain constant under motion [131]. These flexures approximate straight guiding over a relatively small stroke since the body movement in the u_z-direction (see the figure above on the left) is accompanied by a parallel movement in the transverse direction u_x. This is called the shortening effect [55] which can be compensated by a compound flexure. This is an ancillary body which is also guided, and is connected to the second body. The stiffness against displacement under parallel bending for one flexure is given by:

$$c_x = 12 \cdot \frac{E \cdot I}{l^3} \tag{3-7}$$

The maximum bending stress occurs at the end of the leaf springs and is defined as

$$\sigma_{max} = \frac{3 \cdot E \cdot h \cdot \delta_x}{l^2} \tag{3-8}$$

The feasibility of a leaf spring configuration, in which four parallel flexures are axially distributed over the catheter diameter, has been investigated for an inner catheter diameter of 3.3 mm or less and an indenter diameter of at least 1 mm. The maximum length of the flexure hinges can be 1.15 mm, which is very short for the required displacement of 1.5 mm. Potentially a rubber-like material can be used, but these materials exhibit nonlinear material properties and undergo creep and stress relaxation [128]. Only very small deformation for a load of 0.2 N can be achieved when implemented in catheter tips because of the high stiffness in these monolithic structures [15, 9]. Increased force resolution requires larger deformation and therefore this type of monolithic hinges will not be implemented in the catheter tip.

A spring element as part of the force sensing mechanism in the catheter tip allows for larger deflection and therefore force resolution. Therefore, a spring will be used in the catheter tip, as opposed to a flexure.

3-4 Summary

Many choices concerning the catheter tip design were made in this chapter based on theory and assumptions. Table 3-1 provides an overview of the main design features and the associated requirements.

The general measurement concept can be summarized as follows. Force and stiffness sensing is performed based on load-displacement determination, as opposed to e.g. resonance-based sensing. Measurement is performed in a displacement-controlled mode (in which force is measured), which allows more accurate measurement than force-control. Actual measurement is performed with a 3D magnetic Hall sensor and a permanent magnet, with a spring in between. Deflection of the spring creates a changed magnetic field, which is measured by the Hall sensor. Through calibration, the applied force and the spring deformation can be deduced from this magnetic field. Since the actuation displacement is controlled, the tissue indentation can be determined as the difference between the actuation and spring deformation. Tissue stiffness can then be calculated as the ratio of the force and tissue indentation.

Table 3-1: Overview of design choices

Design feature	**Requirement**
Force range	$0 - 0.2$ N
Force resolution	0.01 N
Distance magnet and Hall sensor	$0.5 - 6$ mm
Indentation	1.5 mm
Tool dimensions	≤ 4 mm

Chapter 4

Technical design

In this chapter the technical design of the catheter tip is discussed. This incorporates all analyses and choices concerning materials, sensor, spring characteristics, overall dimensioning and assembly configuration for optimal performance as well as robustness of the catheter tip design.

The chapter starts with a short theoretical introduction on spring terminology and characteristics in section 4-1. This section provides the necessary context for choices with regards to the selection of a commercial spring component made later in this chapter. The theoretical working principle of the Hall sensor is already discussed in section 2-1-7, and will therefore not be elaborated any further. In section 4-2, the technical design of the force sensing system of the catheter tip is discussed. This includes the selection of the Hall sensor, the permanent magnet and the spring in the catheter tip. Assembly of the catheter tip is the topic of section 4-3. In these sections, a commercially available round-wire spring is included in the design.

In section 4-4 a custom-design (rectangular wire) spring is proposed to replace the commercial (round-wire) spring in the tip, because of advantageous assembly possibilities and a decrease in spring dimensions. The catheter tip assembly with this designed rectangular-wire is the topic of section 4-6. Finally, the conclusions of this chapter are provided in section 4-6.

4-1 Spring Theory

In this section, general spring theory is discussed to understand the working principle and characteristics. This is relevant for optimal spring implementation in the catheter tip, to understand for instance what the factors are that influence the spring rate, what limits the working principle, and which material is best to use for a robust design on this scale.

A helical compression spring is a mechanical element that offers resistance to an axially applied compressive force and can store and release mechanical energy [132]. The spring deformation is linearly related to the applied force as long as the elastic limit of the material is not exceeded. When force and displacement are not linearly related as is shown figure

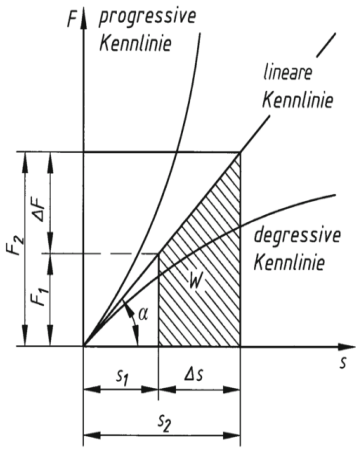

Figure 4-1: Spring force deflection relations

4-1, the spring is either progressive, requiring less force for increased deflection, or degressive which is the inverse relation.

Springs are among the most frequently used machine components in industry and therefore the variety of applications is very broad. Springs are used as energy absorbers in drives and reciprocating devices, interceptors of static and dynamic forces, shock absorbers, elements in force joints and devices for controlling and measuring forces [133]. The latter form of function implementation (measurement of forces) is used in this thesis for the catheter tip force sensing system.

Springs can be classified into many categories based on their characteristic load types and structural designs. Examples are helical springs, flat springs and specially shaped springs. The main focus of this work is put on helical springs, made of either round or rectangular wire. These springs exhibit the function to resist and deflect under tensile, compressive or torsional load.

Most compression springs are constant in diameter. However, other forms such as conical, hourglass, barrel, concave, convex, tapered or a combination of these (selection in figure 4-2), can provide better performance solutions. For example, conical, hourglass and barrel-shaped springs are preferred configurations to achieve greater lateral stability and resistance to surging, while keeping the solid height low [134]. For conical springs, the height can be designed as low as one coil diameter since each coil can nest in the preceding coil. However, round wire springs offer the best performance because of linear motion and stress distribution is along one linear direction in the wire [135]. These are widely commercially available in many different materials and will be used as flexible element in the catheter tip.

Spring rate of helical compression spring

To determine the deformation of elastic bodies under external loading and support reactions, Castigliano's theorem can be used [136]. Note that his theorem is restricted to linear elastic materials which obey Hooke's law for load and deformation (stress and strain). Castigliano's theorem is defined as:
"When forces act on elastic systems subject to small displacements, the displacement corresponding to any force, collinear with the force, is equal to the partial derivative of the total

(a) Conical **(b)** Barrel **(c)** Hourglass

Figure 4-2: Spring geometries

strain energy with respect to that force."

For a compression spring, the total strain energy (U) is composed out of a torsional component and a shear component, as shown in the free body diagram in figure 4-3 [137]. The total strain energy U can be calculated using equation (4-1), in which T is the torsion moment, l is the spring wire length, G is the shear modulus, J is the polar moment of inertia, F is the force on the spring, and A is the spring wire area.

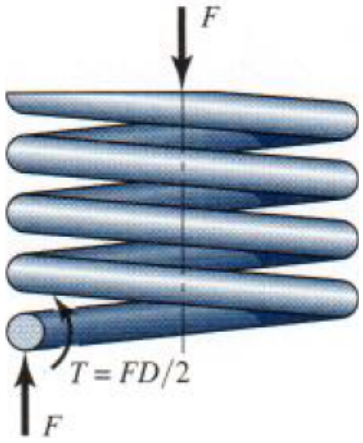

Figure 4-3: Free body diagram of helical compression spring

$$U = \frac{T^2 l}{2GJ} + \frac{F^2 l}{2AG} \tag{4-1}$$

Several parameters in equation (4-1) can be substituted: the torsion can be described as $T = FD/2$, where D is the mean coil diameter. Furthermore, wire length l can be expressed as $l = \pi DN$, where n is the number of of active spring coils. Lastly, one can substitute $J = \pi d^4/32$ and $A = \pi d^2/4$, in which d is the spring wire diameter. This results in equation (4-2) [137].

$$U = \frac{4F^2 D^3 n}{d^4 G} + \frac{2F^2 Dn}{d^2 G} \tag{4-2}$$

Total spring deflection y is obtained by the partial derivative of the strain energy, as is shown in equation (4-3).

$$y = \frac{\partial U}{\partial F} = \frac{8FD^3n}{d^4G} + \frac{4F^2Dn}{d^2G} \tag{4-3}$$

For known deflection and spring rate, the associated force can be measured. Note that the rate equation is accurate between 15 and 80% of the deflection range of maximum spring deflection [134].

Stresses in helical compression spring

To prevent failure, maximum shear stress τ_{max} needs to be calculated in the wire of a helical compression spring. The maximum stress levels occur at the inside of the wire and can be calculated by superposition of the torsional shear stress and the direct shear stress, as is shown in equation (4-4).

$$\tau_{max} = \frac{Td}{2J} + \frac{F}{A} \tag{4-4}$$

Substituting $T = FD/2$, $J = \pi d^4/32$ and $A = \pi d^2/4$ yields equation (4-5).

$$\tau_{max} = \frac{8FD}{\pi d^3} + \frac{4F}{\pi d^2} \tag{4-5}$$

Note that under elastic conditions the stress in the cross section of the wire is not uniform due to the curvature of the coil. The formula described above considers only a straight wire and does not account for increased stress in the material and direct shear loading caused by the helical curvature.

The spring index C is a direct measure for coil curvature and is defined as $C = D_m/d$, where D_m is the mean coil diameter as indicated in figure 4-3. The highest stress levels occur at the surface on the inside of the spring, and the curvature correction factor K_c is defined as in equation (4-6) (based on Bergsträsser factor [134]).

$$K_c = \frac{2C(4C+2)}{(4C-3)(2C+1)} \tag{4-6}$$

The curvature stress can normally be neglected for static loading, which is the loading type applied in the catheter tip, because with the first application of load strain-strengthening occurs [138, 139]. The shear stress correction factor K_s, defined in equation (4-7) cannot be neglected however.

$$K_s = \frac{2C+1}{2C} \tag{4-7}$$

Therefore equation 4-5 can be rearranged to equation (4-8) using the shear stress correction factor and spring index.

$$\tau_{max} = K_s \frac{8FD}{\pi d^3} \tag{4-8}$$

The choice for operation stress depends on the type of loading which can be static, cyclic or dynamic. Only static loading is relevant in the force sensing system, which means that the spring is deformed for less than 10^4 cycles or is under constant load for a long time. For static applications it is important to realize that the load-carrying ability is limited by the yield strength or stress-relaxation resistance of the material. The maximum torsional stresses for static applications are therefore determined as percentages of material tensile strength and have to be compared to the stresses calculated by equation 4-8 to prevent failure.

Spring material and buckling Springs are designed to undergo large deformation in their elastic range, this function requires springs to be made of material with an extensive elastic range [134]. Elasticity is the property of a material to regain its original configuration after deformation [137]. There are some very well-known spring materials, such as music wire, stainless steel wire and oil-tempered wire. During spring manufacturing, deformation induces residual stresses in the material, but these can be released by mild heat treatment.

Mostly spring materials are compared by means of tensile strength. However, the tensile strength of the wire varies inversely with the wire diameter, see appendix A. Therefore, just the tensile strength values of a material do not provide real insight, and the effect of wire diameter needs to be assess as well.

Buckling is a phenomenon, which describes the bending or snapping behavior of a spring at large deflections and is common for compression springs with a free length (L_f) larger than four times the mean coil diameter D_m. The critical deflection y_{cr} depends on the slenderness ratio (L_0/D), end condition constant α (the clamping/supporting configuration can be fixed, hinged or free for which α increases respectively [140]) and material properties (E and G) [137], as is shown in equation (4-9).

$$y_{cr} = L_0 C_1' \left[1 - \left(1 - \frac{C_2'}{\lambda_{eff}^2} \right) \right] \tag{4-9}$$

$$\lambda_{eff}^2 = \frac{\alpha L_0}{D}, \quad C_1' = \frac{E}{2(E-G)}, \quad C_2' = \frac{2\pi^2(E-G)}{2G+E} \tag{4-10}$$

4-2 Force Sensing System

The force sensing mechanism described in this thesis consists of three linked components, which are the permanent magnet, the spring and the Hall sensor. The characteristics of the individual components determine the force sensing range, accuracy, sensitivity and disturbances such as noise. The components as well as the relation between them are the topic of this section. Section 4-2-1 discusses the Hall sensor, section 4-2-2 discusses the selection of the permanent magnet, and section 4-2-3 discusses spring selection.

4-2-1 Hall sensor selection

The first step in the design of the force sensing system is selection of the Hall sensor. Since the Hall sensor has the largest cross-section dimensions of the catheter tip components, it

determines the catheter tip diameter. The main selection criteria for the Hall sensor are its dimensions, sensitivity and noise level.

For this thesis research, one 3D Hall sensor was available, which was also suitable for this purpose: the Infineon TLV493D-A1B6 [141]. This sensor is suitable because of the very low noise level, and the difficulty to saturate while still being able to achieve relatively high sensitivity. Its dimensions are a width of 2.5 mm, a height of 1.1 mm and a length of 3 mm, excluding connection pins. In order to minimize the catheter diameter, the sensor is positioned with the longest dimension over the spring axis, as indicated in figure 4-4. Note that the maximum working temperature of this sensor is 125°C, which makes it possible to ablate in close proximity.

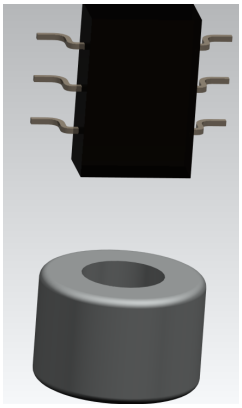

Figure 4-4: Orientation of the Hall sensor with respect to magnet and spring axis

Now that the Hall sensor has been determined, the catheter tube material can be selected. The outer diameter of the tube should be a small as possible, but the inner diameter should be large enough, so that the Hall sensor, and its connection pins, fit inside. Additional design requirements are that the tube should be biocompatible, and that it should have a smooth surface to reduce friction during tube movement. A Polytetrafluoroethylene (PTFE) tube created by Polyfluor was found that has an inner diameter of 3.17 mm that is just large enough to include the Hall sensor and connection pins. Its outer diameter is 3.89 mm and it satisfies the additional design requirements as well [142].

4-2-2 Permanent magnet selection

After the Hall sensor and catheter diameter have been determined, the permanent magnet is selected. The goal is to find a magnet that is as small as possible, and with advantageous magnetic field characteristics. The permanent magnet is a crucial component for measurement of the deflection of the spring, which is the basis for force and stiffness sensing.

A first selection has lead to four magnets that are further investigated. They all have a ring geometry, such that sensor cables in the tip can run through. Furthermore, the outer diameter (D_{outer}) of these magnets should be smaller than 3.17 mm, so that it can fit inside the catheter tube, which was dimensioned based on the Hall sensor.

For these four magnets, the magnetic field decay has been analyzed. This is an important characteristic, since it determines the optimal measurement range, i.e. the most linear part

of the magnetic field decay curve. Based on this optimal measurement range, the spring deflection range can be determined, as well as the initial distance between the magnet and Hall sensor.

Figure 4-5 shows this analysis. The magnetic field strength of the four magnets is plotted against the axial distance from the magnet surface based on a COMSOL simulation. For the magnetic field decay to be quasi-linear, the range of motion should either be before the maximum value or in the longer decaying part after the maximum value. Since the quasi-linear working ranges on the right side of the magnetic maxima are longer, this part is better suited for the catheter tip.

Of these four magnets, magnet 2 has the strongest magnetic field gradient in the quasi-linear regime after the maximum, which is desirable because it increases measurement accuracy. Now a trade-off must be made, based on these field characteristics and on magnet dimensions, which are shown in table 4-1. This trade-off leads to selection of magnet 1, since it has clearly the smallest volume of the four magnets and its magnetic field gradient is almost the same to that of magnet 2. Note that magnet 3 would have been too large, since it would not fit inside of the catheter tube (with an inner diameter of 3.17 mm).

The working range can now be determined based on the quasi-linear part of the magnetic field decay curve of magnet 1. From figure 4-5 it can be concluded that the distance between the Hall sensor and the permanent magnet should be 0.7 mm to 2.5 mm, which results in a spring deflection range of 1.8 mm.

Note that because of limited availability of magnet 1, magnet 4 has been used in the catheter prototype.

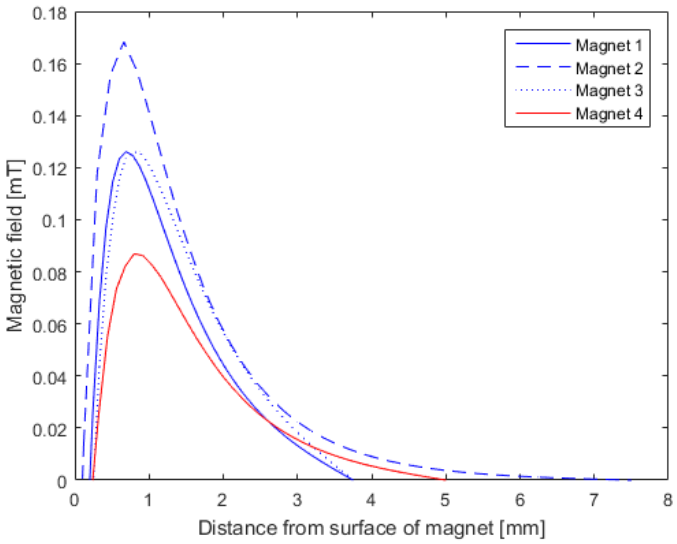

Figure 4-5: Magnetic field decay for the four magnets of interest

Table 4-1: Dimensions of the magnets in figure 4-5 [143]

Number	D_{outer}	D_{inner}	h
Magnet 1	3.0 mm	1.0 mm	1.5 mm
Magnet 2	3.0 mm	1.0 mm	3.0 mm
Magnet 3	3.5 mm	1.1 mm	1.5 mm
Magnet 4	3.0 mm	1.5 mm	2.0 mm

4-2-3 Spring selection

A spring can be selected to complete the force sensing system. This spring should fit inside of the catheter tube, which has an inner diameter of 3.17 mm. Furthermore it should have the right spring rate, which will first have to be determined. The desired spring deflection range is known to be 1.8 mm, as was determined in the selection of the permanent magnet. Furthermore, it is known from literature, that the force that should be applied on tissue can be approximately 0.17 N [120]. This leads to a desired spring rate of roughly 0.09 N/mm. Moreover, the force of 0.17 N, and the displacement of 1.8 mm, should fall within the linear region of the spring.

A spring that satisfies these design requirements has been found: the N-87 made by Century Spring [144]. Table 4-2 shows its characteristics in comparison to the design requirements.

Table 4-2: Comparison between design requirement and commmercial selected spring

Charactertistic	Design requirement	Commercial spring
Spring rate (k)	Approx. 0.09 N/mm	0.067 N/mm
Outer spring diameter (D_{outer})	<3.17 mm	1.98 mm
Inner spring diameter (d_{inner})	-	1.73 mm
Free spring length (L)	-	6.35 mm
Number of coils (n)	-	8.00 windings
Wire diameter (d_{wire})	-	0.127 mm
Solid length (L_s)	-	1.27 mm
Suggested max deflection (s_{max})	> 1.8 mm	5.33 mm
Suggested max load (F_{max})	> 0.17 N	0.356 N
Material	-	Music wire
Ends	Grounded	Grounded

This spring is made out of music wire, which is used for springs, because it is the toughest and strongest of all materials for manufacturing of small springs [145]. The main advantage is that it can withstand higher stresses under repeated loading than springs made of another material. Moreover it has the highest tensile strength and is available in diameters as small as 0.12 mm. Therefore, this material is a perfect choice for a micro-spring in the catheter tip. The specific material properties are provided in table 4-3 [146].

Table 4-3: Material properties of Music wire

Material	Tensile strength	Young's modulus
Music wire (ASTM A228)	2.8 GPa	207 MPa

The materials tensile strength depends on the wire cross section (discussed discussed in section 4-1), and is based on figure A-1 in appendix A.

The material's tensile strength determines the maximum operating stress, which should not exceed 45 - 50 % of tensile strength. The maximum operating stress therefore is 1.26-1.4 GPa. Using equation (4-11), which is based on equation (4-8), the stress in the spring for a maximum force of 0.17 N can be calculated. This resulting maximum operating stress of 431.882 MPa is almost 3 times below the maximum operating stress, which was expected as the spring is designed for a maximum force of 0.356N and this linearly scales in equation 4-11.

$$\tau = K_s \frac{8FD}{\pi d^3} = \frac{2C+1}{2C} \cdot \frac{8FD}{\pi d^3} = \frac{2 \cdot 15.5906 + 1}{2 \cdot 15.5906} \cdot \frac{8 \cdot 0.17 \cdot 1.98}{\pi \cdot (0.127)^3} = 431.882 \quad MPa \quad (4\text{-}11)$$

4-3 Catheter Tip Assembly

Four catheter tip assembly configurations are considered for fabrication resulting in a prototype. In figure 4-6, schematic cross sections of the possible configurations are given.

In the first configuration, the spring is inside the tube which is sealed by a membrane to which an indenter is attached.

For the second concept design, the Hall sensor is mounted in a cap which is attached by means of glue to the end of the spring. The magnet is located at the other end of the spring, which is fixed. The membrane is removed in this configuration; instead a cap covers the free end of the spring and the Hall sensor.

In the third concept configuration, a cap covers the whole spring. This cap is secured by the stoppers on the inside of the tube. The spring is kept in position by the inner tube in such a way that deflection is still possible. The advantage of this concept is that its parts can not detach from the assembly in use, however there might be friction between the parts.

In the fourth concept configuration, the sensor is mounted at a closer distance to the magnet and a rod inside the spring translates the spring motion to the sensor. This increases the sensor sensitivity because the signal is much stronger and smaller displacement can be measured with increased accuracy. Furthermore, the diameter of both the catheter cap and of the spring can be small, since the sensor is not enclosed in the cap nor the spring. Because of the higher accuracy and lower dimensions, this fourth configuration is chosen for the catheter tip design.

These four configurations describe the assembly of the hall sensor, magnet and spring, which constitute the force sensing system. Furthermore, two elements have been included in the design that increase the catheter tip's functionality: a guidance tube and mechanical stoppers. The guidance tube is a stiff tube that concentrically encloses the catheter. Not only does this

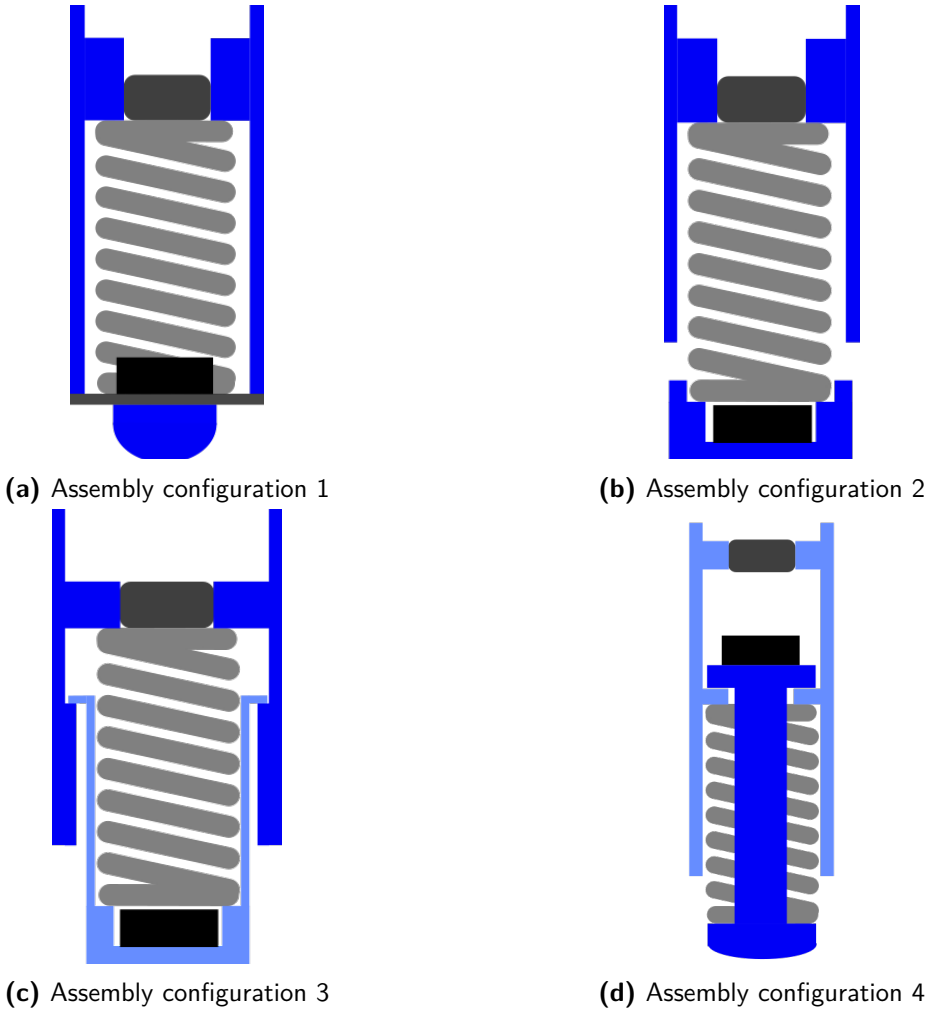

(a) Assembly configuration 1 **(b)** Assembly configuration 2

(c) Assembly configuration 3 **(d)** Assembly configuration 4

Figure 4-6: Assembly configurations for commercial round wire spring

provide protection to the device, it also enables *ex vivo* actuation. This is the case because a force can be applied outside of the body, which is then transferred to the catheter tip without influencing the catheter position in the body, due to the high stiffness of the guidance tube. *Ex vivo* actuation is a key design feature, since it makes miniaturization possible and furthermore decreases catheter tip cost. The mechanical stoppers in the design serve three purposes. Firstly, they prevent parts from falling out, which is of course important during *in vivo* operations. Secondly, they protect the Hall sensor by preventing extensive spring deformation. Lastly, and most importantly, the spring can be pre-loaded because of the stoppers. Therefore, the initial spring length (before actuation) is always the same, which is essential to achieve repeatable and reliable results.

4-4 Custom Designed Spring

In general, round wire springs offer better stress performance than compression springs with a rectangular cross section. This is caused by the fact that for the fabrication of these springs,

the formation of rectangular rods induces a lot of deformation on the material and therefore a nonuniform stress profile in the cross section [147]. Therefore, in general, it is recommended to avoid springs with a rectangular cross-section. However, when rectangular springs are manufactured from a tube, these stresses can be avoided. This can be achieved by means of laser cutting in which the laser removes material by means of heat.

The advantage of laser cutting a spring from a tube is that very small structures, e.g. spring windings as small as 150 μm can be cut from a tube as long as the wall thickness of the tube is small enough [148]. The disadvantage is that the heat changes the material properties, which can partly be recovered by means of heat and chemical treatment but will not remain unaltered. The effect on the designed spring stiffness and material properties depends on the tube material, spring dimensions and power of the laser. Little research has been published in this field, however, and all analysis is experimental.

The main advantage of rectangular wire springs is that they can be used in applications where the solid height of the spring is limited and relatively low stresses are required [134]. By using rectangular wire, instead of round wire, the material volume can be increased while the maximum solid height is maintained.
Especially when a large ratio between s/L_c needs to be achieved, rectangular wire springs having a cross-section with large b/h or h/b ratio offer much better performance than round wire springs [147]. See figure 4-9 for an explanation of these variables.

Additionally, more energy can be stored in a smaller space than for equivalent round-wire springs, when the long side of the rectangular cross section is perpendicular to the longitudinal axis because of the increased material volume [147].

Rectangular springs can have two configurations, either $b/h \geq 1$ or $h/b \geq 1$, both configurations are given in figure 4-9 respectively. Configuration (b) has a higher spring rate than (a) for similar deflection, ratio between the sides, number of windings and D/b ratio, such that the same deflection requires more force. This is explained by the fact that for $b < h$ the mean diameter (D_m) is smaller, resulting in a lower spring rate.

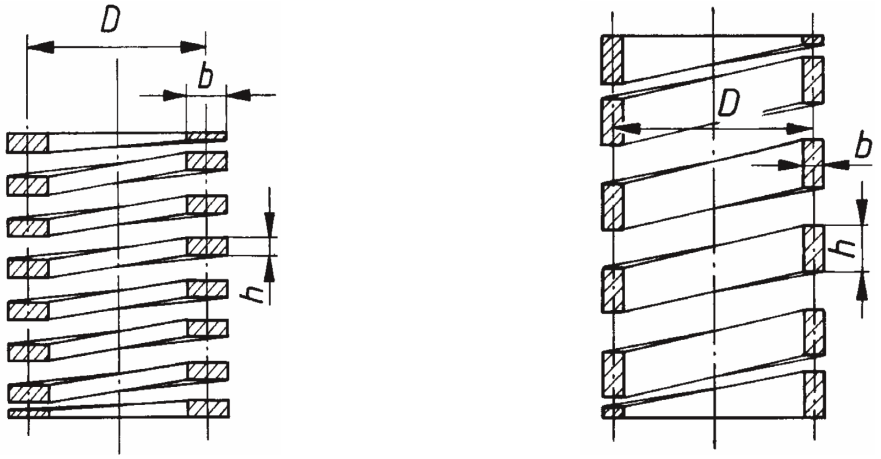

(a) Rectangular spring configuration; h, b **(b)** Rectangular spring configuration; $h > b$

Figure 4-7: Cross-sectional configurations for rectangular-wire spring

4-4-1 Motivation

There are four reasons for using a custom made rectangular-wire spring instead of a commercial round-wire spring in the force sensing system of the catheter tip:

- **Spring rate not influenced by glue**: Glue stiffens the spring and reduces the free length of the spring, both of which result in a higher spring rate.
- **Limited additional housing required**: The spring does not require an additional tube that sticks through since the sensor can be mounted in the tip itself. This reduces the volume and weight of the catheter.
- **The whole tip is one item**: Decreased chance of failure or items breaking of and causing *in vivo* damage.
- **Increased energy storage in smaller space**: For an equivalent spring rate the rectangular spring requires less length than a round wire spring.

4-4-2 Spring design

To achieve the associated assembly benefits of a rectangular spring design, the Hall sensor needs to fit inside the tube. This requires the inner diameter of the tube to be at least 2.5 mm plus additional space for the soldering of the cables (at least 0.5 mm) on the Hall sensor connectors. Med-tube offers tubes, made of biocompatible steel alloys (302/304, 304L, 316, 316L, 321, 430). The tube with smallest wall thickness (which determines the b value of the spring's cross section) and minimum inner tube diameter is K9-TW with dimensions specified in table 4-4.

Table 4-4: Tube dimensions for laser cutting of rectangular spring design

Gage	**Wall type**	$\mathbf{D_{outer}}$ [mm]	$\mathbf{d_{inner}}$[mm]	**Wall, b** [mm]
9	TW	$3.7846 - 3.7338$	$3.3274 - 3.17500$	0.254

The spring rate of a rectangular wire spring is defined as follows [149]:

$$k = \frac{G \cdot b^2 \cdot h^2}{\varepsilon \cdot n \cdot D_m^3} \tag{4-12}$$

In this equation, G is the shear modulus of the tube material, b is the tube thickness, h is the height of the rectangular cross section, ϵ is a shape factor which depends on the ratio of b/h or h/b depending on the spring configuration, n is the number of active coils and D_m the mean spring diameter.

There are three known parameters (G, b, D_m) and three design parameters (h, n, ϵ) that can be used to influence the spring rate. The value for ϵ is nonlinear and defined in literature [149].

Table 4-5: Design requirements for rectangular spring

Design requirement	Formula	Criterium
Spring index	$C = D_m/b$	Cold worked : 4-16, Hot formed : 3-12
Ratio b/h	b/h	1:5 - 5:1
Min pitch	-	$> 1.5d_{inner}$
Max pitch	$(0.3 - 0.6)D_m$	$> 0.3D_m$
Max hear stress	$\tau = \frac{\psi \cdot F \cdot D}{b \cdot h \cdot \sqrt{b \cdot h}}$	$<$ 69 GPa [150]
Spring index	$w = D_m/b$	≥ 4
Slenderness ratio	L_0/D_m	1 - 10

The design parameters are bound by ratios which need to be satisfied for proper design as well as remain within the maximum allowed shear stress levels for the spring dimensions and material. These are summarized in table 4-5 [133].

The value for ψ in the shear stress calculation can be determined from a reference graph [149] and is determined by the values of $h/b, b/h$ and w. This value is unique for any value of these two parameters and therefore needs to be read out individually each time since data is protected and automation of spring design is not possible.

The rectangular spring design is performed in MATLAB. For spring designs in which $h > b$, given the fixed dimension for b, the spring rate remains too high for the design target compared to designs where $b < h$ as is in line with the statement made earlier in this section. The desired spring rate can be achieved by values of $0.1 - 0.2$ mm for h. The stress levels increase for decreasing values of h, which also follows from the equation in table 4-5. Moreover, for very small values of the height in the cross sectional profile, the resolution of the laser cutting machine is approached. This may result in poor spring quality because of an uneven pitch profile.

The final spring design is given in figure 4-8 and table 4-6.

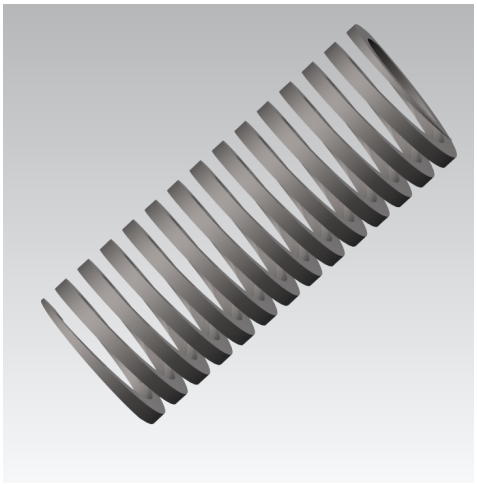

Figure 4-8: Spring design

Table 4-6: Final spring dimensions

Parameter	Dimension
h	0.2 mm
L_0	5.5 mm
n	14
$pitch$	0.3929 mm
k	$0.0669(0.08945 - 0.04184)$ N/mm
τ	$79.596(111.183 - 62.4239)$ MPa

4-4-3 FEM - prototype comparison

Since the custom spring has not arrived yet, this section will be completed as soon as analysis of the prototype can be performed.

4-5 Custom Spring Assembly

Three catheter tip assembly configurations for the rectangular spring are considered for prototype fabrication. In figure 4-9, schematic cross-sections of the possible configurations are given.

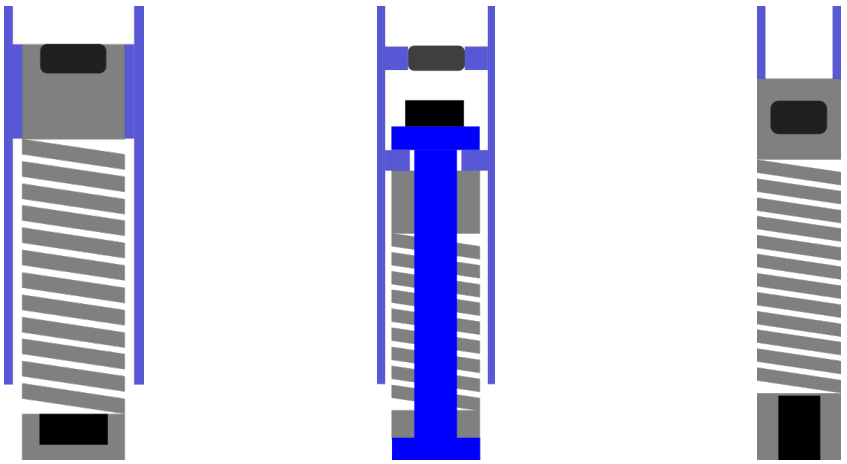

(a) Assembly configuration 1 **(b)** Assembly configuration 2 **(c)** Assembly configuration 3

Figure 4-9: Assembly configurations for rectangular spring

In the first configuration, the Hall sensor is mounted on the one end of the elongated spring while the magnet is mounted on the other side. This end of the rectangular spring is fixed on the inside of a PTFE or 3D printed tube. In the second configuration, a stick is pushed through the inside of the tube, which is quite similar to the fourth round wire concept assembly. In the last configuration the tube is directly attached to the custom spring.
The third configuration is preferred, since it uses the volume most effectively, driving drown catheter dimensions. A prototype based on this configuration is currently being developed.

4-6 Conclusion

In this chapter, the force sensing mechanism for the catheter tip has been designed and different assembly configurations have been discussed. Initially, a commercially available round wire spring of music wire is proposed having a spring stiffness of 0.067 N/mm. Four assembly configurations are reviewed and the fourth assembly configuration (stick through spring) is chosen to be fabricated, in order to test the working principle and efficiency of the design concept.

Furthermore, a rectangular wire spring is designed to replace the commercial round wire spring. The primary reason is because of increased assembly opportunity without influencing the spring rate and fitting the sensor inside the spring while minimizing overall size. The spring rate is designed such that it corresponds to the round wire spring.

Chapter 5

Further design study: DACM

This chapter describes a design study which has been undertaken as an additional project during the research. The goal for this study is to make the first steps towards addressing the challenge of high accuracy and resolution measurement of small contact force during MIS. Therefore the use of a displacement amplifying compliant mechanism (DACM) is proposed, to increase the force resolution and signal-to-noise ratio. Because the small input displacement is amplified by the mechanism, and then measured Hall sensor.

This chapter starts with a brief background on compliant mechanisms in section 5-1, and in specific displacement amplifying compliant mechanisms are discussed. Section 5-2 presents the design methodology. The results and discussion are given in section 5-3. Finally, the conclusions of this study and recommendations are presented in section 5-4.

5-1 Background

A mechanism is defined as a mechanical device used to transfer motion, force or energy [151]. Compliant mechanisms are single piece, flexible structures having the mobility of a conventional mechanism with the stiffness of a conventional structure [152]. The mobility in a compliant mechanism is based on the structural deformation, induced at the input side of the mechanism.

Compliant mechanisms are used in applications to reduce friction, wear, noise, assembly cost and to perform unconventional actuation schemes [153]. Over the last 10 years, complaint mechanism structures have increasingly been used in MEMS. For example in a linear comb-drive to match load characteristics (see figure 5-1a [154]), as micro-accelerometers to reduce the electrical noise (which dominates the mechanical noise) [155] and as displacement amplification by factors as large as 20:1 without significant reduction in output force [156, 157], see figure 5-1b.

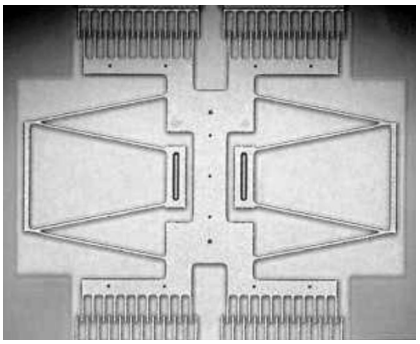

(a) Compliant suspension in linear MEMS comb drive actuator [154]

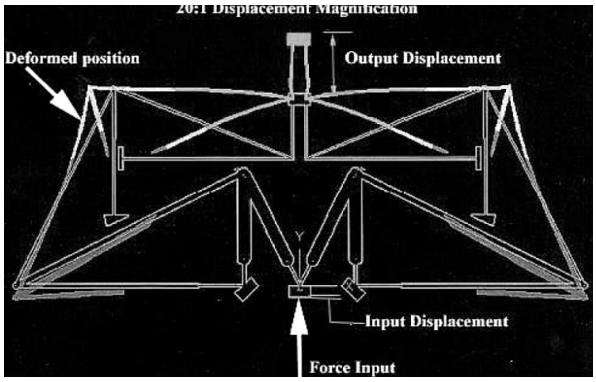

(b) 20:1 stroke amplification mechanism [156]

Figure 5-1: Examples of compliant mechanisms in MEMS

5-2 Design Methodology

In literature, two approaches for compliant mechanism design can be distinguished, which are a kinematic based and a structural optimization/continuum based approach. In the kinematic based approach [158], rigid-body linkage with joint springs are used to synthesize known compliant topology, this is also called a pseudo-rigid body model. In the second approach, computational techniques are used to optimize the topology, shape and size of the mechanism [159, 160].

Design of compliant mechanisms by means of topology optimization is performed by Sigmund [159] by optimizing the mechanical advantage. This is the ratio between the output forces to the input forces, $M = F_{out}/F_{in}$, and is dependent on the size and stiffness of the compliant mechanism [161]. The maximum stress levels are constrained by boundary conditions on the displacement at the input ports. A multicriteria optimization for topology optimization of compliant mechanisms has been proposed by Saxena and Ananthasureth [162] by seeking an optimal continuum to: i) satisfy the kinematic requirements with flexibility, ii) withstand external mechanical loads. An alternative objective function is based on the maximization of energy throughput in the structure [163].

Both of these techniques are time consuming and it is not known a priori whether the set of design requirements and boundary conditions will result in a feasible solution, and therefore design, with the desired amplification [164]. Therefore a new technique based on a lumped model for describing single-input-single-output compliant mechanisms is applied.

Each compliant mechanism can be described by a complementary spring (mass)-lever (SML) model, having an input stiffness k_{in}, output stiffness k_{out} and amplification factor n, see figure 5-2 [165]. The methodology is based on this characterization of compliant mechanism by mapping the input stiffness against the output stiffness [166]. A stiffness map of compliant mechanisms can be created for a database of existing compliant mechanisms. Based on the design requirements, the range of input and output stiffness values for the compliant design can be calculated. These values can be plotted as a feasible region in a stiffness map, which includes the SML parameters of existing compliant mechanisms. Therefore, this analysis pro-

vides insight in the existence of a feasible solution. Furthermore, this technique provides a first starting point for size and shape optimization of existing compliant mechanisms in or close to the feasible region. By redesign of parameters, the existing compliant mechanism can move in the stiffness map towards or inside the feasible region. In order to obtain the desired amplification factor, the dimensions can be scaled along one or multiple axis of the mechanism, in combination with varying material properties.

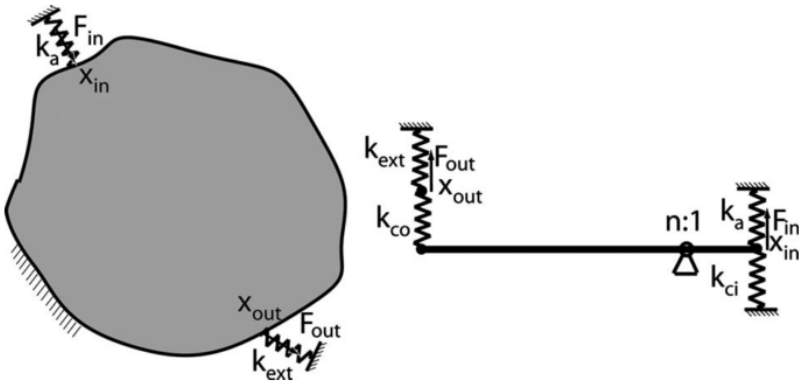

Figure 5-2: SL model of a single-input-single-output compliant mechanism [165]

In the next step, the designs can be analyzed in ANSYS to determine i) the achieved amplification from the input to the output, ii) the maximum stress levels for a maximum input force of 0.2 N. Finally, the maximum displacement for this input force needs to be determined because of stored strain energy.

5-2-1 Spring Mass-Lever model

Three main assumptions are made in the spring-mass lever model:

1. The compliant mechanisms are a single-input-single-output system
2. It is common to model for the purpose of design an elastic structure as a lumped spring-mass (SML) system with one degree of freedom
3. A DACM can not be modeled as a simple rigid-body lever; it is a lever having non-zero stiffness at the input side as well as non-zero stiffness at the output side [157]

Important to note is that the amplification and deamplification of force or displacement because of the geometrical advantage of a DACM are not reciprocal to each other. This means that the ratio of the input and output displacements is different when an input force or displacement is applied at either two of the points [157].

The input stiffness k_{ci} and output stiffness k_{co} in the model are defined in equation (5-1).

$$k_{ci} = \frac{F_{in}}{u_{out}} = \frac{F_{in} - k_a u_{in} - n(F_{out} - k_{ext} u_{out})}{u_{in}} \tag{5-1}$$

$$k_{co} = \frac{F_{out} - k_{ext} u_{out}}{u_{out} - n u_{in}} \tag{5-2}$$

The database with input and output stiffness values for existing compliant mechanisms is given in table 5-1. Note that a negative sign is inverting an inverting displacement amplifying compliant mechanism. The corresponding stiffness map is given in figure 5-3a. The influence of the external stiffness on the geometrical amplification is plotted for the purpose of illustration, figure 5-3b. In the next section, the feasible region based on the design parameters is described.

Table 5-1: Database with existing compliant mechanisms [167]

Mechanism number	Input stiffness [N/m]	Output stiffness [N/m]	Amplification
M_1	$6.26 \cdot 10^2$	$3.90 \cdot 10^2$	-5.91
M_2	$1.78 \cdot 10^2$	2.93	10.57
M_3	$1.25 \cdot 10^5$	$3.60 \cdot 10^2$	7.90
M_4	$7.15 \cdot 10^3$	$3.96 \cdot 10^2$	-10.2
M_5	$1.78 \cdot 10^2$	2.93	10.57

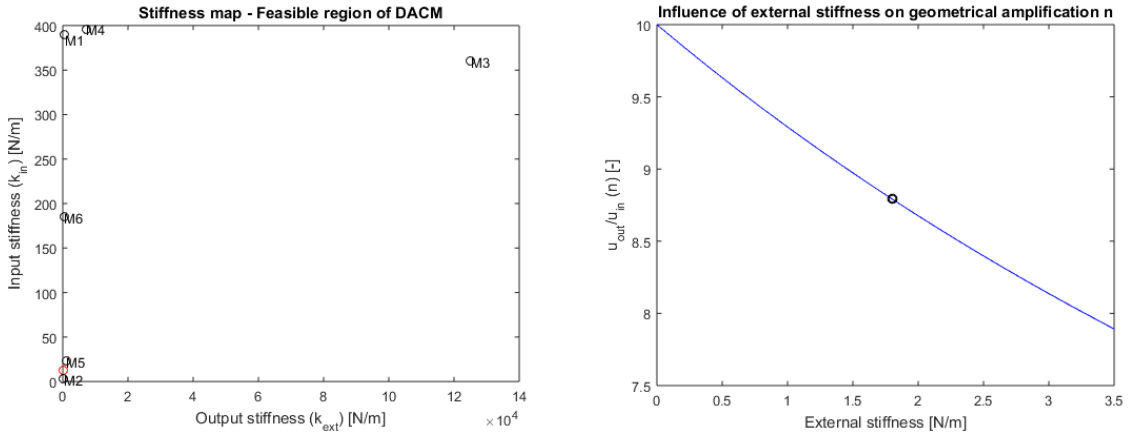

(a) Stiffness map of database with compliant mechanisms

(b) Influence of external stiffness on the amplification factor

Figure 5-3: Database stiffness map and external stiffness influence on amplification

5-2-2 Feasible region

The feasible region can be described as the feasible set of the SML parameters that satisfy the compliant mechanism design specifications. According to Hedge and Ananthasuresh [167], the feasible region can be described by the equality expressions for k_{ci} and k_{co} which involve the variable design specifications as well as the SML parameters.

In order to select and/or redesign the compliant mechanism, the feasible region of SML parameters needs to be determined. The methodology to determine the feasible region is based on calculating the full feasible solution set. This set is created by calculating all possible combinations of the design variables by varying all variables from the lower to the upper bound. The ranges for the SML parameters are given in table 5-2.

The feasible region and database of existing compliant mechanisms are plotted in a stiffness map, but none of the existing compliant mechanisms are in the feasible region, see figure 5-6. Compliant mechanism 2 is in close proximity to the feasible region. Size and shape optimization of mechanism 2 is performed in MATLAB, see figure 5-4b, based on geometrical relations and constraints of rigid linkages [168]. To perform the size and shape optimization, the additional lever close to the output of the mechanism is removed such that the mechanism is statically determined. This lever is added afterwards, see figure 5-5. For catheter implementation, the structure has been made three dimensional, thereby superimposing boundary conditions on the beam deflections in the mechanism.

Table 5-2: Design parameters for SML variables

Parameter	Range	Description
k_{ext}	$1-2$	Tissue stiffness in [N/mm]
F_{max}	$0.05-0.27$	Maximum force [N]
sf	0.75	Safety factor [-]
u_{in}	$0.1-2$	Input displacement [mm]
u_{out}	$0.4-8$	Output displacement [mm]
F_{in}	$0.1-2.7$	Input force [N]
F_{out}	$0.04-1.08$	Output force [N]
n	4	Amplification [-]
m_a	0	Actuator mass [kg]
k_a	0	Actuator stiffness [N/mm]
m_{ext}	0	External mass [kg]

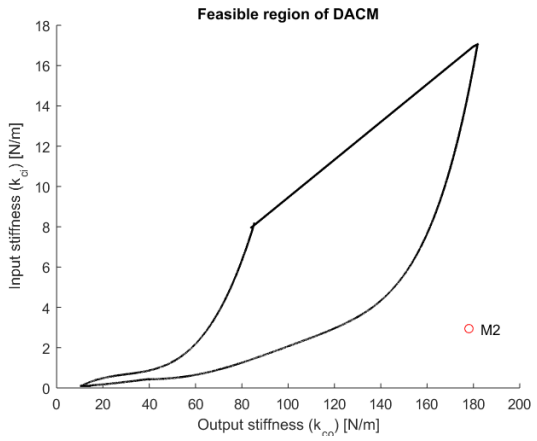

(a) Feasible region and existing compliant mechanism M2

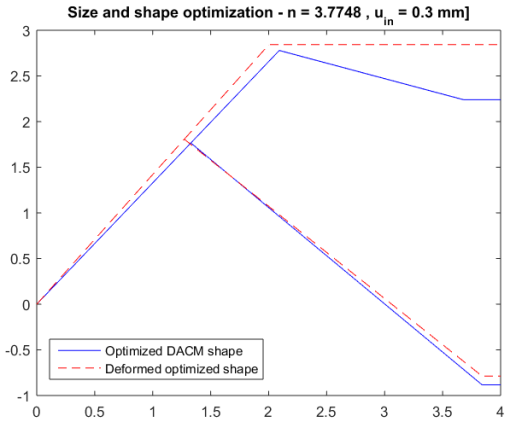

(b) Size and shape optimization of mechanism 2

Figure 5-4: Selection and optimization of compliant mechanism 2

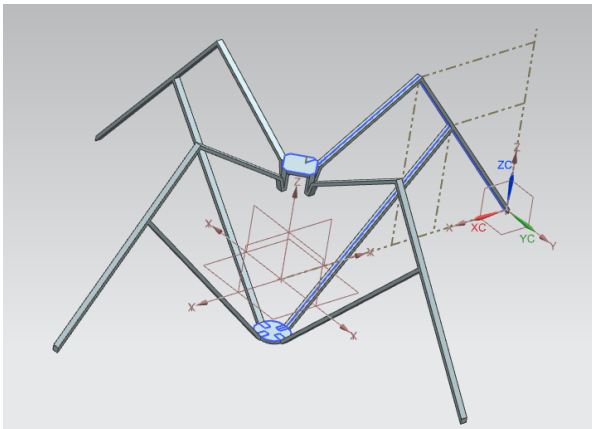

Figure 5-5: Three-dimensional model of the mechanism

5-3 Results and discussion

For the geometrical model obtained during the size and shape optimization, the thickness and width of the beams are varied and accordingly analyzed in ANSYS. The material model used for analysis is stainless steel (E = 210, ν=0.3). The beam width and beam thickness are 0.1 and 0.05 mm respectively. A force of 0.2 N is applied on the bottom area in z-direction, and the element is constrained by boundary conditions in all directions on the vertical side area. Note that because of symmetry only one quarter or half of the amplifying mechanism needs to be modeled, which reduces computational effort. The amplification of the design is 2.2, the stress levels are however above the maximum and therefore result in failure.

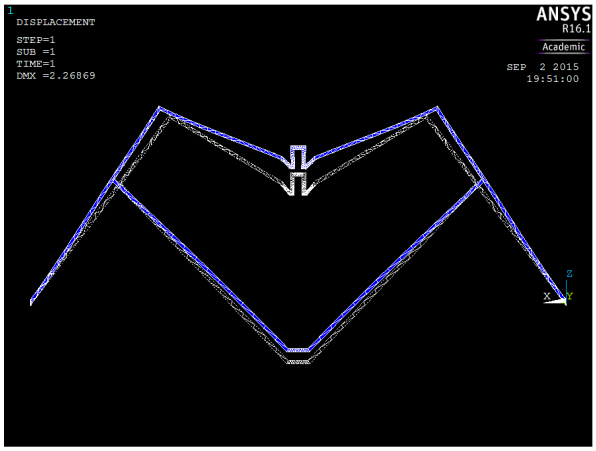

Figure 5-6: Displacement amplification of 2.2

The mechanism has been 3D printed several times, based on ANSYS analysis with 3D printing material models instead of the preferred material choice (steel). Unfortunately, the fabrication of the device has not been successful yet. The trade-off between material flexibility and material strength for the thin structure requires more in-depth analysis of the mechanism requirements.

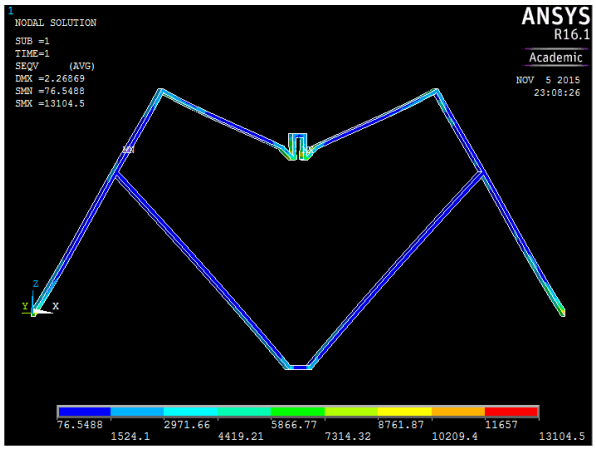

Figure 5-7: Stress levels (half of the model)

5-4 Conclusions and Recommendations

A displacement amplifying compliant mechanism has been designed to increase the force resolution and signal-to-noise ratio in a catheter tip. Deformation amplification of the resilient structure increases the magnetic field strength which can be measured by the Hall sensor. This is desired because of the very small catheter contact forces.

Based on spring-mass lever models, compliant mechanisms can be plotted based on their input and output stiffness. Size and shape optimization is performed on an existing compliant mechanism, close to the feasible region which is drawn based on the design parameters.

The final amplification of the compliant mechanism determined in ANSYS is 2.2, the stress levels exceed the maximum resulting in failure of the mechanism. The first steps towards fabrication of the amplifying mechanism have been taken. Recommendations for further design are in the direction of material choice and other methods of fabrication. Currently, failure mechanisms of the device have not been studied, which is especially important for implementation in medical devices.

Chapter 6

Fabrication

This chapter discusses the fabrication methods used for prototyping of the catheter tip designs. In section 6-1, the fabrication of all components, except for the commercial spring and Hall sensor, are discussed. This section also describes the prototype assembly. Section 6-2, elaborates on the fabrication of the custom designed spring. The conclusion of this chapter is given in section 6-3.

6-1 Catheter tip (commercial spring)

The fabrication of the components for the commercial spring prototype, as well as the assembly, is discussed in section 6-1-1. Section 6-1-2 discusses the iterations that have been executed to overcome challenges in earlier prototypes. Lastly, a short discussion on the fabrication method and success is the topic of section 6-1-3.

6-1-1 Fabrication method

The parts that cannot be bought in the catheter tip design are 3D printed, which allows fast and cheap fabrication. The material choice is therefore limited to materials that are engineered for 3D printing technology. The hardest possible printing material, Veroclear (Shore Hardness D-85), is chosen for fabrication to ensure that very thin parts, which reach the printer resolution, do not break easily [169]. Moreover, the compliance of the printed catheter tip material should be as low as possible to avoid bending and provide optimal force transduction, which requires the stiffest possible material.

Figure 6-1a shows the printed components for the final prototype. Just after printing, the components are surrounded by support material, since the 3D printer requires a material base to deposit a new layer and is therefore not capable to print in air. This material needs to be removed after printing to allow assembly of all parts. The material is quite easy to remove, however because of the length of the printed tubes and the small diameter, residual support

(a) Tip tube, stick, spring and cap

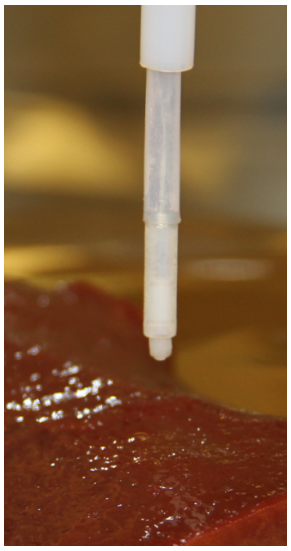

(b) Final prototype indenting a liver

Figure 6-1: 3D components and assembled prototype

material easily remains inside. Small micro-cleaning brushes, used by dentists, are used to remove all material inside the tube.

The prototype assembly is performed in four steps, of which the first one is the most critical

- Hall sensor and cables: The six output pins of the Hall sensor need to be connected to an external display by means of soldering signal cables to the sensor. To avoid six separate cables running through the catheter and to prevent signal interference, the signal cables are organized in a plastic sheath. There are four cables of 50 μm in this plastic sheath (custom made) connecting the output of the Hall sensor to a controller (Arduino), which was discussed in chapter 7. In order to make soldering of the wires possible, they need to be exposed from the plastic sheath. This is done with a lighter, because of the very small wire diameter. This needs to be done with caution to avoid oxidation of the wires, which would make the wires difficult to solder and useless.
  The 4 cables are soldered to the 6 output pins of the Hall sensor, which are shown in figure 6-2. First, two neighboring grounds (GND) are soldered together. Then the cable is soldered to the pin and folded over to the other side of the sensor, such that it can be soldered to the third ground. Thus, three ground pins are all connected to one cable. The other three cables are attached to the voltage pin (VDD) and two signal output pins (SDA and SCL). The cables are glued to the housing of the Hall sensor to provide additional strength to the connections, for when the sensor displaces during force sensing, and to secure cable isolation now that the plastic sheath is removed to solder.

- The Hall sensor (with attached cables) is positioned between the small walls at the end of the catheter stick and fixated by means of glue, which is hardened under UV light. These walls primarily serve to mount the sensor at the right location (middle of the

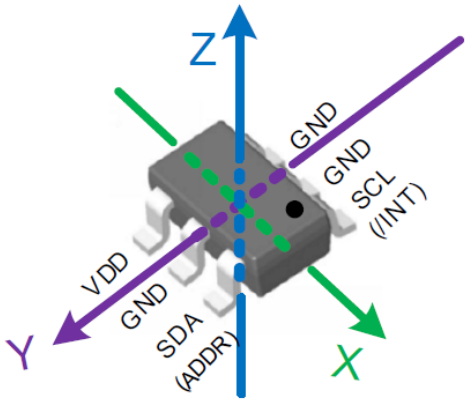

Figure 6-2: Pin configuration of the Hall sensor

stick) and to avoid tilting during fixation with glue, see figure 6-3a. Note that these walls have been added from the third prototype onward, based on lessons learned from previous prototypes.

- The stick with Hall sensor is inserted at the back side of the tip tube, see figure 6-3b.
- The commercial spring is shoved over the stick from the front and kept in place by the cap, see figure 6-3c. The tolerance between cap and stick is very low, and only a little bit of glue is used to fixate the cap.
- Finally, the ring magnet is positioned at the end of the tube, with the cables pushed through its center, see figure 6-3d. The surface of the magnet is aligned with the end of the tip tube. The magnet is positioned at such a location, that for a maximum spring deflection of 1.5 mm, the measurements are conducted in the desired magnetic field range, as discussed in section 4-2-2.

The weight of the assembled catheter tip is 0.3164 gram and costs are below €4 (Hall sensor: €1.25, magnet: €0.90, 3D printing: €1.58).

6-1-2 Fabrication challenges and iterations

The concept design has been fabricated three times to overcome challenges and implement improvements. In the first prototype, figure 6-4a, the connection between the catheter tip and the PTFE tube is made by overlap of the tip tube inside the PTFE tube. Note that in the figure, the magnet (in the PTFE tube), spring and Hall sensor are not displayed. There is a significant amount of side deflection in this prototype when a force is applied outside the longitudinal axis. This is caused by a gap between the tube wall and spring causing play.

In the second prototype, shown in figure 6-4b, two improvements have been made. First of all, the play is decreased by making sure that the cap is inside the catheter tube and therefore guides the spring deflection. An additional benefit is that the cap is always inside the tube and does not hit the tube wall at the tip. Secondly, the tip tube length is increased

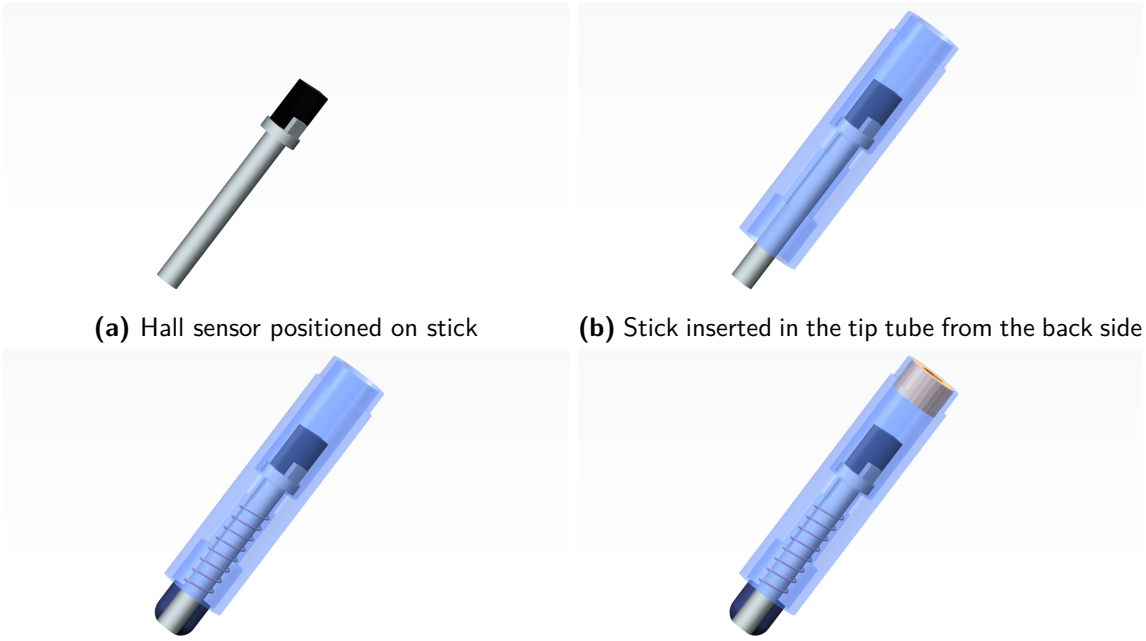

(a) Hall sensor positioned on stick

(b) Stick inserted in the tip tube from the back side

(c) The spring and cap are shoved over the stick

(d) The magnet is placed (and glued) in position

Figure 6-3: Steps for final prototype assembly

and the magnet is pushed inside the tube, increasing the magnetic field strength because of closer proximity to the Hall sensor. In the previous configuration, the overlap between tip and PTFE tube caused an increase in distance between the sensor and the magnet.

In the final prototype, shown in figure 6-4c, three improvements have been made. Firstly, a mechanical stopper is implemented with additional material at the inside of the tube such that the cap can travel 1.5 mm, in order to prevent sensor damage and reduce friction. Secondly, the cap is increased in length to pre-load the spring such that a deflection of $15-20\%$ of the maximum spring displacement is reached. The advantage of pre-loading the spring is that the indenter always returns to the same initial position, and that the sensing platform prevents the spring and cap from coming out of the catheter tip tube. Lastly, the 'sensor platform' is reduced in diameter. The main advantage is that the gap between this platform and the inner diameter of the printed tube tip increases, which reduces friction.

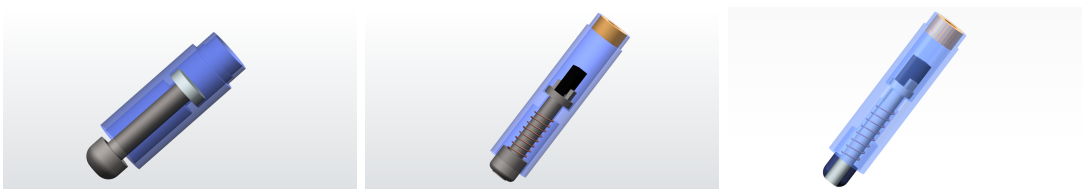

(a) First prototype

(b) Second prototype

(c) Third and final prototype

Figure 6-4: Designs for the three prototypes

6-1-3 Comments on fabrication

The current fabrication method, i.e. using 3D printing, has been very convenient for this research since it was very fast and cheap. The drawback is the limited amount of material choice and the relatively low printing resolution. Furthermore, from experience it depends on the 3D printer how accurately the printed part resembles the CAD model when approaching the printer resolution.

This method of fabrication is not compatible for actual *in vivo* usage and primarily serves the purpose of a proof of concept. In order to pursue a commercially available version of this prototype, the 3D printed parts need to be manufactured from biocompatible material.

6-2 Catheter tip (custom spring)

A catheter tip with a custom-made rectangular spring has also been designed, for further catheter tip miniaturization and for biocompatibility. Its fabrication has been outsourced to the University of Istanbul at the end of August. Unfortunately there has been some unforeseen delay and, as of October, the springs have not arrived yet. Therefore, the fabrication is not discussed in this report and will be described upon arrival of the springs.

6-3 Conclusion

In this chapter the catheter tip fabrication and assembly has been discussed. For the commercial spring, the stick, cast and cap are 3D printed. This results in a very cheap prototype, since the cost of 3D printing, as well as that of the Hall sensor and magnet, are very low. The whole tip design is optimized in three iteration cycles resulting in a very small, almost frictionless prototype. The mechanical stoppers, and spring pre-loading guarantee an increase in repeatability and robustness of the catheter tip design.

The custom designed spring offers many advantages over the commercial spring in terms of miniaturization and biocompatibility. The performance, in terms of volume compared to spring rate, and opportunities for biocompatible treatments are more favorable than for the commercial spring. However the fabrication is more lengthy and expensive than for the commercial spring and catheter tip design.

Chapter 7

Measurement

The manufactured prototypes are tested to determine the capability and efficiency in generating load-displacement data to extract meaningful mechanical properties. Therefore, the device is tested on samples which mimic soft tissue characteristics. Section 7-1 discusses the method for testing device effectiveness. Section 7-2 presents the calibration procedure and results. In section 7-3, the sample material choice, as well as the sample preparation, are discussed. Data processing is discussed in section 7-4. Finally, section 7-5 presents a conclusion of this chapter.

7-1 Method

This section describes the method to verify three aspects of the design concept by using of a prototype. The first is to test the effectiveness of the design towards its main goal: distinguishing different materials with different stiffness values, in particular ablated versus non-ablated tissue. The second is to verify the precision of the device which encompasses the repeatability for similar indentation. The third is to test the accuracy of the measured values compared to a verified machine. The measurement set-up is described in section 7-1-1, which discussed all materials and software. The measurement procedure is described in section 7-1-2.

7-1-1 Set-up

The measurement set-up consists of an actuation system, two concentric sliding tubes and the catheter tip. Note that the displacement sensing system, which is used to measure the indentation at initial tool-tissue contact, is not implemented in the measurement set-up. The software for the magnetic linear displacement encoder was not robust and therefore the actuator displacement is only controlled, and not measured.

The actuation system is a fixed reference frame consisting of an (outer) guidance tube and the actuator. These are attached to a specifically designed stage which can be fixated on any

location, as is shown in figure 7-1. The (inner) catheter tube is connected to the actuator shaft (within the outer guidance tube) to perform the required tissue indentation. A linear actuator with lead screw and linear slidestepper motor (model: nanotech L20-A) is implemented in the set-up to perform the linear precision actuation. The (peak) power of the actuator is chosen to be much higher than necessary (i.e. 40 N), in order to prevent a power shortage or pushing the actuation limits. The actuator resolution is 0.005 mm per actuation step and can be performed with a speed of up to 40 mm/s. The whole datasheet is attached in appendix A.

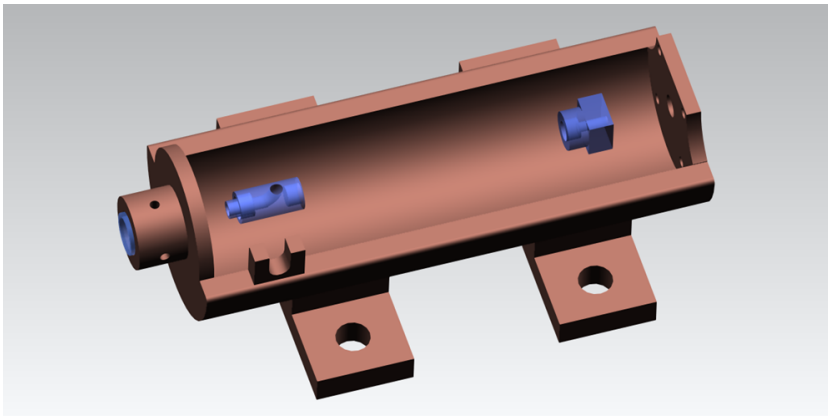

Figure 7-1: Reference frame for actuator (on the right) and guidance tube (on the left)

The catheter tip, which includes the sensor system, is fixed to the (inner) catheter tube and guided by the (outer) guidance tube. It can therefore be actuated remotely. Attached to the Hall sensor are cables that run all the way to the actuator connection, where they leave the tube via specifically designed hole in the connection, see figure 7-2.

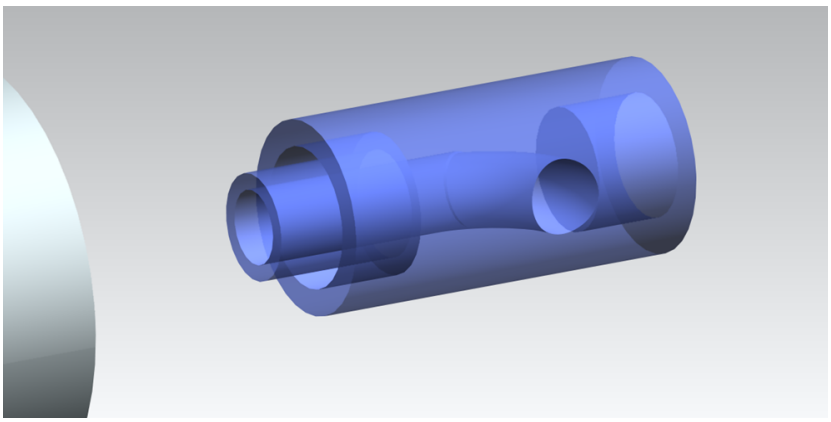

Figure 7-2: Actuator connection with holes for Hall sensor cables

A closed-loop control system is implemented for movement control of the actuator and measurement of the corresponding change in magnetic field in the catheter tip. The implemented controller is called 'Arduino', and is an 8-bit microcontroller. This software is used to actuate the stepper motor and subsequently measure the magnetic field. The magnetic field data generated by the Hall sensor is sampled multiple times at each step and the average

value is written to the output screen. The magnetic field data has been analyzed and for static measurement, the output field converges within a second and is very stable. The whole interaction between user, software and hardware is summarized in figure 7-3.

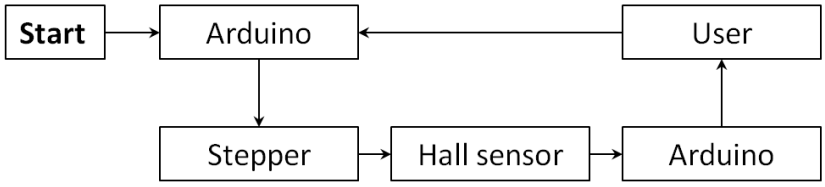

Figure 7-3: Schematic flow of the catheter tip load-displacement measurement.

7-1-2 Procedure

For soft tissue characterization, three different types of measurements can be conducted to obtain different mechanical properties. The first are so called 'tensile tests', in which a sample is firmly clamped and stretched until it breaks [170, 171]. Another type of characterization is 'indentation' measurement, in which load-displacement data is generated [95, 172, 101]. Material stiffness values, and also Young's modulus if geometrical initial and boundary conditions are specified, can be obtained by measurement [170] or FEM inverse analysis [172], as was also discussed in chapter 2. The last type of measurements are 'creep experiments', in which the time-dependent deformation (creep-behavior) of the sample is investigated by implementing so-called hold periods. These are periods in which the displacement is kept constant and the change in stress distribution under the indenter is analyzed by continuous force measurement [173].

The focus in this research is, as discussed in the introduction of this chapter, on distinguishing materials with different stiffness values. Therefore, the measurement scope is on indentation measurements generating load-displacement data. The accuracy of the catheter device will be determined by comparison to a verified load-displacement machine. Both measurement procedures will shortly be discussed.

Catheter measurement: Prototype
The catheter indentation is performed in a displacement-controlled mode. Therefore, control of indentation strain and strain rate can be achieved [174]. Note that displacement-controlled indentation is preferred over force-controlled indentation to analyze time-dependent behavior of soft material, during so-called creep-experiments [72]. These will however not be conducted in this research.

The sample is placed on a rigid and horizontal surface, aligned such that the deformation is in the middle of the test specimen [175]. The catheter is brought in close proximity to the sample surface and further lowered with the actuator until the first force value is measured (upon first catheter-sample contact).

The indentation is performed with a speed of 25 μm/s, and performed until the specimen does not allow for further indentation or the catheter force measurement is saturated. This implies that the spring deflection in the indenter is at its maximum level. Each sample is indented three times at the same location, and in between the indentation measurements a

hold period is implemented to allow the samples to relax. The indentations are performed consecutively to prevent aging effects in the sample.

Verified measurement: Stentor II
A verified load-displacement machine, called the Stentor II, is used to test the catheter accuracy for all samples. The force-sensing resolution of the machine is 0.005 N, which is measured with a load cell (SPIP S2) having a capacity of 50 N. The displacement resolution is 0.02 mm and the minimum indentation speed of the machine is 10 mm/min (167 μm/s).

The indenter on the test arm is exchanged by a version of the catheter tip for comparison purposes. This version does not include the spring, and thus the stick and cap are fixed in a screw which is attached to the test arm. The sample is placed on a rigid surface and the middle of the specimen is aligned with the fixed catheter tip. Subsequently, the arm is lowered until it is in close proximity to the sensor and the machine is set to indent the material automatically with 10 mm/min up to a force value of 1 N. Further analyses will focus on force values up till 0.2 N, corresponding to the force range of the catheter prototype.

7-2 Calibration

System calibration is the procedure by which the output of the instrument under test is compared to the output of an instrument with known accuracy applying the same input (measured quantity) to both instruments [176]. The calibration needs to be carried out for the full measurement range, i.e. all possible values the input can adopt, to ensure that the accuracy is known for the whole range. Calibration only holds as long as the environmental conditions do not alter with respect to the conditions under which calibration has taken place. Moreover, system calibration needs to be repeated from time to time to prevent change in characteristics because of mechanical wear, dirt, chemicals and temperature changes reflecting on the measurement data. The significance of drift depends on the amount of use and operating environment, although drift also can occur on shelve because of aging effects in the components.

In theory, for a controlled displacement of the magnet with respect to the Hall sensor (or vice versa), the corresponding magnetic field can be measured. If the spring constant is known, the force-displacement curve can then be determined based on this magnetic field. However, friction forces in the catheter tip need to be accounted for. For the catheter tip, friction is caused by the stick sliding through the stopper opening, and also occurs between the spring and the stick. Furthermore, possible small side-deflection of the spring causes non-linear behavior and influences the displacement. Therefore, calibration of the catheter tip is performed by displacement-controlled measurement of the Hall sensor signal and determination of the corresponding force using a precision scale.

The calibration set-up consists of a position stage, catheter tip and scale positioned as indicated in figure 7-4. The calibration components and procedure are briefly discussed in section 7-2-1. The calibration results are presented in section 7-2-2.

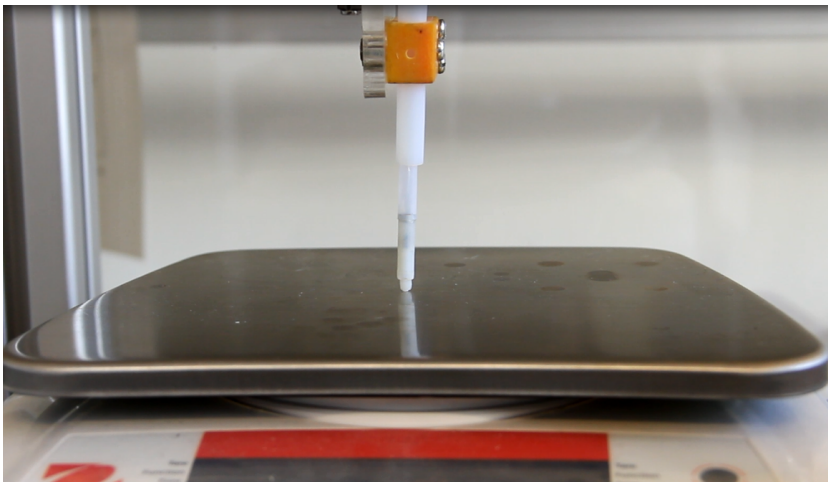

Figure 7-4: Calibration set-up with position stage, catheter tip and scale

7-2-1 Calibration components and procedure

The outside of the catheter tip is fixated on a position stage, called SmartAct, which can perform three-dimensional controlled displacement and has a positioning resolution of 0.2 μm. The SmartAct is a position stage based on capacitive actuation and is controlled manually. The total travel range of this system is limited and therefore the scale is placed in vicinity of the tip such that limited displacement is required before contact.

A precision electronic balance is used to measure the force for every step of the controlled position. The scale has a resolution of 0.01 N. The whole calibration set-up is enclosed by a glass box to the reduce influence of airflow on the measurement.

The calibration has been performed according to the following procedure:
The catheter tip is brought in very close proximity to the scale, such that with an additional displacement step the scale displays a non-zero value. The corresponding magnetic field value is then measured with the Hall sensor and saved. The displacement steps are performed with the actuator and are 50 μm. The calibration is performed for the full displacement range of the spring, which is determined prior to calibration by measuring the magnetic field strength for zero spring deflection and maximum spring deflection. These values are on average 8.738 mT and 23.871 mT, respectively (based on 40 sample points).

Using this procedure, the magnetic field values, as measured by the Hall sensor, are related to the force (using the scale) and to the spring deflection. The spring deflection is equal to the controlled actuation displacement, since the catheter tip is placed on a rigid surface.

7-2-2 Calibration result and discussion

Two calibration measurements are performed, the results for the spring deflection and force values for the measured magnetic field are given in figures 7-5a and 7-5b, respectively.

For zero spring deflection and force, the measured magnetic field value is 8.728 mT because of constant presence of the permanent magnet. The magnetic field increases quasi-linearly

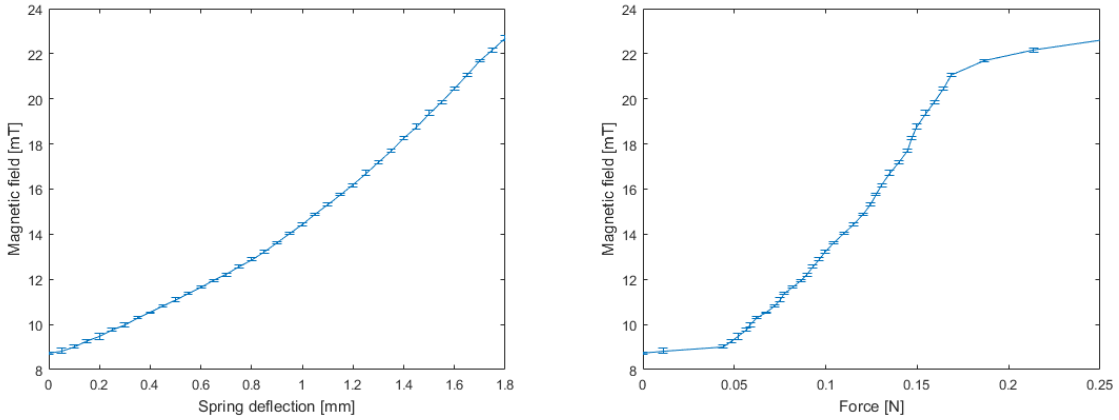

(a) Calibrated magnetic field vs spring deflection **(b)** Calibrated magnetic field vs force

Figure 7-5: Results of the prototype calibration

for increasing spring deflection. This is the case, since the spring deflection range has been specifically designed to be in the quasi-linear region of the magnetic field versus distance relationship (as was discussed in section 4-2-2). Note that this calibration is almost equivalent to the calibration of the spring stiffness constant, but also takes into account internal friction forces in the catheter.

The magnetic field also increases quasi-linearly for increasing force, with two exceptions. Firstly, for force values smaller than 0.05 N, the magnetic field hardly increases. This happens because the spring is not deflected due to friction forces which have not been overcome yet. Secondly, for force values larger than approximately 0.17 N, the magnetic field hardly increases either. This happens because the spring has been saturated and further spring compression requires a higher force than would be expected from a linear force-displacement approximation.

7-3 Materials

In this research, three materials are indented which are specifically chosen to mimic soft tissue stiffness before and after ablation. This is done to investigate the effectiveness in distinguishing ablated and non-ablated tissue (see section 8-3). Ecoflex 10 (E-10) is selected, since the Young's modulus of this material is in the range of that of non-ablated soft tissue. Two other materials, Ecoflex 5 (E-5) and Vytaflex 10 (V-10), have been selected to mimic ablated tissue. Ecoflex 5 and Ecoflex 10 are platinum-catalyzed silicon rubbers, composed of polyorganosiloxanes and amorphous silica [177]. Vytaflex 10 is a urethane rubber, and consists of a mixture of TDI prepolymers and isocyanates [178].

The three materials are shown in figure 7-6 and their properties are summarized in table 7-1. Note that the figure also includes the sample holders, which are discussed in section 7-3-1.

Other materials that are often used for representing soft tissue are Agarose gel [179, 72], which requires lengthy sample preparation, and gelatin concentrations [80, 62]. The choice

for above materials is based on the high repeatability of sample preparation and additional material properties provided by the manufacturer.

Table 7-1: Mechanical properties of sample materials

Material	**Tensile strength** $[N/mm^2]$	**Young's modulus** $[N/mm^2]$	**Shore hardness**
Ecoflex 5	2.41	0.10	5A
Ecoflex 10	0.38	0.06	00-10
Vytaflex 10	1.38	0.17	10A

7-3-1 Sample preparation

The sample preparation is performed in two phases: development of the sample holder, discussed in section 7-3-1, and the preparation of the materials, discussed in section 7-3-1.

Sample holder

The stabilization of sample boundary conditions is essential in achieving good measurement accuracy in load-displacement data [175]. Direct measurement of the Young's modulus based on load-displacement data can only be achieved when all sample boundary conditions are known. By constraining the sample, the knowledge of the boundary conditions of the sample is increased which allows for more reliable data processing for the Young's modulus.

Cylindrical sample holders are used to minimize the boundary area between the sample and the inside of the holder, compared to sample volume [175, 170]. Moreover, this shape is relatively easy to produce, especially by making use of 3D printing. Boundary condition effects are further reduced by using a high diameter-to-height ratio and by preventing geometrical imperfections [175].

The height of the sample holder relates to the sample thickness and is determined based on a relative indentation depth and sample aspect ratio. The relative indentation depth is defined as the ratio between the indentation depth and the sample thickness while the aspect ratio is defined as the radius of the indenter with respect to the sample thickness [172]. These values, especially the aspect ratio (a/h) where a is the indenter radius and h the sample thickness, are important for the influence of stiffness on the friction between the indenter tip and sample surface. Miniaturizing the diameter of the indenter further reduces the influence of boundary conditions [175] as well as these friction forces [172]. Since the aspect ratio influences the geometry and material-dependent factor (κ) and is preferably under <0.2 to keep the values for κ low. However, the indenter diameter can not be further decreased. The final dimensions for the sample holder are therefore 10 mm (aspect ratio of : 0.13) in height and 20 mm in diameter, see figure 7-6.

Procedure

The samples are prepared in laboratory environment at room temperature, and all glass mixing containers, sticks and syringes are either new or thoroughly cleaned with alcohol,

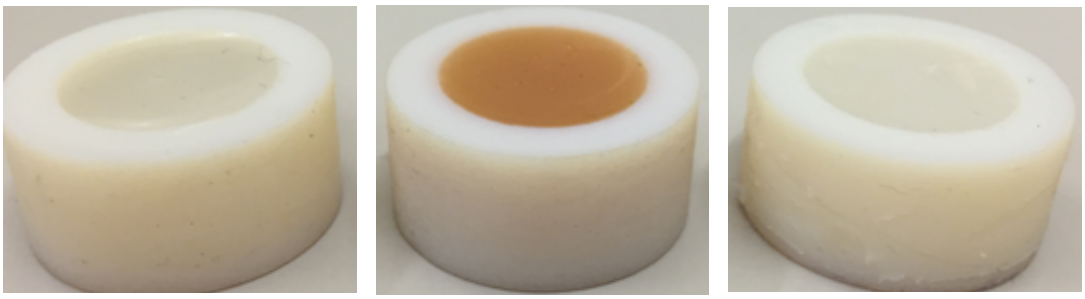

(a) Ecoflex 10 **(b)** Vytaflex 10 **(c)** Ecoflex 5

Figure 7-6: Selected sample materials in sample holders

purified water and special wipes. All three sample materials consist of two components, A and B, which need to need to be mixed on a 1:1 mass ratio. Therefore a precision electronic balance is used, which is calibrated prior to use to achieve the desired measurement accuracy ($< 10^{-4}$g). During calibration, care has to be taken that the glass doors surrounding the scale are closed and no objects are placed on the table to reduce vibrations.

The small glass mixing containers are placed in the middle of the scale. The following procedure consists of eight steps, which apply to all three materials unless specifically stated otherwise:

1. The content of material B is mixed (around 30 s), a syringe is used to extract material and deposit 10 g in the glass container;
2. The content in the glass container is mixed thoroughly for 3 minutes (except for the Ecoflex 5, which is stirred a couple of times because of very fast curing time);
3. The content of material A is mixed (around 30 s), a syringe is used to extract material and deposit 10 g in the glass container;
4. The glass container is taken of the scale and the sample material is mixed by hand for 3 minutes;
5. To improve the sample quality, the samples are placed in a vacuum machine for 3 minutes, to extract most air bubbles from the mixture. The pressure in the vacuum chamber rises to 25 kPa and is removed after three minutes with approximately 1.5 kPa/s. This step is not executed for Ecoflex 5 because of fast curing time;
6. The sample holders are filled to the top by hand and are lightly trimmed to evenly distribute the material and prevent curvature in the sample surface;
7. A needle is used to remove surface forces between the sample holder and the materials, and to puncture air bubbles which have not been removed with vacuuming. This step is especially crucial for the Ecoflex 5 which is not placed in the vacuum machine. By using the needle, air bubbles which are trapped inside the sample can be removed as well;
8. Finally, the samples are placed in a box for protection and cured at room temperature.

7-4 Data processing

This section describes the data processing of the catheter tip in section 7-4-1 and of the verified measurements with the STENTOR II in section 7-4-2.

7-4-1 Catheter data processing

The acquired data during the sample indentation with the catheter consists of the measured magnetic field values and the controlled actuation of the catheter tip. The number of actuation steps, as well as their size, are defined a piori in the Arduino code. Since all catheter measurements run through Arduino, the corresponding magnetic field data in x, y and z-direction for each actuation step is written in this environment. At the end of each measurement, this data is transferred to a text file such that the raw data can easily be imported in MATLAB for processing and analysis.

Therefore the output data consists of the full catheter tip displacement (h_a in equation 7-1), i.e the actuation performed by the stepper motor, and the magnetic field measured by the Hall sensor. The spring deflection (d_{spring}) and force value are determined based on the magnetic field in x-direction by means of the calibration curves, discussed in section 7-2-2. The indentation of the sample, h_i can then be calculated with equation 7-1.

$$h_i = h_a - d_{spring} \tag{7-1}$$

7-4-2 STENTOR II data processing

The load-indentation data generated with the STENTOR II is stored in a text file. Based on this information, two data processing steps are required to make a comparison in load-displacement data between the catheter and STENTOR.

The first step involves the removal of all data before making contact with the sample. The point of initial tool-sample contact needs to be set to 0. In the second step, a correction has to be made for the reversed vertical coordinate system of the STENTOR compared to the catheter measurement. Finally, the values can be imported and plot in MATLAB.

7-5 Conclusion

In this chapter, the measurement method of the catheter prototype has been discussed. The measurement goal to test the effectiveness of the design in distinguishing materials with different stiffness, to verify the precision (i.e. repeatability) of the design and to determine the accuracy of the design. These are respectively tested based on indenting three sample materials of different stiffness, performing multiple indentation cycles on the same specimen and performing indentation of the sample materials by a certified machine. The sample material is specifically selected to mimic soft tissue stiffness before ablation (Ecoflex 10) and soft tissue stiffness values after ablation (Vytaflex 10 and Ecoflex 5).

Calibration is performed for the spring deflection as well as force values based on the measured magnetic field. The error on the calibration curves is very small, enhancing the overall accuracy of the catheter when these curves are used for raw magnetic field data processing.

Chapter 8

Results and discussion

In this chapter the results of the prototype measurements are presented and discussed. The aim of this section is to evaluate the capability of the proposed prototype to extract meaningful mechanical properties of samples by generating load displacement data. A detailed description of the experimental setup has been discussed in detail in chapter 7, and investigates the prototype capability in three ways. First, the repeatability of the measurements is determined, which is discussed in section 8-1. Second, the accuracy of the measurements is determined by comparing the results of the prototype measurements to results determined using a verified load-displacement machine. This is discussed in section 8-2. Third, the effectiveness of the prototype, i.e. the capability to distinguish materials with different stiffness values, is discussed in section 8-3. Final conclusions of this chapter are summarized in section 8-4.

8-1 Repeatability

As discussed in chapter 7, multiple measurements have been performed for three different materials, in order to assess the repeatability of the prototype measurements. High repeatability is desired, since it is a primary prerequisite for high-quality stiffness measurement and it allows effective distinction between materials with different stiffness values (also see section 8-3).

Three measurements each have been performed on Ecoflex 5 (E-5), Ecoflex 10 (E-10) and Vytaflex 10 (V-10). The measured load-displacement curves are shown in figs. 8-1a, 8-1c and 8-1e. Note that these graphs do not include the origin, since the corresponding forces and displacements are outside of the prototype measurement range, due to inaccuracies related to the exact determination of first tip-tissue contact [180]. However, this problem can be circumvented since the stiffness can be determined from the part of the load-displacement curves shown in the figure. As expected, these curves show a quasi-linear relationship between force and displacement, of which the gradient reflects the material stiffness. The stiffness values, as well as a comparison between the different materials, will be further discussed in sections 8-2 and 8-3, respectively.

For each of the different materials, the gradient of the three measured load-displacement curves show a small deviation. For each of these materials, figs. 8-1b, 8-1d and 8-1f shows the absolute percentage deviation from the mean measured force at different indentation values, averaged for the three different measurements. Two main conclusions can be drawn from these results. The first is, that for higher indentation, the percentage deviation decreases, which corresponds to a higher repeatability. Therefore, it is best to determine the stiffness based on this part of the curves, as was also concluded in section 4-2-2. The second observation is that Ecoflex 10 (figure 8-1d) has a higher deviation, and therefore a lower repeatability. This is the case because Ecoflex 10 has a lower stiffness than the other materials, which causes it to 'overflow' above the sample holder upon indentation. This 'overflow' can occur in varying forms, which creates an uncontrollable (and therefore not repeatable) factor that slightly influences the force-displacement measurement [181].

To summarize, the deviation in the right part of the curves is mostly between 0% and 5%. This deviation, and therefore the repeatability, is adequate for the prototype and will be further discussed in section 8-3.

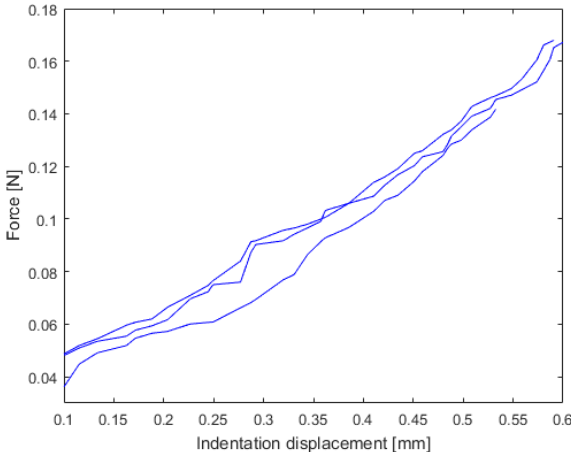

(a) Load-displacement measurements of E-5

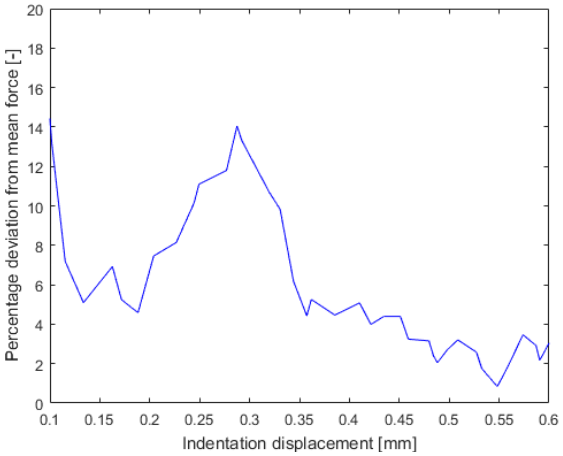

(b) Force deviation (%) of E-5 measurements

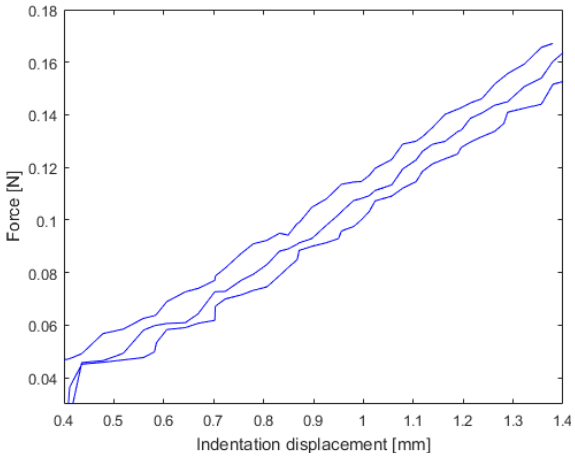

(c) Load-displacement measurements of E-10

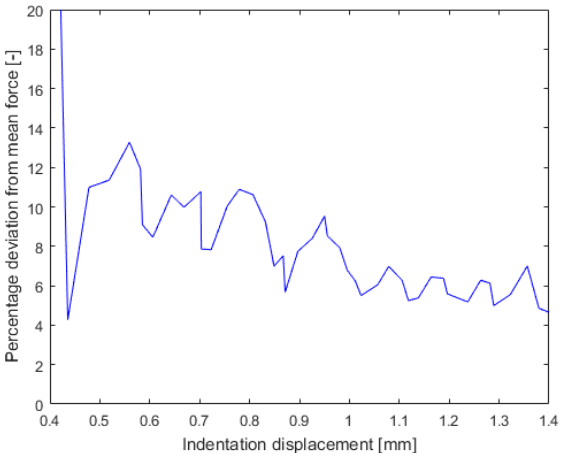

(d) Force deviation (%) of E-10 measurements

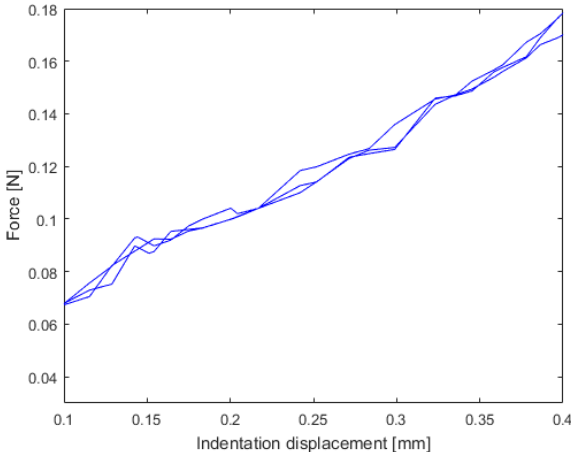

(e) Load-displacement measurements of V-10

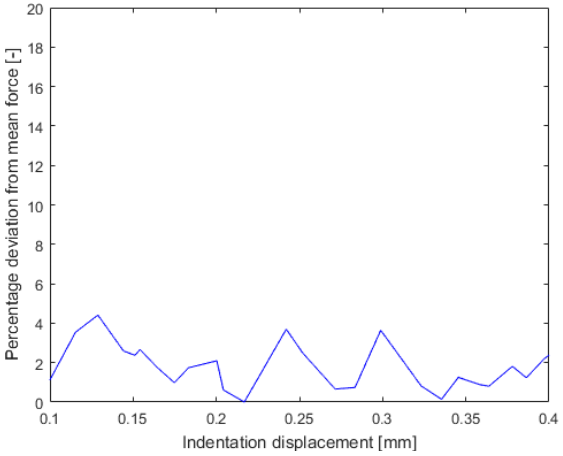

(f) Force deviation (%) of V-10 measurements

Figure 8-1: Load-displacement curves and force deviations among multiple measurements

8-2 Accuracy

As discussed in chapter 7, samples of the three materials have been measured both with the prototype and with a commercial load-displacement machine. By comparing the measurement results of both, the accuracy of the prototype can be determined.

Figure 8-2 shows the load-displacement curves for the three materials, as measured with the prototype and the verified load-displacement machine. Furthermore, table 8-1 presents the corresponding stiffness values. The prototype measurements underestimates the stiffness by approximately 30-40% in comparison to the commercial measurements. However, both the figure and table show that the load-displacement curves and stiffness values of the different materials can still be distinguished despite this underestimation. This will be discussed further in section 8-3.

The underestimation appears to be systematic, and can be explained by a dependency of stiffness on indentation speed. This effect is described in literature, and shown in figure 8-3, in which a higher indentation speed corresponds to a different load-displacement curve and a higher stiffness [182]. The stiffness underestimation of the prototype measurements is influenced by this effect, since the indentation speed of the prototype measurement (approximately $25\mu m/s$)is lower than that of the verified load-displacement machine (approximately $167\mu m/s$). Unfortunately, different indentation speeds had to be used during the measurements because of machine limitations. As is stated in chapter 10, it is recommended to repeat the verified machine measurements, using a machine that can indent with a similar speed as the prototype.

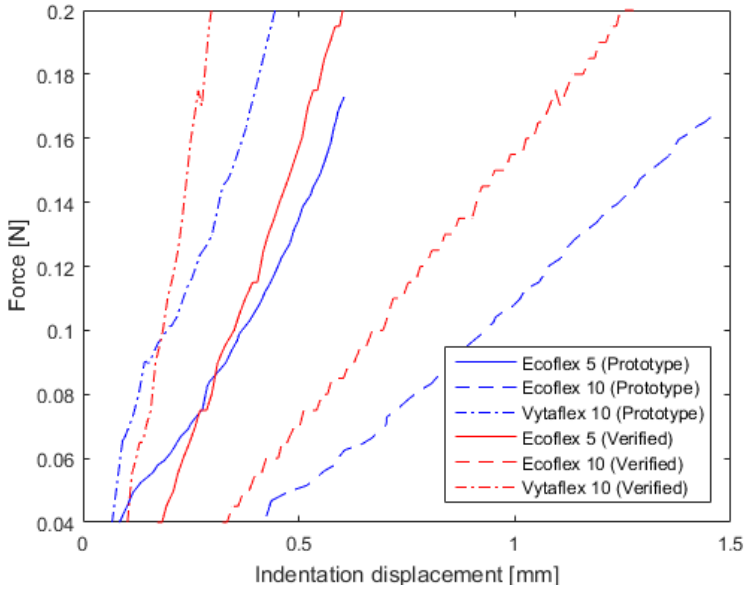

Figure 8-2: Load-displacement curves from both the prototype and a verified machine for each sample material

Table 8-1: Stiffness of different materials, as determined by the prototype and a verified machine

Material	Prototype stiffness $[N/mm]$	Verified stiffness $[N/mm]$	Difference
Ecoflex 5	0.352	0.502	-29.7%
Ecoflex 10	0.129	0.182	-29.3%
Vytaflex 10	0.547	0.953	-42.6%

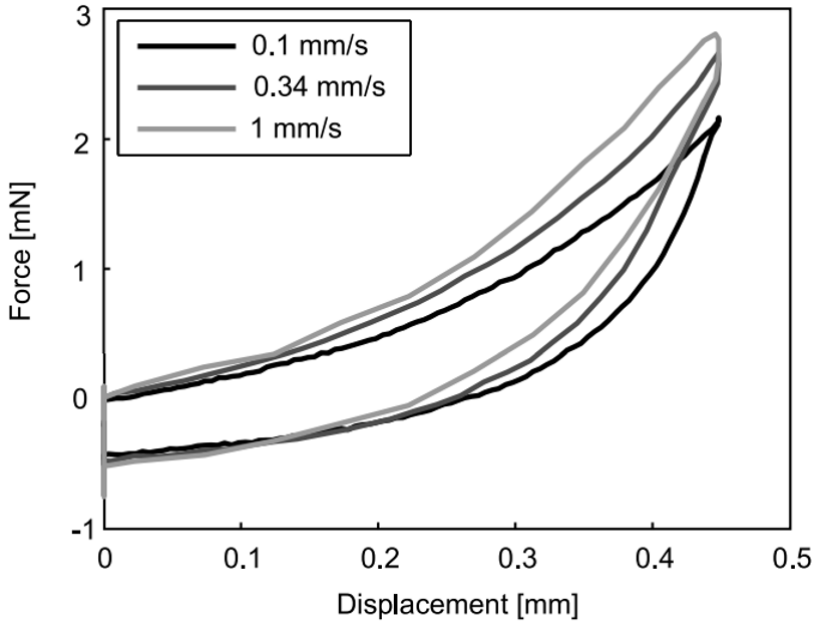

Figure 8-3: Effect of indentation speed on load-displacement curve and stiffness [182]

8-3 Effectiveness

This section discusses the effectiveness of the prototype towards its goal: distinguishing materials with different stiffness values, in order to recognize ablated and non-ablated tissue. As was discussed in chapter 7, specific sample materials have been selected to mimic heart tissue stiffness. Ecoflex 10 reflects non-ablated tissue, and Ecoflex 5 and Vytaflex 10 both reflect ablated tissue.

The effectiveness of the prototype was evaluated upon the consistent discrimination of different materials based on the obtained stiffness measurements. Figure 8-4 shows that this is indeed the case for the prototype. The prototype effectively measures different load-displacement curves for ablated versus non-ablated materials (mimicked by Ecoflex 10 versus Ecoflex 5 and Vytaflex 10, respectively). Furthermore, it can even distinguish different types of ablated materials, since the load-displacement curves of Ecoflex 5 and Vytaflex 10 are also dissimilar. Therefore, the prototype is effective in achieving the goal for which it was designed.

This effectiveness is achieved despite the accuracy limitations described in section 8-2. This is the case since this inaccuracy is systematic and therefore influences the measurements of

the different materials in the same way. Furthermore, the effectiveness is achieved because of the high precision of the measurements (as discussed in section 8-1 on repeatability).

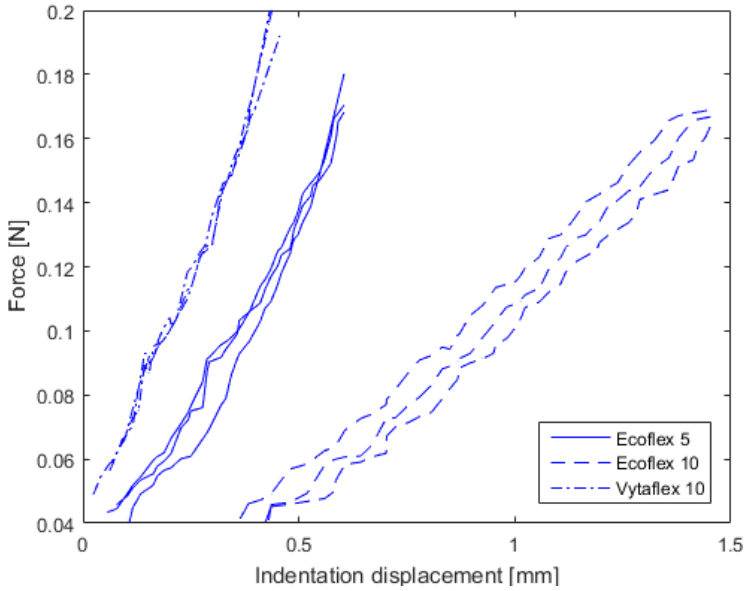

Figure 8-4: Load-displacement curves for different measurements of three samples

8-4 Conclusions

This chapter investigated the repeatability, accuracy and effectiveness of the prototype, based on several measurements. The main conclusions are:

- The prototype measurements are repeatable, with a measured force deviation of up to 5% for different measurements of the same material.
- The prototype measurements directionality correspond to measurements with a commercial load-displacement machine. However, the prototype systematically underestimates the stiffness by approximately 30% to 40%, due to an indentation speed difference between the measurements with the prototype and with the verified machine.
- The prototype is effective towards its goal of distinguishing non-ablated and ablated tissue, and even different ablated tissues. This is mainly the case because of the high measurement repeatability (i.e. precision) and the fact that the lower accuracy was mainly caused by a systematic error (instead of a random one).

Chapter 9

Conclusions

The main goal of this research is to develop a catheter capable of contact force and soft tissue stiffness measurement in the human heart. The purpose is to to assist the surgeon during thermal ablation and assess treatment effectiveness by stiffness measurement of the lesion (ablated tissue). This is reflected in the research objective:

Develop an accurate and robust micro-scale catheter tip prototype for combined stiffness and force sensing of soft biological heart tissue during minimally invasive surgery by making use of a 3D magnetic Hall sensor and micro-indentation technique.

Subordinate to the main objective are three sub-objectives:

1. To create effective catheter tip concept design(s) for the combined stiffness and 3D force sensing by making use of a Hall sensor and fixed permanent magnet;

2. To study the design and application of a displacement-amplifying compliant mechanism to amplify the indentation displacement and thereby improve the force and stiffness sensing accuracy;

3. To perform experiments with the assembled prototypes on samples of varying stiffness under prescribed boundary & environmental conditions.

The research objective has been met: a robust and effective catheter tip prototype has been designed for combined stiffness and force sensing of soft biological heart tissue. This will be substantiated in the following sections, which correspond to the three research sub-objectives.

9-1 Catheter tip design

An effective catheter tip has been designed, the key design choices and the catheter's key features are presented in this section.

Load-displacement based stiffness sensing, also called indentation, is applied in the catheter tip design, as opposed to resonance-based sensing. Measurement is performed in a displacement-

controlled mode, while the force is measured. Force-control would result in inaccurate measurement, since the force would be controlled *ex vivo*, but the force applied on the tissue (*in vivo*) would be different because of friction forces and moments on the catheter.

As stated in the objective, a 3D magnetic Hall sensor is used, together with a permanent magnet, which allows measurement of their relative location. Because of this sensor choice, force-sensing requires a deformable element, which translates this force to a displacement. For this reason a spring is implemented in the design, and its force-dependent deflection can be measured using the Hall sensor. In the design, the Hall sensor is placed at the free end of the spring ('free end' is inside the tip by making use of a stick to improve sensitivity and robustness) and the magnet is placed on the other end. The magnet is thus fixated, which enables guidance of the whole catheter based on an external (i.e. *ex vivo*) magnetic field.

Through calibration, the applied force and the spring deformation can be deduced from the magnetic field measured by the Hall sensor. Since the actuation displacement is controlled, and thus known, the tissue indentation can be determined as the difference between the actuation and spring displacement. Lastly, tissue stiffness is calculated from the generated load-displacement curve as the ratio of the force and tissue indentation (gradient).

The above describes the measurement principles behind the design. Furthermore, two elements have been included in the design that increase the catheter tip's functionality: a guidance tube and mechanical stoppers. The guidance tube is a stiff tube that concentrically encloses the catheter. Not only does this provide protection to the device, it also enables *ex vivo* actuation. This is the case because a force can be applied outside of the body, which is then transferred to the catheter tip without influencing the catheter position in the body, due to the high stiffness of the guidance tube. *Ex vivo* actuation is a key design feature, since it makes miniaturization possible and furthermore decreases catheter tip cost. The mechanical stoppers in the design serve three purposes. Firstly, they prevent parts from falling out, which is of course important during *in vivo* operations. Secondly, they protect the Hall sensor by preventing extensive spring deformation. Lastly, and most importantly, the spring can be pre-loaded because of the stoppers. Therefore, the initial spring length (before actuation) is always the same, which is essential to achieve repeatable and reliable results.

Most of the components of the catheter tip are 3D printed out of VeroClear. The only two exceptions are the spring and Hall sensor, which are both commercially available at low cost. Consequentially, the catheter tip weighs only 0.32 gram and costs less than €4, making it disposable. Other key design features of the catheter tip are its diameter of 4 mm and its force range of 0 - 0.2 N.

All in all, the catheter tip performs force and load-displacement based stiffness sensing, in a displacement-controlled mode, based on magnetic measurement of spring deflection and on calibration. Actuation of the catheter can occur *ex vivo* (because of the guidance tube), as well as guidance of the catheter (because of the fixed magnet). The catheter tip design ensures protection of both its own components and human tissue (non-destructive technique), and has a low weight, a low cost and a small size.

9-2 Displacement amplifying compliant mechanism

To increase the force resolution and signal-to-noise ratio of the catheter tip, a design study has been undertaken as a side-project during the research. Based on this study, the use of a displacement amplifying compliant mechanism (DACM) is proposed based on a spring-mass lever model and stiffness mapping. A mechanism with an amplification of 2.2 has been designed, and a review of fabrication methods is recommended.

9-3 Prototypes and experiments

The third sub-objective has been achieved since several prototypes have been produced and calibrated. Experiments have been performed on the final prototype to assess the repeatability, accuracy and effectiveness of the catheter tip design.

The main conclusions of these experiments were:

- The prototype measurements are repeatable, with a measured force deviation of mostly 0% to 5% in different measurements of the same material.
- The prototype measurements directionally correspond to measurements with a verified load-displacement machine. However, the prototype systematically underestimates the stiffness by approximately 30% to 40%, due to an indentation speed difference between the measurements with the prototype and with the verified machine.
- The prototype is effective towards its goal of distinguishing non-ablated and ablated tissue, and even different ablated tissues. This is mainly the case because of the high measurement repeatability (i.e. precision) and the fact that the lower accuracy was mainly caused by a systematic error (instead of a random one).

Based on these measurement results, it can be concluded that the developed catheter tip meets the main objective of robust and effective force and stiffness sensing of soft biological heart tissue. Although there seems to be a systematic inaccuracy (to be verified, see chapter 10) in stiffness measurement, the catheter tip is still effective in reaching its goal of distinguishing ablated and non-ablated tissue.

Chapter 10

Recommendations

Much work has been performed for the current research. The research is not finished, however, several recommendations can be given regarding the next steps that can be taken. The recommendations fall into three categories: increasing biocompatibility, increasing accuracy and decreasing catheter size, which will be discussed.

Increase biocompatibility

Biocompatibility is a crucial requirement for the catheter tip, especially for its commercialization. Although the catheter tip will only remain *in vivo* for a short amount of time, improvements on its biocompatibility are desirable. Four suggestions for further research on this topic are presented in this section.

Firstly, all components of the catheter should be made of verified biocompatible materials. In the current prototype, VeroClear is used for the 3D printed parts, because of limited availability of other 3D printer materials. VeroClear is already used for long-term tissue studies [183], but further research is required to verify its biocompatibility, or to investigate alternative biocompatible materials that are fit for 3D printing.

Secondly, hermetical sealing for the catheter tip could be designed to prevent blood from entering the catheter tip, which has several potential negative effects. It can cause measurement inaccuracy, since flowing blood or blood in the compression region of the tip influences spring behavior. Furthermore, blood in the tip can cause corrosion of tip components, and non-biocompatible material of the tip interior could enter the patient's blood stream. This can be solved with e.g. a highly elastic 'glove' around the catheter tip, so that spring behavior is not influenced (compared to its calibration). Further research on the hermetical sealing is required, and should focus on the choice of material, fabrication process and assembly technique.

Thirdly, the optimal stiffness of the guidance tube should be determined. As was stated in section 3-3-3, the guidance tube should be stiff enough to make *ex vivo* actuation possible. On the other hand, it should be flexible enough that the catheter can be easily and safely

guided through the body. Further investigation is required to determine the optimal between these conflicting requirements.

Fourthly, the catheter tip should be tested in an *in vivo* environment to determine its effectiveness, accuracy and repeatability in realistic conditions. This is an important step in the eventual commercialization of the catheter tip design. Accurate measurement in an *in vivo* environment creates several challenges, caused by the fluid surroundings, the curvature of the tube system and motion of the measurement site (e.g. due to heart beat or patient movement). Further research is required to determine the effect of these challenges on force and stiffness measurement.

Increase accuracy

The catheter is already accurate enough to distinguish ablated and non-ablated tissue. Increased accuracy would create new possibilities, such as measuring absolute stiffness values to estimate lesion size. Two suggestions for further research are presented in this section.

Firstly, the accuracy of the current catheter tip design should be investigated in more detail. As was discussed in chapter 8, accuracy was determined by comparing measurement results of the catheter tip to those of a commercial machine. However, it was not possible to perform this comparison with the same indentation speeds, resulting in apparent inaccuracies. Further research could use a different commercial or verified machine to determine accuracy with matching indentation speeds.

Secondly, the accuracy of the catheter tip could be improved by automation of actuation. This would result in a smoother indentation process than in the current situation, which used manual timing of actuation steps. A smoother process would increase accuracy, since the indentation process during measurements can be matched exactly to the indentation processes used in calibration. In the current situation these are not precisely matched, which causes inaccuracies because of visco-elastic effects, such as stress relaxation.

Decrease catheter size

The current catheter diameter is 4 mm (not considering the custom designed spring. Further miniaturization would be beneficial, since it would reduce the surgery impact on the patient. Two improvements are suggested in this section.

Firstly, a custom-made rectangular spring can be used instead of the commercially available round wire spring, used in the current prototype. This rectangular spring has already been designed and is currently in production, as discussed in section 4-4. With this custom-made spring, the catheter diameter can be decreased to approximately 3.7 mm, which is the minimum size because of the Hall sensor dimensions. Once its fabrication is finished, experiments can be performed to determine the effectiveness, repeatability and accuracy of the catheter tip with this custom spring.

Secondly, the catheter tip can be further miniaturized if the Hall sensor size is decreased, since this imposes the current size limit. Either a smaller 3D Hall sensor should be developed, or a smaller, commercially available 1D Hall sensor should be used.

Appendix A

Appendix

Figure A-1 shows the minimum ultimate tensile strength for different springs wires. It shows that the tensile strength of spring wire varies inversely with the wire diameter.

Figure A-2 shows the datasheet of the actuator used for the measurements.

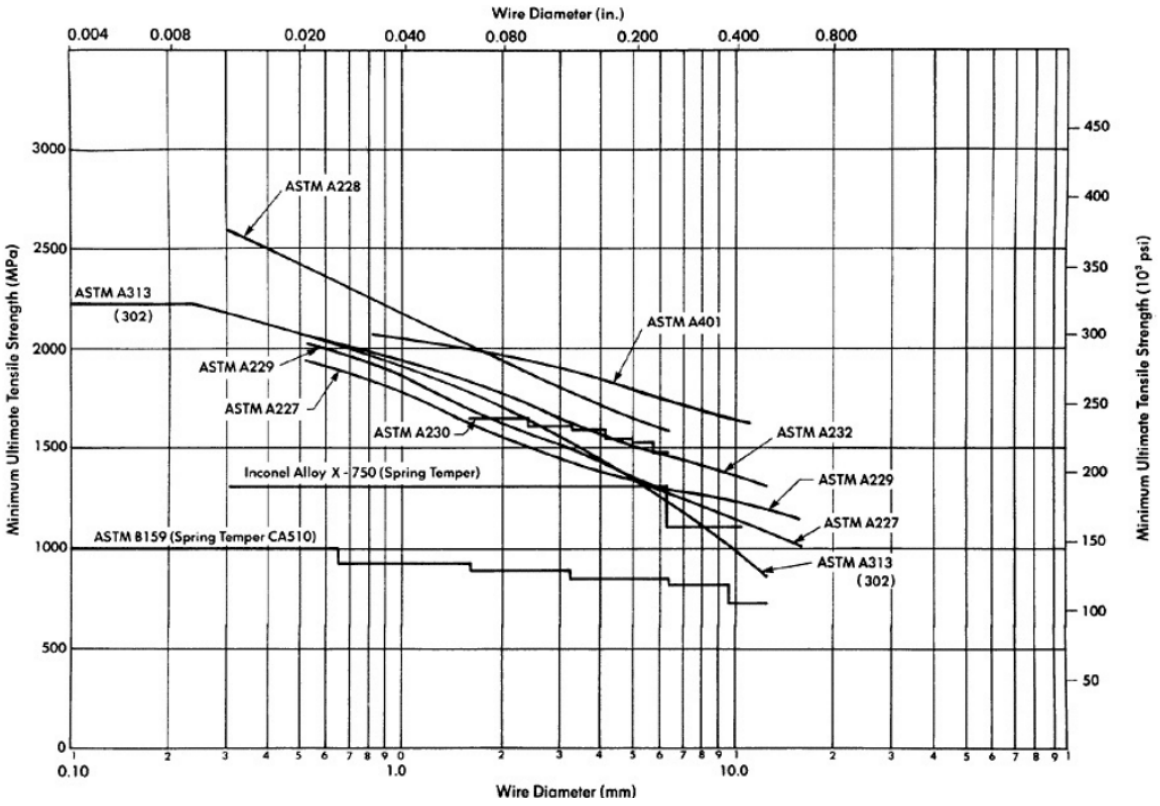

Figure A-1: Minimum tensile strengths of spring wire [134]

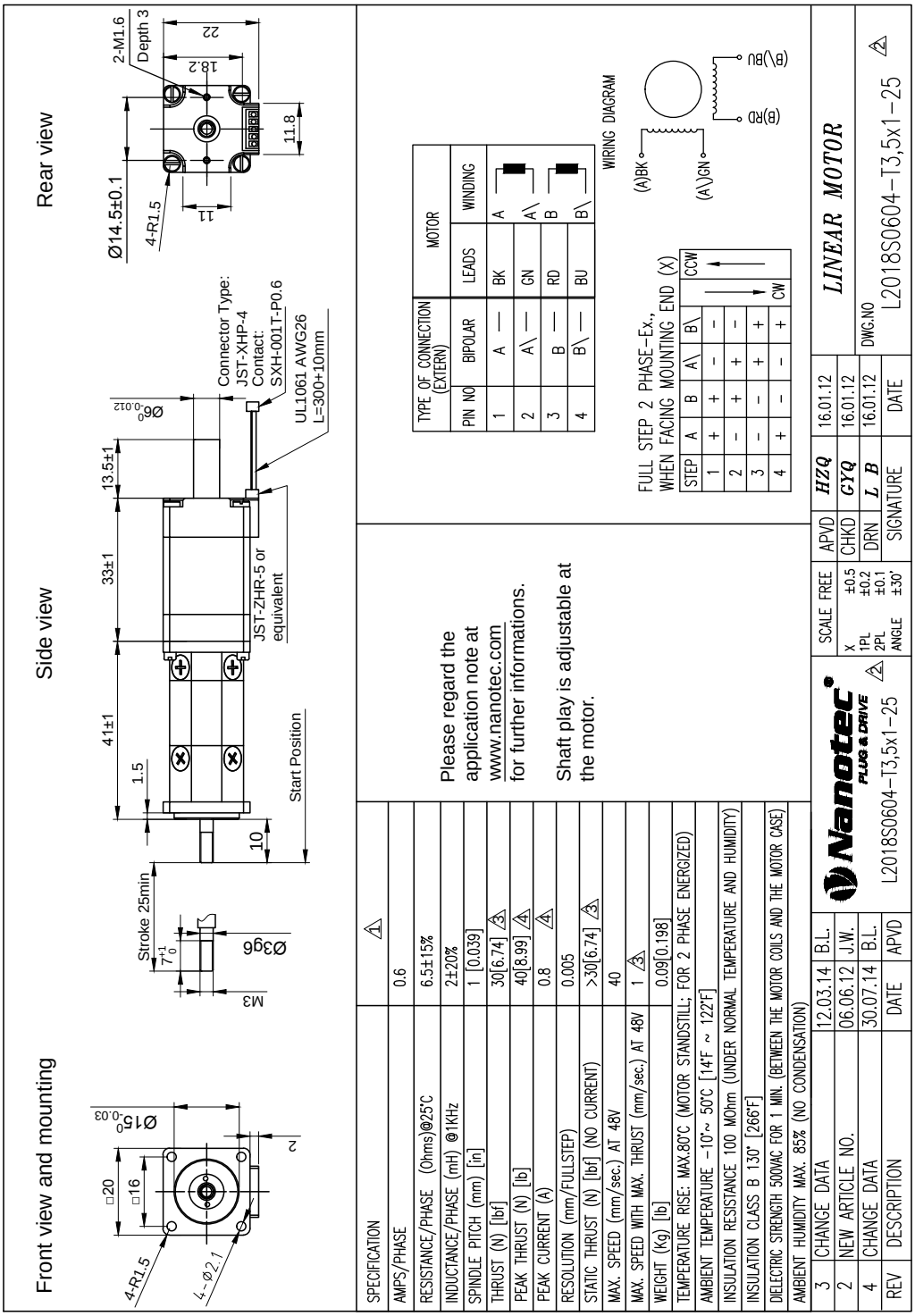

Figure A-2: Measurement actuator datasheet [184]

Bibliography

[1] B. Deml, T. Ortmaier, and U. Seibold, "The Touch and Feel in Minimally Invasive Surgery," *HAVE 2005 âĂŞ IEEE International Workshop on Haptic Audio Visual Environments and their Applications*, no. October, pp. 1–6, 2005.

[2] A. Trejos, R. Patel, and M. Naish, "Force sensing and its application in minimally invasive surgery and therapy: a survey," *Proceedings of the Institution of Mechanical Engineers, Part C: Journal of Mechanical Engineering Science*, vol. 224, no. 7, pp. 1435–1454, 2010.

[3] H. Iwata and K. Itoigawa, "Catheter having pressure detecting ability," 1996.

[4] The Electronics Tutorial, "The Hall effect sensor." [Online] http://www.electronics-tutorials.ws/electromagnetism/hall-effect.html [Accessed: 1 November 2015].

[5] M. Farine, *Instrumented Indentation of Soft Materials and Biological Tissues*. PhD thesis, ETH Zurich, 2013.

[6] G. Holzapfel, *Nonlinear Solid Mechanics*. Wiley, 2006.

[7] K. Hayashi, "Mechanical properties of soft tissues and arterial walls," *Biomechanics of Soft Tissue in Cardiovascular Systems*, no. 441, pp. 15–64, 2003.

[8] S. Hegde and G. K. Ananthasuresh, "Design of Single-Input-Single-Output Compliant Mechanisms for Practical Applications Using Selection Maps," *Journal of Mechanical Design*, vol. 132, no. 8, p. 081007, 2010.

[9] J. A. W. van Dommelen, T. P. J. van der Sande, M. Hrapko, and G. W. M. Peters, "Mechanical properties of brain tissue by indentation: Interregional variation," *Journal of the Mechanical Behavior of Biomedical Materials*, vol. 3, no. 2, pp. 158–166, 2010.

[10] R. E. Joerres, "Chapter 6: Springs," in *Standard Handbook of Machine Design*, vol. 2, pp. 6.3–6.70, McGraw-Hill, third ed., 2004.

[11] Nanotec, "L2018S0604-T3, 5x1-25." [Online] Available: http://de.nanotec.com/fileadmin/files/Datenblaetter/Linearaktuatoren/L20mV/L2018S0604-T3_5x1-25.pdf [Accessed: 2 November 2015], 2015.

[12] HKCM Engineering, "Ring Magnet Selection." [Online] https://www.hkcm.de/expert.php?fav= [Accessed: 15 September 2015].

[13] S. Hegde and G. K. Ananthasuresh, "A spring-mass-lever model, stiffness and inertia maps for single-input, single-output compliant mechanisms," *Mechanism and Machine Theory*, vol. 58, pp. 101–119, 2012.

[14] A. Bicchi, G. Canepa, D. De Rossi, P. Iacconi, and E. P. Scillingo, "A sensor-based minimally invasive surgery tool for detecting tissue elastic properties," *Proceedings of the IEEE International Conference on Robotics and Automation*, vol. 1, no. April, pp. 884–888, 1996.

[15] S. J. Lederman and R. L. Klatzky, "Sensing and Displaying Spatially Distributed Fingertip Forces in Haptic Interfaces for Teleoperator and Virtual Environment Systems," *Presence: Teleoperators and Virtual Environments*, vol. 8, pp. 86–103, 1999.

[16] D. E. Discher, P. Janmey, and Y.-L. Wang, "Tissue cells feel and respond to the stiffness of their substrate.," *Science (New York, N.Y.)*, vol. 310, no. 5751, pp. 1139–1143, 2005.

[17] J. F. Greenleaf, M. Fatemi, and M. Insana, "Selected methods for imaging elastic properties of biological tissues.," *Annual review of biomedical engineering*, vol. 5, pp. 57–78, 2003.

[18] P. Puangmali, K. Althoefer, L. D. Seneviratne, D. Murphy, and P. Dasgupta, "State-of-the-art in force and tactile sensing for minimally invasive surgery," *IEEE Sensors Journal*, vol. 8, no. 4, pp. 371–380, 2008.

[19] M. Tavakoli, R. V. Patel, and M. Moallem, "Robotic Suturing Forces in the Presence of Haptic Feedback and Sensory Substitution," *Proceedings of the 2005 IEEE Conference on Control Applications*, pp. 1–6, 2005.

[20] P. Polygerinos, D. Zbyszewski, T. Schaeffter, R. Razavi, L. D. Seneviratne, and K. Althoefer, "MRI-compatible fiber-optic force sensors for catheterization procedures," *IEEE Sensors Journal*, vol. 10, no. 10, pp. 1598–1608, 2010.

[21] P. Polygerinos, P. Puangmali, T. Schaeffter, R. Razavi, L. D. Seneviratne, and K. Althoefer, "Novel miniature MRI-compatible fiber-optic force sensor for cardiac catheterization procedures," *Proceedings - IEEE International Conference on Robotics and Automation*, pp. 2598–2603, 2010.

[22] R. Razavi, D. L. G. Hill, S. F. Keevil, M. E. Miquel, V. Muthurangu, S. Hegde, K. Rhode, M. Barnett, J. van Vaals, D. J. Hawkes, and E. Baker, "Cardiac catheterisation guided by MRI in children and adults with congenital heart disease.," *Lancet*, vol. 362, no. 9399, pp. 1877–82, 2003.

[23] V. Muthurangu, "The value of magnetic resonance guided cardiac catheterisation," *Heart*, vol. 91, no. 8, pp. 995–996, 2005.

[24] J. F. Greenleaf, M. Fatemi, and M. Insana, "Selected methods for imaging elastic properties of biological tissues.," *Annual review of biomedical engineering*, vol. 5, pp. 57–78, 2003.

[25] Ningbo Yu and R. Riener, "Review on MR-Compatible Robotic Systems," *The First IEEE/RAS-EMBS International Conference on Biomedical Robotics and Biomechatronics, 2006. BioRob 2006.*, no. FEBRUARY 2001, pp. 661–665, 2015.

[26] J. Peirs, J. Clijnen, D. Reynaerts, H. Van Brussel, P. Herijgers, B. Corteville, and S. Boone, "A micro optical force sensor for force feedback during minimally invasive robotic surgery," *Sensors and Actuators, A: Physical*, vol. 115, pp. 447–455, 2004.

[27] P. Puangmali, H. Liu, L. D. Seneviratne, P. Dasgupta, and K. Althoefer, "Miniature 3-axis distal force sensor for minimally invasive surgical palpation," *IEEE/ASME Transactions on Mechatronics*, vol. 17, no. 4, pp. 646–656, 2012.

[28] J. J. van den Dobbelsteen, A. Schooleman, and J. Dankelman, "Friction dynamics of trocars," *Surgical Endoscopy*, vol. 21, no. 8, pp. 1338–1343, 2007.

[29] T. Katsumata, Y. Haga, K. Minami, and M. Esashi, "Micromachined 125μm diameter ultra miniature fibre-optic pressure sensor for catheter," *Transactions IEE Japan*, vol. 120, no. 2, pp. 58 –63, 2000.

[30] S. Charles, H. Das, T. Ohm, C. Boswell, G. Rodriguez, R. Steele, and D. Istrate, "Dexterity-enhanced telerobotic microsurgery," in *1997 8th International Conference on Advanced Robotics. Proceedings. ICAR'97*, pp. 5–10, 1997.

[31] G. Dogangil, B. L. Davies, and F. Rodriguez y Baena, "A review of medical robotics for minimally invasive soft tissue surgery.," *Proceedings of the Institution of Mechanical Engineers. Part H, Journal of engineering in medicine*, vol. 224, no. 5, pp. 653–679, 2010.

[32] S. C. Low and L. Phee, "A review of master-slave robotic systems for surgery," *International Journal of Humanoid Robotics*, vol. 3, no. 4, pp. 547–567, 2006.

[33] G. Guthart and J. Salisbury, "The Intuitive telesurgery system: overview and application," *Proceedings 2000 ICRA. Millennium Conference. IEEE International Conference on Robotics and Automation. Symposia Proceedings (Cat. No.00CH37065)*, vol. 1, pp. 618–621, 2000.

[34] Intuitive Surgical Inc, "http://www.intuitivesurgical.com/." [Online] http://www.intuitivesurgical.com/.

[35] A. R. Lanfranco, A. E. Castellanos, J. P. Desai, and W. C. Meyers, "Robotic Surgery," *Annals of Surgery*, vol. 239, no. 1, pp. 14–21, 2004.

[36] A. Madhani, *Design of Teleoperated Surgical Instruments for Minimally Invasive Surgery*. PhD thesis, Massachusetts Institute of Technology, 1998.

[37] J. Peirs, H. V. Brussel, D. Reynaerts, and G. D. Gersem, "A flexible distal tip with two degrees of freedom for enhanced dexterity in endoscopic robot surgery," *MME - Micromechanics Europe Workshop*, pp. 271–274, 2002.

[38] H. Fischer, B. Vogel, W. Pfleging, and H. Besser, "Flexible distal tip made of nitinol (NiTi) for a steerable endoscopic camera system," *Materials Science and Engineering: A*, vol. 273-275, pp. 780–783, 1999.

[39] K. Cleary and C. Nguyen, "State of the art in surgical robotics: Clinical applications and technology challenges," *Computer Aided Surgery*, vol. 6, no. 6, pp. 312–328, 2001.

[40] M. Zoni-Berisso, F. Lercari, T. Carazza, and S. Domenicucci, "Epidemiology of atrial fibrillation: European perspective.," *Clinical epidemiology*, vol. 6, pp. 213–20, 2014.

[41] M. Haissaguerre, P. Jais, D. C. Shah, A. Takahashi, M. Hocini, G. Quiniou, S. Garrigue, A. Le Mouroux, P. Le Metayer, and J. Clementy, "Spontaneous Initiation of Atrial Fibrillation by Ectopic Beats Originating in the Pulmonary Veins," *N Engl J Med*, vol. 339, no. 10, pp. 659–666, 1998.

[42] H. Calkins, K. Kuch, R. Cappato, and J. Brugada, "Expert Consensus Statement on Catheter and Surgical Ablation of Atrial Fibrillation: Recommendations for Patient Selection, Procedural Techniques, Follow-up, and Research Trial Design : A report of Task Force on Catheter and Surgical Ablation of Atrial Fi," *Heart Rythm*, vol. 9, no. 4, pp. 632 – 696, 2012.

[43] A. Thiagalingam, A. D'Avila, L. Foley, J. L. Guerrero, H. Lambert, G. Leo, J. N. Ruskin, and V. Y. Reddy, "Importance of catheter contact force during irrigated radiofrequency ablation: Evaluation in a porcine ex vivo model using a force-sensing catheter," *Journal of Cardiovascular Electrophysiology*, vol. 21, no. 7, pp. 806–811, 2010.

[44] S. N. Goldberg, G. S. Gazelle, and P. R. Mueller, "Thermal Ablation Therapy for Focal Malignancy :," *American Roentgen Ray Society*, no. February, pp. 323–331, 2000.

[45] R. Righetti, F. Kallel, R. J. Stafford, R. E. Price, T. a. Krouskop, J. D. Hazle, and J. Ophir, "Elastographic characterization of HIFU-induced lesions in canine livers," *Ultrasound Med Biol*, vol. 25, no. 7, pp. 1099–1113, 1999.

[46] R. Souchon, O. Rouvière, A. Gelet, V. Detti, S. Srinivasan, J. Ophir, and J.-Y. Chapelon, "Visualisation of HIFU lesions using elastography of the human prostate in vivo: preliminary results," *Ultrasound in Medicine and Biology*, vol. 29, no. 7, pp. 1007–1015, 2003.

[47] T. Varghese, J. A. Zagzebski, and F. T. Lee, "Elastographic imaging of thermal lesions in the liver in vivo following radiofrequency ablation: Preliminary results," *Ultrasound in Medicine and Biology*, vol. 28, no. 11-12, pp. 1467–1473, 2002.

[48] T. Wu, J. P. Felmlee, J. F. Greenleaf, S. J. Riederer, and R. L. Ehman, "Assessment of thermal tissue ablation with MR elastography," *Magnetic Resonance in Medicine*, vol. 45, no. September 2000, pp. 80–87, 2001.

[49] S. Bharat, U. Techavipoo, M. Z. Kiss, W. Liu, and T. Varghese, "Monitoring stiffness changes in lesions after radiofrequency ablation at different temperatures and durations of ablation," *Ultrasound in Medicine and Biology*, vol. 31, no. 3, pp. 415–422, 2005.

[50] K. B. Yesin, K. Vollmers, and B. J. Nelson, "Analysis and design of wireless magnetically guided microrobots in body fluids," *Robotics and Automation, 2004. Proceedings. ICRA '04. 2004 IEEE International Conference on*, vol. 2, no. October, pp. 1333–1338 Vol.2, 2004.

[51] L. Han, J. A. Noble, and M. Burcher, "A novel ultrasound indentation system for measuring biomechanical properties of in vivo soft tissue," *Ultrasound in Medicine and Biology*, vol. 29, no. 6, pp. 813–823, 2003.

[52] Farlex, "The free dictionary." [Online] http://medical-dictionary.thefreedictionary.com/catheterization [Accessed: 30 July 2015].

[53] Farlex, "The free dictionary." [Online] http://medical-dictionary.thefreedictionary.com/cardiac+catheterization [Accessed: 7 September 2015].

[54] B. Demi, T. Ortmaier, and U. Seibold, "The touch and feel in minimally invasive surgery," in *Haptic Audio Visual Environments and their Applications, 2005. IEEE International Workshop on*, 2005.

[55] L. D. Harmon, "Automated Tactile Sensing," *The international journal of roboi*, pp. 3–32, 1981.

[56] D. Hristu, N. Ferrier, and R. Brockett, "The performance of a deformable-membrane tactile sensor: basic results on geometrically-defined tasks," *Proceedings 2000 ICRA. Millennium Conference. IEEE International Conference on Robotics and Automation. Symposia Proceedings (Cat. No.00CH37065)*, vol. 1, pp. 508–513, 2000.

[57] S. Sokhanvar, M. Packirisamy, and J. Dargahi, "A multifunctional PVDF-based tactile sensor for minimally invasive surgery," *Smart Material Structures*, vol. 16, pp. 989–998, 2007.

[58] M. I. Tiwana, S. J. Redmond, and N. H. Lovell, "A review of tactile sensing technologies with applications in biomedical engineering," *Sensors and Actuators, A: Physical*, vol. 179, pp. 17–31, 2012.

[59] M. Lee and H. Nicholls, "Review Article Tactile sensing for mechatronicsâĂŤa state of the art survey," *Mechatronics*, vol. 9, pp. 1–31, 1999.

[60] A. Govari, Y. Altmann, Y. Karkur, and H. Schwartz, "Catheter with pressure sensing," 2013.

[61] J. Clark, M. Bar-Tal, G. Karim, A. Montag, and M. Stanley, "Catheter with combined position and pressure sensing structure," 2013.

[62] A. Govari, A. Altman, and Y. Ephrath, "Estimation and mapping of ablation volume," 2011.

[63] M. Tanimoto, F. Arai, T. Fukuda, H. Iwata, K. Itoigawa, and Y. Gotoh, "Micro force sensor for intravascular neurosurgery and in vivo experiment," in *Micro Electro Mechanical Systems, 1998. MEMS 98. Proceedings., The Eleventh Annual International Workshop on*, pp. 504–509, 1998.

[64] J. Craig, *Introduction to robotics: Mechanics and Control*. Englewood Cliffs, NJ: Prentice-Hall, 2003.

[65] H. Soemers, *Design Principles for precision mechanisms*. 2011.

[66] T. Selkee, "Catheter having a force sensing distal tip," 2011.

[67] A. Govari, "Catheter with strain gauge sensor," 2011.

[68] Biosense Webster Inc, "Navistar Thermocool Diagnostic/Ablation catheter: Instructions for use."

[69] Business Wire, " Webster Receives FDA Approval for First Catheter Ablation Therapy in the U.S. to Feature Direct Contact Force Technology for Treatment of Atrial Fibrillation." [Online.] http://www.businesswire.com/news/home/20140225005610/en/Biosense-Webster-Receives-FDA-Approval-Catheter-Ablation [Accessed: 1 September 2011], 2014.

[70] R. Klafter, T. Chmielewski, and M. Negin, *Robotic Engineering: An integrated approach*. Englewood Cliffs, NJ: Prentice-Hall, 1989.

[71] B. Gray and R. Fearing, "A surface micromachined microtactile sensor array," in *Proceedings - IEEE International Conference on Robotics and Automation1*, pp. 1–6, 1996.

[72] M. E. H. Eltaib and J. R. Hewit, "Tactile sensing technology for minimal access surgery - A review," *Mechatronics*, vol. 13, pp. 1163–1177, 2003.

[73] K. Yokoyama, H. Nakagawa, D. C. Shah, H. Lambert, G. Leo, N. Aeby, A. Ikeda, J. V. Pitha, T. Sharma, R. Lazzara, and W. M. Jackman, "Novel contact force sensor incorporated in irrigated radiofrequency ablation catheter predicts lesion size and incidence of steam pop and thrombus.," *Circulation. Arrhythmia and electrophysiology*, vol. 1, pp. 354–362, 2008.

[74] E. Cibula, D. Donlagic, and C. Stropnik, "Miniature fiber optic pressure sensor for medical applications," in *Proceedings of IEEE*, vol. 1, pp. 711–714, 2002.

[75] C. Strandman, L. Smith, and L. Tenerz, "A production process of silicon sensor elements for a fibre-optic pressure sensor," *Sensors and Actuators, A: Physical*, vol. 63, no. 1, pp. 69–74, 1997.

[76] St. Jude Medical, "St. Jude Medical Receives FDA Approval of TactiCath Quartz Contact Force Ablation Catheter for Treatment of Atrial Fibrillation." [Online.] http://media.sjm.com/newsroom/news-releases/news-releases-details/2014/St-Jude-Medical-Receives-FDA-Approval-of-TactiCath-Quartz-Contact-Force-Ablation-Catheter-for-Treatment-of-Atrial-Fibrillation/default.aspx [Accessed: 10 September 2015], 2014.

[77] St. Jude Medical, "Ablation Catheter." [Online] http://www.medicalexpo.com/prod/st-jude-medical/product-70886-517930.html [Accessed:10 September 2015].

[78] C. Ledermann, S. Wirges, D. Oertel, M. Mende, and H. Woern, "Tactile sensor on a magnetic basis using novel 3D Hall sensor - First prototypes and results," in *INES 2013 - IEEE 17th International Conference on Intelligent Engineering Systems, Proceedings*, pp. 55–60, 2013.

[79] M. Epstein, "Hall-effect devices," *Magnetics, IEEE Transactions on*, vol. 3, no. 3, pp. 352–359, 1967.

[80] Pacific Scientific, "Understanding Hall effect devices." [Online] http://www.oeco.com/wp-content/uploads/2015/01/Hall_Effect_Devices.pdf [Accessed: 6 October 2015].

[81] V. Jalkanen, B. M. Andersson, A. Bergh, B. Ljungberg, and O. A. Lindahl, "Explanatory models for a tactile resonance sensor system-elastic and density-related variations of prostate tissue in vitro.," *Physiological measurement*, vol. 29, no. 7, pp. 729–745, 2008.

[82] B. Klein, W. Kuschinsky, H. Schröck, and F. Etterlein, "Interdependency of local capillary density, blood flow, and metabolism in rat brains," *Am J Physiol*, vol. 251, no. 6, pp. 1333–1340, 1986.

[83] V. Jalkanen, B. M. Andersson, A. Bergh, B. Ljungberg, and O. A. Lindahl, "Prostate tissue stiffness as measured with a resonance sensor system: A study on silicone and human prostate tissue in vitro," *Medical and Biological Engineering and Computing*, vol. 44, no. 7, pp. 593–603, 2006.

[84] O. A. Lindahl, C. E. Constantinou, A. Eklund, Y. Murayama, P. Hallberg, and S. Omata, "Tactile resonance sensors in medicine.," *Journal of medical engineering & technology*, vol. 33, no. 4, pp. 263–273, 2009.

[85] O. Lindahl, S. Omata, and K. Angquist, "A tactile sensor for detection of Physical Properties of Human," *Change*, vol. 22, no. 4, pp. 147–153, 1998.

[86] C. Kleesattel and G. Gladwell, "The contact-impedance meter-1," *Ultrasonics*, pp. 175–180, 1986.

[87] S. Omata and Y. Terunuma, "New tactile sensor like the human hand and its applications," *Sensors and Actuators, A: Physical*, vol. 35, pp. 9–15, 1992.

[88] Y. Murayama, C. E. Constantinou, and S. Omata, "Micro-mechanical sensing platform for the characterization of the elastic properties of the ovum via uniaxial measurement," *Journal of Biomechanics*, vol. 37, pp. 67–72, 2004.

[89] H. E. V. Gierke, H. L. Oestreicher, E. K. Franke, H. O. Parrack, and W. W. V. Wittern, "Physics of vibrations in living tissues.," *Journal of applied physiology (Bethesda, Md. : 1985)*, vol. 4, no. 12, pp. 886–900, 1952.

[90] A. Eklund, A. Bergh, and O. A. Lindahl, "A catheter tactile sensor for measuring hardness of soft tissue: measurement in a silicone model and in an in vitro human prostate model.," *Medical & biological engineering & computing*, vol. 37, no. 5, pp. 618–624, 1999.

[91] W. Oliver and G. Pharr, "Measurement of hardness and elastic modulus by instrumented indentation: Advances in understanding and refinements to methodology," *Journal of Materials Research*, vol. 19, no. 01, pp. 3–20, 2004.

[92] E. Samur, M. Sedef, C. Basdogan, L. Avtan, and O. Duzgun, "A robotic indenter for minimally invasive measurement and characterization of soft tissue response," *Medical Image Analysis*, vol. 11, no. 4, pp. 361–373, 2007.

[93] B. Ahn and J. Kim, "Estimation of soft tissue's mechanical properties with the indentation experiments and optimization algorithm," in *Third Asian Pacific conferencce on Biomechanics*, (Tokyo, Japan), 2007.

[94] K. Johnson, *Contact mechanics*. Cambridge University Press, 1985.

[95] R. Hill, B. Storakers, and A. B. Zdunek, "A Theoretical Study of the Brinell Hardness Test," in *Proceedings A*, vol. 423, 1989.

[96] S. I. Bulychev, V. P. Alekhin, M. K. Shorshorov, A. P. Ternovskii, and G. Shnyrev, "Determination of young's modulus according to indentation diagram," *Industrial Laboratory*, vol. 41, pp. 1409 – 1412, 1975.

[97] M. F. Doerner and W. D. Nix, "A method for interpretating the data from depth-sensing indentation instruments," *Journal of Materials Research*, vol. 1, no. 4, 1986.

[98] W. C. Oliver and G. M. Pharr, "An improved technique for determining hardness and elastic modulus using load and displacement sensing indentation experiments," *Materials Research Society*, vol. 7, no. 6, pp. 1564–1583, 1992.

[99] E. H. Lee and J. R. M. Radok, "The Contact Problem for Visooelastia Bodies 1," *Journal of applied mechanics*, pp. 438–444, 1960.

[100] D. Tabor, "A simple theory of static and dynamic hardness," *Proceedings of the Royal Society of London A: Mathematical, Physical and Engineering Sciences*, vol. 192, no. 1092, 1948.

[101] K. W. McElhaney, J. J. Vlassak, and W. D. Nix, "Determination of indenter tip geometry and indentation contact area for depth-sensing indentation experiments," *Journal of Materials Research*, vol. 13, no. 05, pp. 1300–1306, 1998.

[102] G. Picinbono, H. Delingette, and N. Ayache, "Nonlinear and anisotropic elastic soft tissue models for medical simulation," vol. 2, no. 2, pp. 1370–1375 vol.2, 2001.

[103] B. Ahn and J. Kim, "Measurement and characterization of soft tissue behavior with surface deformation and force response under large deformations," *Medical Image Analysis*, vol. 14, no. 2, pp. 138–148, 2010.

[104] M. G. Zhang, Y. P. Cao, G. Y. Li, and X. Q. Feng, "Spherical indentation method for determining the constitutive parameters of hyperelastic soft materials," *Biomechanics and Modeling in Mechanobiology*, vol. 13, no. 1, pp. 1–11, 2014.

[105] T. Lyyra, J. Jurvelin, P. Pitkanen, U. Vaatainen, and I. Kiviranta, "Indentation instrument for the measurement of cartilage stiffness under arthroscopic control," *Medical Engineering and Physics*, vol. 17, no. 5, pp. 395–399, 1995.

[106] M. Ottensmeyer and J. Salisbury, "In Vivo Data Acquisition Instrument for Solid Organ Mechanical Property Measurement," *Medical Image Computing and Computer-Assisted Intervention âĂŞ MICCAI 2001*, vol. 2208, pp. 975–982–982, 2001.

[107] F. J. Carter, T. G. Frank, P. J. Davies, D. McLean, and A. Cuschieri, "Measurements and modelling of the compliance of human and porcine organs," *Medical Image Analysis*, vol. 5, no. 4, pp. 231–236, 2001.

[108] J. P. A. Arokoski, J. Surakka, T. Ojala, P. Kolari, and J. S. Jurvelin, "Feasibility of the use of a novel soft tissue stiffness meter.," *Physiological measurement*, vol. 26, no. 3, pp. 215–228, 2005.

[109] E. Samur, M. Sedef, C. Basdogan, L. Avtan, and O. Duzgun, "A robotic indenter for minimally invasive characterization of soft tissues," *International Congress Series*, vol. 1281, pp. 713–718, 2005.

[110] J. T. Iivarinen, R. K. Korhonen, and J. S. Jurvelin, "Experimental and numerical analysis of soft tissue stiffness measurement using manual indentation device - significance of indentation geometry and soft tissue thickness," *Skin Research and Technology*, vol. 20, no. 3, pp. 347–354, 2014.

[111] R. A. Lange and D. L. Hillis, "Diagnostic Cardiac Catheterization," *Circulation*, vol. 107, no. 17, pp. 111–113, 2003.

[112] S. Guo, T. Fukuda, F. Arai, and K. Ogura, "Micro active guide wire catheter system-characteristic evaluation, electrical model and operability evaluation of micro active catheter," *Proceedings of the Sixth International Symposium on Micro Machine and Human Science*, pp. 131–136, 1995.

[113] H. Takizawa, H. Tosaka, R. Ohta, S. Kaneko, and Y. Ueda, "Development of a microfine active bending catheter equipped with MIF tactile sensors," in *Micro Electro Mechanical Systems, 1999. MEMS'99. Twelfth IEEE International Conference on. IEEE*, pp. 412 – 417, 1999.

[114] J. D. Humphrey and A. D. McCulloch, *The Cardiovascular System - Anatomy, Physiology and Cell Biology*. Springer, 2003.

[115] DuPont, "Properties Handbook: Teflon PTFE." [Online] http://www.rjchase.com/ptfe_handbook.pdf [Accessed:18 September 2015], 2013.

[116] M. Paun, J. Sallesse, and M. Kayal, "Offset and drift analysis of the Hall effect sensor. The geometrical parameters influence," *Journal of Nanomaterials and Biostructures*, vol. 7, no. 3, pp. 883 – 891, 2012.

[117] J. D. Humphrey, "Review Paper: Continuum biomechanics of soft biological tissues," *Proceedings of the Royal Society A: Mathematical, Physical and Engineering Sciences*, vol. 459, no. 2029, pp. 3–46, 2003.

[118] J. Oden, *Finite elements of non-linear continua*. mcgraw-hil ed., 1972.

[119] Y. C. Fung, *Biomechanics: motion, flow, stress and growth*. Springer, 1990.

[120] M. G. Wertheim, "Memoire sur l' eastocote et la cohesion des principaux tissues du corp humain," *Ann. Chim. Phys.*, vol. 21, p. 385414, 1847.

[121] C. Roy, "The elastic properties of the arterial wall," *Phil. Trans. R. Soc. Lond.*, vol. B99, pp. 1–31, 1880.

[122] P. S. L. Centre, "Elastomers." [Online] http://pslc.ws/macrog/elas.htm [Accessed: 2 September 2015], 2005.

[123] R. W. Ogden, "Nonlinear Elasticity , Anisotropy , Material Stability and Residual stresses in Soft Tissue Nonlinear Elasticity , Anisotropy , Material Stability and Residual Stresses in Soft Tissue," vol. 108, no. 441, pp. 65–108, 2003.

[124] C. Chuong and Y. Fung, "Compressibility and constitutive equation of arterial wall in radial compression experiments," *Biomechanics*, vol. 17, no. 1, pp. 35–40, 1984.

[125] Y. C. Fung, *Mechanical properties of living tissue.* Springer-Verlag, 2nd ed., 1993.

[126] A. Natale, V. Y. Reddy, G. Monir, D. J. Wilber, B. D. Lindsay, H. T. McElderry, C. Kantipudi, M. C. Mansour, D. P. Melby, D. L. Packer, H. Nakagawa, B. Zhang, R. B. Stagg, L. M. Boo, and F. E. Marchlinski, "Paroxysmal AF Catheter Ablation With a Contact Force Sensing CatheterResults of the Prospective, Multicenter SMART-AF Trial," *Journal of the American College of Cardiology*, vol. 64, no. 7, pp. 647–656, 2014.

[127] A. M. Okamura, C. Simone, and M. D. O'Leary, "Force modeling for needle insertion into soft tissue," *IEEE Transactions on Biomedical Engineering*, vol. 51, no. 10, pp. 1707–1716, 2004.

[128] F. Tendick, S. Sastry, R. Fearing, and M. Cohn, "Applications of Microelectromechanics in Minimally Invasive Surgery," *IEEE/ASME Transactions on Mechatronics*, vol. 3, no. 1, pp. 34–42, 1998.

[129] H. Wheat, L. Salo, and A. Goodwin, "Human Ability to Scale and Discriminate Forces Typical of Those Occurring during Grasp and Manipulation," *Journal of Neuroscience*, vol. 24, no. 13, pp. 3394 – 3401, 2004.

[130] St. Jude, "TactiCath Quartz Contact Force Ablation." [Online] http://professional-intl.sjm.com/products/ep/therapy/advanced-ablation/tactisys-quartz#tech-specs [Accessed:21 October 2015].

[131] Elmwood Electric Inc., "The Fatal Current." [Online] Available:https://www.physics.ohio-state.edu/˜p616/safety/fatal_current.htmlhttps://www.physics.oh state.edu/˜p616/safety/fatal_current.html [Accessed: 20 May 2015], 1987.

[132] E. W. Stockert and A. Langerman, "Assessing the magnitude and costs of intraoperative inefficiencies attributable to surgical instrument trays," *American College of Surgeons*, vol. 219, no. 4, pp. 646 – 655, 2014.

[133] S. Rush, J. a. Abildskov, and McFEER, "Resistivity of body tissues at low frequencies.," *Circulation research*, vol. 12, pp. 40–50, 1963.

[134] S. Smith, *Flexures, Elements of of Elastic Mechanisms*. North Carolina: Gordon and Breach Science Publishers, 2000.

[135] Precision Point, "Construction and Design, Leaf Springs." [Online] http://www.jpe.nl/downloads/Leaf-spring-or-flexure-Reinforced.pdf [Accessed:20 October 2015].

[136] S. Sirouspour, *Advanced Engineering and Computational Methodologies for Intelligent Mechatronics and Robotics*. 2013.

[137] L. Howell, *Compliant mechanisms*. Provo, Utah: john Wiley & Sons, Inc., first ed., 2001.

[138] Lee Spring Limited, "Designing & Specifying Compression, Extension and Torsion Springs," tech. rep., 2002.

[139] Massuchutes Institute of Technolohy, "Spring Calculation." [Online] http://mitcalc.com/doc/springs/help/en/springstxt.htm [Accessed: 24 June 2015].

[140] Newcomb Spring Comb, "Compression spring shapes." [Online] http://www.newcombspring.com/compression-spring-shapes.html [Accessed: 12 September 2015].

[141] N. Lobontiu, *Compliant mechanisms: design of flexure hinges*, vol. 23. 2002.

[142] J. Shigley, C. Mischke, and R. Budynas, *Mechanical Engineering Design*. Mc Graw Hill, seventh ed., 2004.

[143] G. Krauss, *Steels processing, structure, and performance*. 2015.

[144] University of Virginia, "Dislocations and Strengthening Mechanisms." [Online] http://www.virginia.edu/bohr/mse209/chapter7.htm [Accessed: 27 Ooctober 2015].

[145] J. A. Collins, H. R. Busby, and G. H. Staab, *Mechanical Design of Machine Elements and Machines: A Failure Prevention Perspective*. Hoboken, USA: Wiley, 2 ed., 2009.

[146] Infineon Technologies AG, "Technical Product description of 3D Magnetic Sensor TLV493D-A1B6." [Online.] http://www.infineon.com/dgdl/Infineon-3D+Magnetic+Sensor+-+Technical+Product+Description-ATI-v01_02-EN.pdf?fileId=5546d4624d6fc3d5014de2c7dc8030eb [Accessed: 20 June 2015], 2015.

[147] Polyfluor, "PTFE Tubes." [Online] http://www.polyfluorâĂŃ.nl/nl/materialen/ptâĂŃfe/ [Accessed: 10 July 2015].

[148] Century Spring, "Compression spring characteristics, N-78." [Online] http://www.centuryspring.com/Store/globalresults.php [Accessed: 4 September 2015].

[149] H. Carlson, "Selection and Application of Spring Materials," *Mechanical Engineering*, vol. 78, pp. 331 – 334, 1956.

[150] Associated Spring, *Design Handbook*. 1987.

[151] H. Wittel, D. Muhs, D. Jannasch, and J. Voß iek, *Roloff/Matek Maschinenelemente*. 2011.

[152] Synova, "Precision cutting and grooving with the Laser MicroJet." [Online] http://www.swissphotonics.net/libraries.files/PAUCHARD_EPMT2010.pdf [Accessed: 15 October 2010]], 2010.

[153] Deutsches Institut fur Normung, "Engineering standard: DIN2090."

[154] P. Childs, *Mechanical Design*. 2004.

[155] A. Erdman and G. Sandor, *Mechanisms Design: Analysis and Synthesis*. Upper Saddle River, New Jersey: Prentice Hall, 3th vol 1 ed., 1997.

[156] K. Lu, *Synthesis of Shape Morphing Compliant Mechanisms*. PhD thesis, 2004.

[157] L. L. Howell and A. Midha, "Parametric deflection approximations for end-loaded, large-deflection beams in compliant mechanisms," *Journal of Mechanical Design*, vol. 117, no. 1, pp. 156–165, 1995.

[158] S. Nishiwaki, S. Min, S. Ejima, and N. Kikuchi, "Structural optimization considering flexibility," *JSME Int. J*, vol. 41, no. 3, pp. 476–484, 1998.

[159] S. Khan and G. K. Ananthasuresh, "A Micromachined Wide-Band In-Plane Single-Axis Capacitive Accelerometer with a Displacement-Amplifying Compliant Mechanism," *Mechanics Based Design of Structures and Machines*, vol. 42, no. 3, pp. 355–370, 2014.

[160] S. Kota, J. Hetrick, Z. Li, and L. Saggere, "Tailoring unconventional actuators using compliant transmissions: design methods and applications," *IEEE/ASME Transactions on Mechatronics*, vol. 4, no. 4, pp. 396–408, 1999.

[161] G. Krishnan and G. K. Ananthasuresh, "Evaluation and Design of Displacement-Amplifying Compliant Mechanisms for Sensor Applications," *Journal of Mechanical Design*, vol. 130, no. 10, p. 102304, 2008.

[162] L. L. Howell and A. Midha, "A loop-closure theory for the analysis and synthesis of compliant mechanisms," *Journal of Mechanical Design*, vol. 118, no. 1, pp. 121–125, 1996.

[163] O. Sigmund, "On the design of compliant mechanisms using topology optimization," *Mechanics of Structures and Machines*, vol. 25, no. 4, pp. 493–524, 1997.

[164] M. I. Frecker, G. K. Ananthasuresh, S. Nishiwaki, N. Kikuchi, and S. Kota, "Topological synthesis of compliant mechanisms using multi-criteria optimization," *Journal of Mechanical design*, vol. 119, no. 2, pp. 238–245, 1997.

[165] B. Salamon and A. Midha, "An introduction to mechanical advantage in compliant mechanisms," *ASME Advances in design automation*, vol. 44, no. 2, pp. 47–51, 1992.

[166] a. Saxena and G. K. Ananthasuresh, "On an optimal property of compliant topologies," *Structural and Multidisciplinary Optimization*, vol. 19, no. 1, pp. 36–49, 2000.

[167] J. a. Hetrick and S. Kota, "An Energy Formulation for Parametric Size and Shape Optimization of Compliant Mechanisms," *Journal of Mechanical Design*, vol. 121, no. 2, p. 229, 1999.

[168] R. Kundu, C. V. Aravind, S. Hegde, and G. K. Ananthasuresh, "An Online Interactive Computer Program for Pragmatic Design of Compliant Mechanisms 1 Introduction," in *15th National Conference on Machines and Mechanisms*, pp. 1–11, 2011.

[169] S. Hegde and G. K. Ananthasuresh, "A spring-mass-lever model, stiffness and inertia maps for single-input, single-output compliant mechanisms," *Mechanism and Machine Theory*, vol. 58, no. I, pp. 101–119, 2012.

[170] J. Juuti, K. Kordas, R. Lonnakko, V. P. Moilanen, and S. Leppaviori, "Mechanically amplified large displacement piezoelectric actuator," *Sensors and Actuators, A: Physical*, vol. 120, pp. 225 – 231, 2005.

[171] Stratasys Ldt., "PolyJet Materials Data Sheet." [Online] http://usglobalimages.stratasys.com/Main/Secure/Material%20Specs%20MS/PolyJet-Material-Specs/PolyJet_Materials_Data_Sheet.pdf?v=635376606224140355 [Accessed:3 Julky 2015], 2014.

[172] A. Samanim, J. Bischop, C. Luginbuhl, and D. Plewers, "Measuring the elastic modulus of ex vivo small tissue samples," *Ultrasonic imaging*, 2003.

[173] I. Edwards, M Draper, E.R. Hand, J.W. Taylor, K.M. Young, "Mechanical Testing of Human Cardiac Tissue Strength and Stiffness : Implications for Mri Safety," in *Proceedings International Society Magnetic Resonance Medicine*, vol. 11, pp. 2003–2003, 2003.

[174] M. Zhang, Y. P. Zheng, and A. F. T. Mak, "Estimating the effective Young's modulus of soft tissues from indentation testsâĂŤnonlinear finite element analysis of effects of friction and large deformation," *Medical engineering & physics*, vol. 19, no. 6, pp. 512–517, 1997.

[175] J. M. Mattice, A. G. Lau, M. L. Oyen, and R. W. Kent, "Spherical indentation load-relaxation of soft biological tissues," *Journal of Materials Research*, vol. 21, pp. 2003–2010, 2006.

[176] M. R. Vanlandingham, "Review of Instrumented Indentation," *Journal Of Research Of The National Institute Of Standards And Technology*, vol. 108, no. 4, pp. 249–265, 2003.

[177] R. Q. Erkamp, P. Wiggins, a. R. Skovoroda, S. Y. Emelianov, and M. O'Donnell, "Measuring the elastic modulus of small tissue samples.," *Ultrasonic imaging*, vol. 20, no. 1, pp. 17–28, 1998.

[178] A. Morris and R. Langari, *Measurement and Instrumentation: Theory and Application*. Elsevier B.V., 2012.

[179] Kaupo, "Ecoflex Series." [Online]. http://www.kaupo.de/produkte/silikonkautschuk-additionsvernetzend/ecoflex-serie/ [Accessed: 3 September 2015], 2014.

[180] Smooth-On, "Vytaflex." [Online] http://www.smooth-on.com/tb/files/Vytaflex_Series_TB.pdf [Accessed: 6 September 2015], 2015.

[181] M. Ahearne, Y. Yang, A. J. El Haj, K. Y. Then, and K.-K. Liu, "Characterizing the viscoelastic properties of thin hydrogel-based constructs for tissue engineering applications.," *Journal of the Royal Society, Interface / the Royal Society*, vol. 2, no. 5, pp. 455–463, 2005.

[182] a.C Fischer-Cripps, "A review of analysis methods for sub-micron indentation testing," *Vacuum*, vol. 58, no. 4, pp. 569–585, 2000.

[183] Y. Huang, Z. Xue, H. Gao, W. D. Nix, and Z. C. Xia, "A Study of Microindentation Hardness Tests by Mechanism-based Strain Gradient Plasticity," *Journal of Materials Research*, vol. 15, no. 08, pp. 1786–1796, 2000.

[184] Cornell NanoScale Facility, "3D Printer FAQ." [Online.] http://www.cnf.cornell.edu/cnf_3dfaqs.html [Accessed: 3 November 2015].

Glossary

List of Acronyms

1D	One-dimensional
3D	Three-dimensional
AF	Atrial Fibrillation
CAD	Computer-aided Design
DACM	Displacement Amplifying Compliant Mechanism
E-5	Ecoflex 5
E-10	Ecoflex 10
FEM	Finite Element Model
ETH	Eidgenössische Technische Hochschule
MIS	Minimally Invasive Surgery
MRI	Magnetic Resonance Imaging
PTFE	Polytetrafluoroethylene
PZT	Lead Zirconate Titanate
UV	Ultraviolet
V-10	Vytaflex 10

List of Symbols

α	Spring end condition constant [−]
ϵ	Shape factor [−]
τ_{max}	Maximum shear stress $[N^2]$
A	Area $[mm^2]$
b	Tube thickness $[mm]$
C	Spring index [−]
D	Mean coil diameter $[mm]$
d	Spring wire diameter $[mm]$
D_m	Mean coil diameter $[mm]$
D_m	Mean coil diameter $[mm]$
d_{spring}	Spring deflection $[mm]$
E	Elastic modulus GPa
F	Force $[N]$
F_1	Force on tissue $[N]$
F_2	Force on catheter spring $[N]$
G	Shear modulus $[GPa]$
h	Cross-section height $[mm]$
h_a	Actuation distance $[mm]$
h_i	Sample indentation $[mm]$
J	Polar moment of inertia $[mm^4]$
k_1	Soft tissue stiffness $[N/mm]$
k_2	Catheter spring stiffness $[N/mm]$
K_c	Curvature correction factor [−]
K_s	Shear-stress correction factor [−]
k_{ci}	Input stiffness $[N/mm^2]$
k_{co}	Output stiffness $[N/mm^2]$
l	Length $[mm]$
L_0	Initial catheter spring length $[mm]$
L_f	Free spring length $[mm]$
n	Number of active spring coils [−]
$P_{actuation}$	Catheter tip actuation force $[N]$
T	Torsion $[Nm]$
U	Total strain energy $[J]$
x_1	Tissue spring deformation $[mm]$
x_2	Catheter spring deformation $[mm]$
$x_{actuation}$	Catheter tip actuation displacement $[mm]$
y	Total spring deflection $[mm]$
y_{cr}	Critical deflection $[mm]$